

THE UNIVERSITY OF MICHIGAN

7848-7-Q

STUDY AND INVESTIGATION OF A UHF-VHF ANTENNA

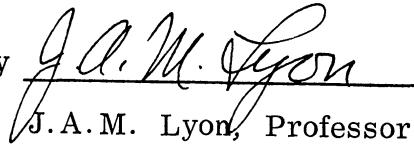
Seventh Quarterly Report  
1 July 1967 through 30 September 1967

October 1967

Prepared by

J. A. M. Lyon, C-C Chen,  
J. C. Parker and D. L. Smith

Approved by

  
J.A.M. Lyon, Professor  
Electrical Engineering

Contract No. AF 33 (615)-3609  
Project 6278, Task 627801  
O.E. Horton, Project Monitor

Air Force Avionics Laboratory, AVWE  
Research and Technology Division, AFSC  
Wright-Patterson Air Force Base, Ohio

This document is subject to special export controls and each transmittal to foreign government or foreign nationals may be made only with prior approval of AFAL(AVPT), Wright-Patterson AFB, Ohio 45433.



# THE UNIVERSITY OF MICHIGAN

7848-7-Q

## FOREWORD

This report, 7848-7-Q, was prepared by the University of Michigan, Radiation Laboratory, Department of Electrical Engineering, under the direction of Prof. Ralph E. Hiatt and Prof. John A. M. Lyon, on Air Force Contract AF 33(615)-3609, under Task 627801 of Project 6278, "Study and Investigation of UHF-VHF Antennas (U)". The work was administered under the direction of the Air Force Avionics Laboratory, Wright-Patterson AFB, Ohio. The task engineer was Mr. Olin E. Horton; the project engineer, Mr. E.M. Turner.

This report covers the period 1 July 1967 through 30 September 1967.

## ACKNOWLEDGEMENTS

The experimental assistance of Mr. U.E. Gilreath and Mr. J. Brooke Hutt is gratefully acknowledged.

ABSTRACT

This report covers the work effort on the various tasks of the project for a three-month period. The report goes into considerable detail since it includes substantial analysis, computer results, and experimental data. In all of the tasks, substantial progress has been made. However, in one task, a complete reorientation of the work program has been made. Under Task II, on slot arrays, it has been found necessary to simplify the work and also to avoid difficulties with materials. This should allow development of a new array utilizing ferrite filled rectangular slots developed in the prior contract work of this group.

LIST OF FIGURES

Figure No.	Caption	Page
2-1:	Antenna 238, A Bifilar Helix Antenna with Shorted Transmission Inductors Used as Loading.	8
2-2:	Dimensions of Inductances of Inductance Loaded Antenna.	9
2-3:	Coordinate System Assumed for the Helix Antenna.	11
2-4a:	Linear Power Patterns of Antenna 238, An Inductor Loaded Bifilar Helix ( $ E_{\theta} ^2$ Patterns in the $\phi = 0$ Plane).	12
2-4b:	Linear Power Patterns of Antenna 238, An Inductor Loaded Bifilar Helix ( $ E_{\theta} ^2$ Patterns in the $\phi = 0$ Plane).	13
2-5:	VSWR of Antenna 238, A Bifilar Helix with Inductance Loading.	14
4-1:	Geometry of the Ferrite Tube Antenna.	28
4-2:	Linear Power Patterns of the Ferrite Tube Antenna ( $ E_{\theta} ^2$ Patterns in the $\phi = 0$ Plane).	30
4-3:	Linear Power Patterns of the Ferrite Tube Antenna ( $ E_{\phi} ^2$ Patterns in the $\phi = 90^{\circ}$ Plane).	31
4-4:	Half-Power Beamwidth Against Frequency of the Ferrite Tube Antenna.	32
4-5:	Side-lobe Level Against Frequency of the Ferrite Tube Antenna.	33
4-6:	Near Field Measurement, the Relative Amplitude and the Phase of $E_{\rho}$ Against the Coordinate Angle $\phi$ , Taken at 5 cm from the Feed End of the Ferrite Tube Antenna.	34

List of Figures (Cont'd)

Figure No.	Caption	Page
4-7:	Near Field Measurement, the Relative Amplitude and The Phase of $E_{\rho}$ Against the Coordinate Angle $\phi$ , Taken at 5 cm from the Free End of the Ferrite Tube Antenna.	35
4-8:	Near Field Measurement, the Relative Amplitude and The Phase of the $E_{\rho}$ Against the Ferrite Tube Axis at 600 MHz in $\phi = \pi/2$ Plane.	36
4-9:	Near Field Measurement, the Relative Amplitude and the Phase of $E_{\rho}$ Against the Ferrite Tube Axis at 900 MHz in $\phi = \pi/2$ Plane.	37
5-1:	Input Resistance R and Reactance X for Folded Dipole Structure where $p_s = 1.0$ , $p_a = 1.0$ .	43
5-2:	Input Resistance R and Reactance X for Folded Dipole Structure where $p_s = 1.0$ , $p_a = 0.8$ .	44
5-3:	Input Resistance R and Reactance X for Folded Dipole Structure where $p_s = 1.0$ , $p_a = 0.6$ .	45
5-4:	Input Resistance R and Reactance X for Folded Dipole Structure where $p_s = 1.0$ , $p_a = 0.4$ ,	46
5-5:	Input Resistance R and Reactance X for Folded Dipole Structure where $p_s = 0.8$ , $p_a = 0.8$ .	47
5-6:	Input Resistance R and Reactance X for Folded Dipole Structure where $p_s = 0.8$ , $p_a = 0.6$ .	48

List of Figures (Cont'd)

Figure No.	Caption	Page
A-1:	Solution of the Characteristic Equation for Helix having Core Parameters $\epsilon_r = 1.00$ , $\mu_r = 1.00$ ; (Air).	53
A-2:	Solution of the Characteristic Equation for Helix having Core Parameters $\epsilon_r = 3.77$ , $\mu_r = 1.00$ ; (EAF-2 Powder Ferrite Biased into Saturation).	54
A-3:	Solution of the Characteristic Equation for Helix having Core Parameters $\epsilon_r = 7.88$ , $\mu_r = 1.00$ ; (Q-3 Ferrite at 150 MHz Biased into Saturation).	55
A-4:	Solution of the Characteristic Equation for Helix having Core Parameters $\epsilon_r = 22.0$ , $\mu_r = 1.00$ ; (Eccosorb CR at 300 MHz Biased into Saturation).	56
A-5a, b:	Solution of the Characteristic Equation for Helix having Core Parameters $\epsilon_r = 3.77$ , $\mu_r = 2.10$ ; (EAF-2 Powder Ferrite).	57, 58
A-6a, b:	Solution of the Characteristic Equation for Helix having Core Parameters $\epsilon_r = 7.96$ , $\mu_r = 12.4$ ; (Q-3 Ferrite at 100 MHz).	59, 60
A-7a, b:	Solution of the Characteristic Equation for Helix having Core Parameters $\epsilon_r = 7.88$ , $\mu_r = 13.2$ ; (Q-3 Ferrite at 150 MHz).	61, 62
A-8a, b:	Solution of the Characteristic Equation for Helix having Core Parameters $\epsilon_r = 7.81$ , $\mu_r = 14.3$ ; (Q-3 Ferrite at 200 MHz).	63, 64
A-9a, b:	Solution of the Characteristic Equation for Helix having Core Parameters $\epsilon_r = 22.0$ , $\mu_r = 4.51$ ; (Eccosorb CR at 300 MHz).	65, 66

TABLE OF CONTENTS

FOREWORD	iii
ABSTRACT	iv
LIST OF FIGURES	v
I INTRODUCTION	1
II FERRITE LOADED CONICAL SPIRALS	3
2.1 Introduction	3
2.2 Anisotropic Ferrite Loaded Helix Antenna.	4
2.3 Discrete Inductance Loading	6
2.3.1 Antenna Description	7
2.3.2 Test Results	10
2.3.3 Conclusions	10
III SLOT ARRAYS	16
IV FERRITE ROD ANTENNAS	17
4.1 Theoretical Analysis	17
4.2 Experimentation	27
V LOW FREQUENCY FERRITE ANTENNAS	39
5.1 Tuning of Linear Elements Via Magnetic Biasing	39
5.2 Computer Analysis of Multiple Linear Elements	41
VI CONCLUSIONS	49
VII FUTURE EFFORT	50
APPENDIX A: DESIGN CURVES FOR SMALL DIAMETER LOADED HELICES	51
REFERENCES	70
DISTRIBUTION	

DD 1473



I

INTRODUCTION

This report indicates the accomplishment in each of four assigned tasks of this project. A separate section is devoted to each task.

Section II describes the work on Task I involving the development of a log conical spiral antenna. Various techniques useful in reducing the size of such an antenna are assessed in this report. For convenience, experiments were confined to the loading of a bifilar cylindrical helix. These results can be transferred to the design of the log conical helix required by this task.

Section III covers the effort under Task II which is devoted to the use of physically small slot antennas as elements of an antenna array. In this section, coverage is given to the new work effort which is quite different from what had been previously recorded under this task. Emphasis is now on an arrangement of ferrite loaded slots connected by a coaxial feed system, with the apertures of the slots mounted in a line in a common ground plane. A description of such a three element array is given in the report.

In previous work under task II, a waveguide with rectangular slots cut in the broad-face was utilized. Some unsatisfactory results were obtained because the ferrite material used (type Q-3) did not have electrical characteristics as good as those published. This necessitated either going to a much lower frequency, with the attendant difficulties due to the required spacing in the array, or going to a new design utilizing better material. The latter course was chosen, and as a result rectangular slots filled with type EAF-2 material were utilized. This choice will permit the array to be studied in a frequency range from 300 MHz up to 600 MHz which will result in more easily obtained experimental patterns.

In Section IV, progress on Task III involving studies of endfire ferrite rod radiators has been described. During this report period, a major part of the effort has been analytical. Also, the important decision has been reached that ferrite rod radiators having only a cylindrical shell are more promising as endfire radiators than solid ferrite cylindrical rod radiators. In addition to analysis, experimentally determined radiation patterns for a ferrite tube antenna are given. Likewise, information is given on experimental measurements of the near field of a ferrite tube antenna.

In Section V, the effort under Task IV devoted to new types of ferrite antennas usable down to 30 MHz is discussed. A considerable part of the effort has been on the tuning of linear elements by utilizing magnetic bias. A computer program study was made on small diameter cylindrical helices utilizing various ferrite material core loadings. The air loaded case was also studied for comparison. For some of the ferrite loading cases, the ferrite has been biased into saturation. Saturated ferrite cores and air core results correspond very well. Studies have also continued on the computer analysis of multi-linear elements. Results on a folded dipole consisting of two similar slow wave elements are presented. The material in Appendix A supplements the coverage given in Section V.

## II

## FERRITE LOADED CONICAL SPIRALS

2.1 Introduction

The objective of this task is to develop a ferrite filled conical spiral antenna that will cover the 200 to 600 MHz range and be approximately one-third the size of an unloaded conical spiral antenna. The antenna is to have circular polarization with a broad forward directional main beam. The antenna should also be capable of employing both the transmit and receive modes simultaneously.

Throughout the course of this contract, emphasis has been placed on size reduction of helix antennas instead of conical spiral antennas. The reasons are three: 1) a helix is a special case of a conical spiral antenna that occurs when the cone angle is 0 degrees; 2) helix antennas are much easier to construct and analyze mathematically; 3) the results of cylindrical helices are directly applicable to conical spirals. Therefore more investigations can be made into reduction techniques with the time and money available.

During this report period, emphasis has been placed on two techniques of reducing the size of a helix antenna. The first is by loading with an anisotropic ferrite; the special case of a ferrite biased into saturation by a d-c magnetic field is explored. This special case is one limiting case of tuning the antenna with a d-c magnetic field. (The other limit is an isotropic material.) A saturated ferrite is also the only low loss ferrite material available above about 400 MHz and therefore is itself an interesting ferrite loading.

The second technique investigated during this report period is discrete inductance loading, inserting inductances in series with the windings of the antenna. The inductors used were shorted sections of transmission line. Due to a miscalculation in the design of the experimental antenna tested, the predicted results were not obtained. However, the antenna is still very interest-

ing because it has the size and shape of a helix antenna, yet operates over almost a 3 to 1 frequency band with a small stop band in the center.

## 2.2 Anisotropic Ferrite Loaded Helix Antenna.

There are several reasons for examining anisotropic ferrite loading in helix antennas. All of these reasons are a consequence of the steady unidirectional magnetic field in the material. First of all, at higher frequencies, a magnetic bias of the ferrite makes a low loss material possible. (Hach, 1966). Second, if a helix is magnetically tuned by adjusting the magnetic field, then the properties of the antenna would be affected by the changes in the characteristics of the material. Third, because a plane wave propagating through a saturated ferrite exhibits circular polarization, precisely the polarization produced by a helix antenna, it may be possible to use anisotropic loading as to mode filter to reduce the high side and backlobes that sometimes result from isotropic loading materials.

Because a saturated ferrite can be expected to represent one limit in the range of operation of a magnetic field tuned ferrite loaded antenna, it poses an interesting special case to study. Fortunately, the anisotropy of the permeability tensor of such a material is relatively simple and can be readily predicted by classical electromagnetic theory. The permeability tensor can be described by the following tensor:

$$\bar{\mu} = \mu_0 \begin{pmatrix} \mu & j\kappa & 0 \\ -j\kappa & \mu & 0 \\ 0 & 0 & 1 \end{pmatrix}$$

where

$$\mu = \left( 1 + \frac{\gamma \omega M_0}{\omega_0^2 - \omega^2} \right)$$

$$\kappa = \left( \frac{\omega \gamma M_0}{\omega_0^2 - \omega^2} \right)$$

and  $M_0$  is approximately  $M_s$ , the saturated magnetization (provided the amplitude of the time varying fields is small),  $\gamma$  is the gyromagnetic ratio,  $\omega_0$  is the Larmor frequency and is equal to  $\gamma B_0$ ,  $B_0$  is the DC magnetic field, and  $\mu_0$  is the permeability of free space (Collin, 1960). The dielectric constant of the material is the same as when no bias is applied.

The permeability tensor, like any tensor, may be transformed to another coordinate system. For the helix antenna, circular cylindrical coordinates are appropriate. Since the transformation matrix from rectangular to circular cylindrical coordinates is:

$$\bar{\bar{C}}_{CR} = \begin{pmatrix} \cos \phi & \sin \phi & 0 \\ -\sin \phi & \cos \phi & 0 \\ 0 & 0 & 1 \end{pmatrix},$$

then the permeability tensor in the new system is:

$$\bar{\bar{\mu}}_C = \bar{\bar{C}}_{CR} \cdot \bar{\bar{\mu}}_R = \begin{pmatrix} \mu \cos \phi - j\kappa \sin \phi & j\kappa \cos \phi + \mu_r \sin \phi & 0 \\ -\mu_r \sin \phi - j\kappa \cos \phi & -j\kappa \sin \phi + \mu \cos \phi & 0 \\ 0 & 0 & 1 \end{pmatrix}$$

which makes the permeability tensor a function of the coordinates. This is true, in general, for any common coordinate system, except rectangular. This dependence on one of the coordinate variables complicates the mathematical solution of any saturated ferrite problem in any coordinate system except rectangular. However, this doesn't make the situation hopeless, and some insight can be obtained by a mathematical analysis.

Details of the mathematical analysis will be given in the final report. The preparation time for this report is insufficient to permit an adequate check of the analysis prior to publication.

### 2.3 Discrete Inductance Loading

If the series inductance of a uniform transmission line is increased, the phase velocity of the wave propagating over the line will be reduced. Since a helix or conical helix antenna can be reasonably approximated by a two wire transmission line having the same wire diameter as the winding of the helix antenna and a wire spacing equal to the diameter of the helix (Rassweiler, 1967) it seems reasonable that if the helix antenna has inductance inserted in series with the winding, then the phase velocity of a wave propagating along the helix, and hence the size of the helix, can be reduced.

To check out this theory, a helix antenna was constructed and tested that had additional inductance inserted in series with the winding. The inductances were shorted coaxial transmission line stubs. The object of the experiment was to check out the concept of using inductors made out of shorted sections of coaxial transmission line. If the concept were substantiated, then a ferrite loaded stub would be used. The advantages of ferrite are that smaller stubs could be used for a given inductance and that more stubs could be used per winding, hence making the discrete inductances approximate more closely a distributed inductance.

Unfortunately, due to an error in calculating the inductance needed, the inductances inserted were too small, and the hoped for performance was not realized. However, the experimental results were so favorable that they are reported here in the hope that the antenna may be useful to someone else. A backward fire pattern is obtained over almost a 3 to 1 band (475 to 1250 MHz) and the VSWR is close to 3 to 1 with respect to a 50 ohm load over this band,

except for a band of 80 MHz centered around 800 MHz. Yet a helix antenna of the same size would have a center of operation around 710 MHz.

### 2.3.1 Antenna Description

The antenna, shown in Fig. 2-1, is a bifilar helix antenna fed at the tip with a hybrid by twin lead consisting of two pieces of RG-58/U coaxial cable on the axis of the antenna. The inductances are inserted every quarter turn, and were designed to produce a 4 to 1 reduction in size assuming the diameter of the two wire line model is the diameter of the helix antenna, and that the diameter of the wire of the parallel wire line is that of the winding of the helix. However, the miscalculation altered this relationship.

The formulas used to calculate the inductance needed to accomplished were derived in an earlier report (Lyon et al., 1966) and are restated here:

$$L = Z_o / V_p \quad L' = L/R$$

where R is the multiplicative reduction factor (0.25 in this case), L is the original inductance per unit length, L' the new inductance per unit length,  $Z_o$  the characteristic impedance, and  $V_p$  the phase velocity.

The antenna is wound on a 4"ID x 1/16" thick piece of NEMA Grade XXX (Mil-P-3115-PBE) paper phenolic tubing. The pitch angle of the helix is  $14^\circ$  and there are 5 turns on the antenna. The winding was cut at the intervals shown in Fig. 2-2. Part of the dielectric and outer shield was removed, and one end of the remaining part of the shield was soldered to the center conductor to produce the inductor.

A helix antenna of this size would have a center frequency of operation of about 710 MHz as can readily be calculated from Fig. 2-3 on page 333 of

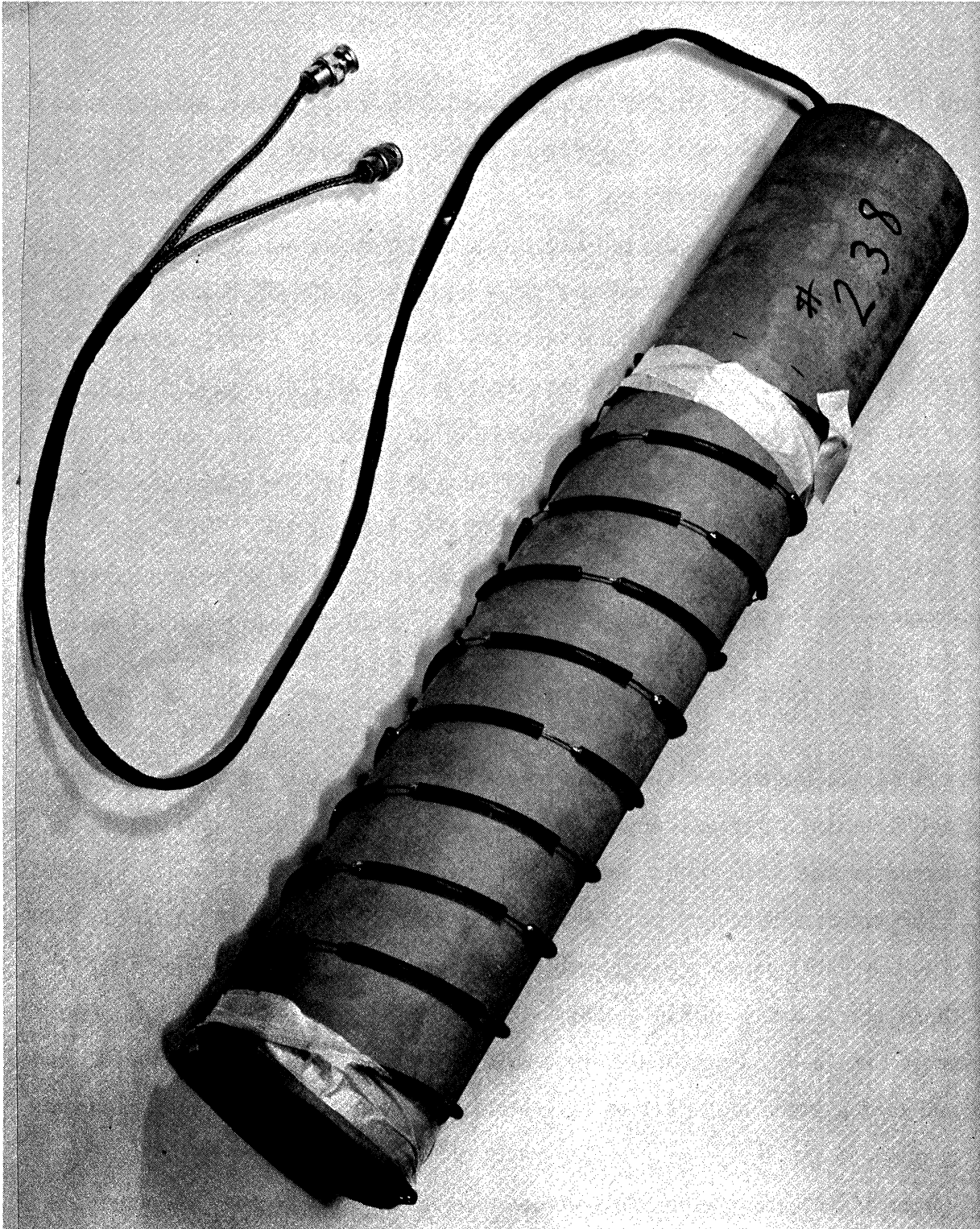


FIG. 2-1: ANTENNA 238, A BIFILAR HELIX ANTENNA WITH SHORTED TRANSMISSION INDUCTORS USED AS LOADING.



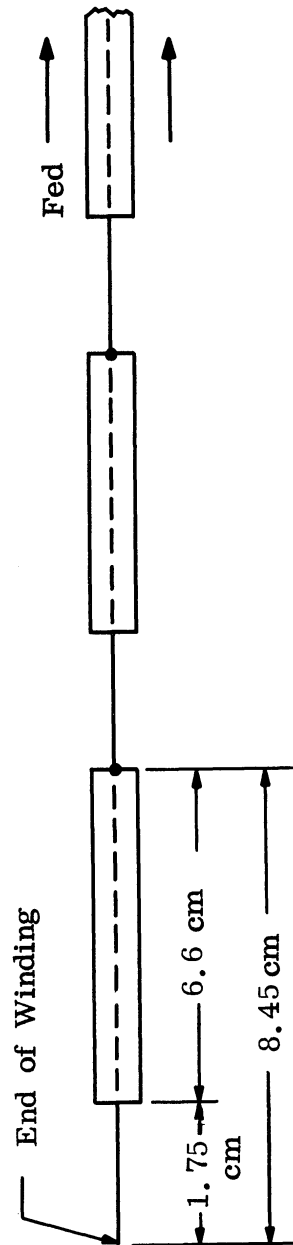


FIG. 2-2: DIMENSIONS OF INDUCTANCES OF INDUCTANCE  
LOADED ANTENNA.

Walter (1965). The antenna described, however, was designed to have a center frequency of operation of 227 MHz, since 910 MHz was assumed to be the unloaded center frequency.

### 2.3.2 Test Results

The radiation patterns taken measuring  $|E_{\theta}|^2$  on the  $\phi = 0$  cut as in Fig. 2-3 show the usual backward fire radiation patterns (low back lobe and side lobes, a well developed main lobe) from 475 to 760 MHz and from 840 to 1250 MHz as can be seen in Fig. 2-4. This gives geometrical mean center frequencies of operation of 600 MHz and 1025 MHz respectively, with corresponding bandwidths of 79 percent and 67 percent.

Between 760 and 840 MHz, the signal amplitude was so small that it was difficult to record patterns. Those that could be recorded were not satisfactory backward fire helix patterns.

The VSWR of the antenna was measured with respect to the input port of the hybrid used to feed the antenna with swept frequency equipment as is indicated in Fig. 2-5. In the lower band, the VSWR was centered around 2.5 with respect to 100 ohms and the variation from this was within  $\pm 0.5$  over most of the band. In the high band, the VSWR centered around 3.0 and the variation from this was less than  $\pm 0.5$  over most of the band. At about 790 MHz the reflection coefficient was almost 1.0. A check of the design indicated that at this frequency, the coaxial stub should be about one-quarter wavelength long, and hence the winding should be effectively open-circuited.

### 2.3.3 Conclusions

1) The transmission line model of the helix antenna presented by Rassewiler (1967) is apparently not quite correct. Assuming that the lower band of operation was caused by the inductive loading and working backwards from its

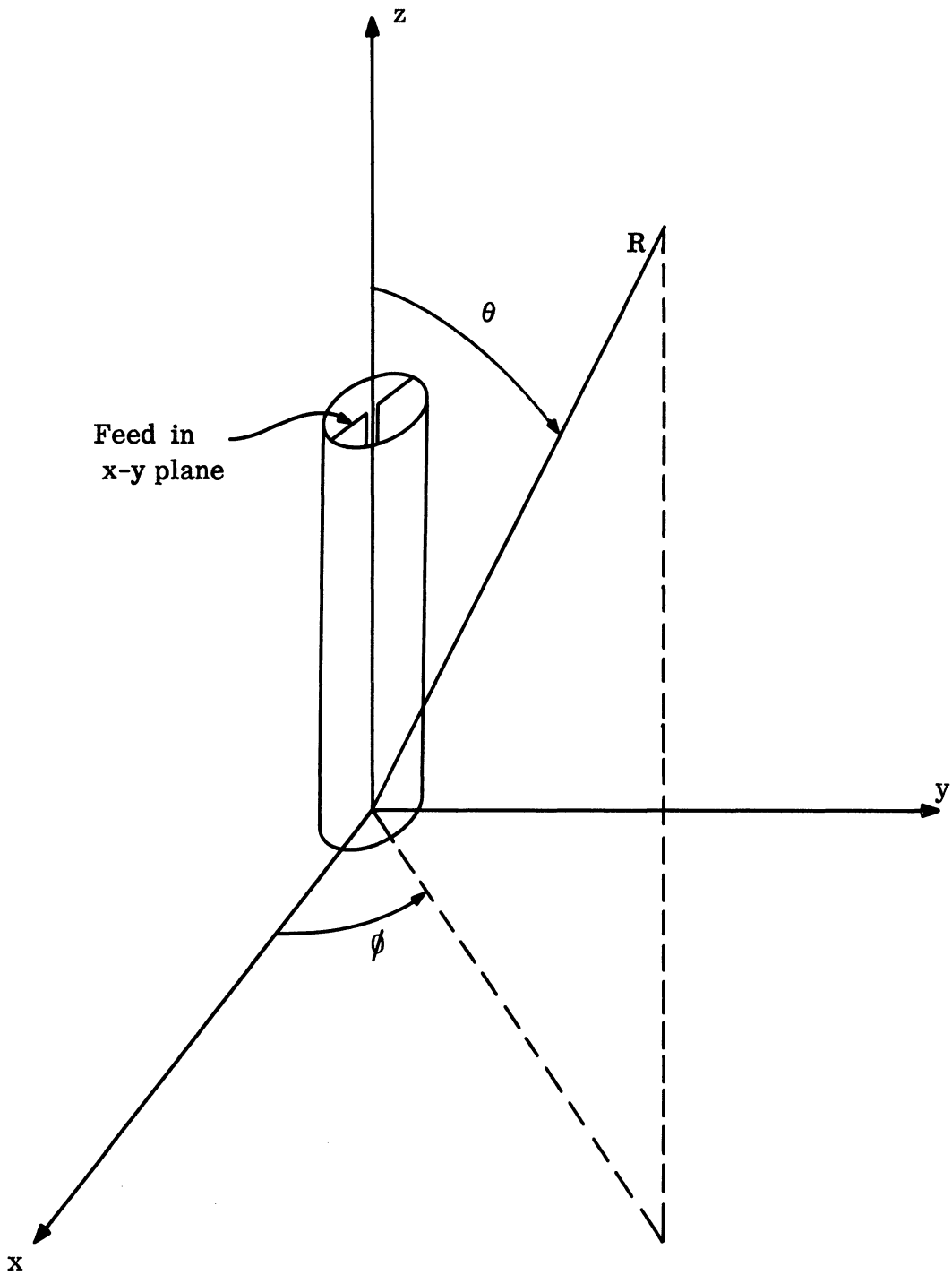


FIG. 2-3: COORDINATE SYSTEM ASSUMED FOR THE HELIX ANTENNA.

THE UNIVERSITY OF MICHIGAN

7848-7-Q

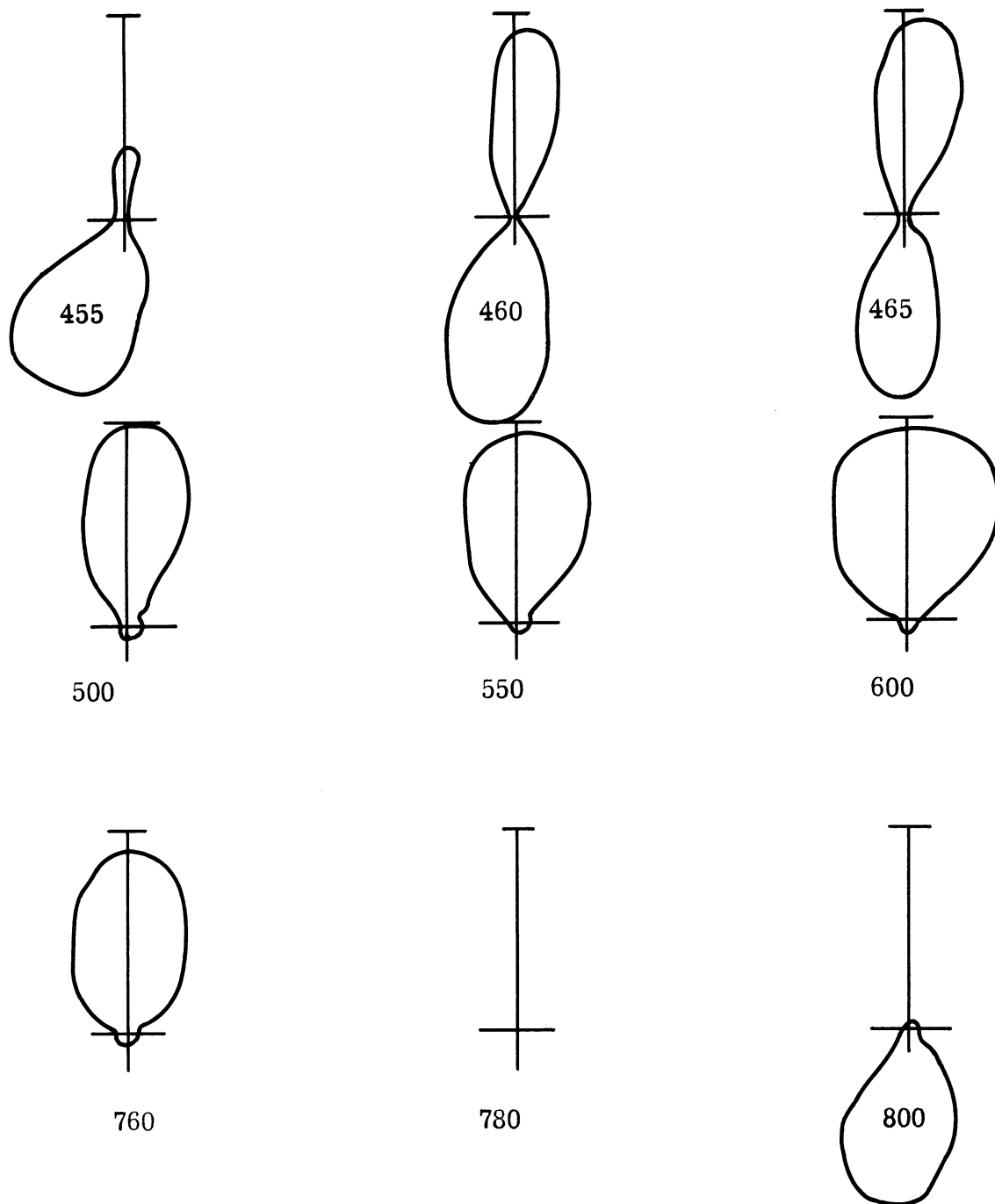


FIG. 2-4a: LINEAR POWER PATTERNS OF ANTENNA 238, AN INDUCTOR LOADED BIFILAR HELIX. ( $|E_{\theta}|^2$  Patterns in the  $\phi = 0$  plane.)

THE UNIVERSITY OF MICHIGAN

7848-7-Q

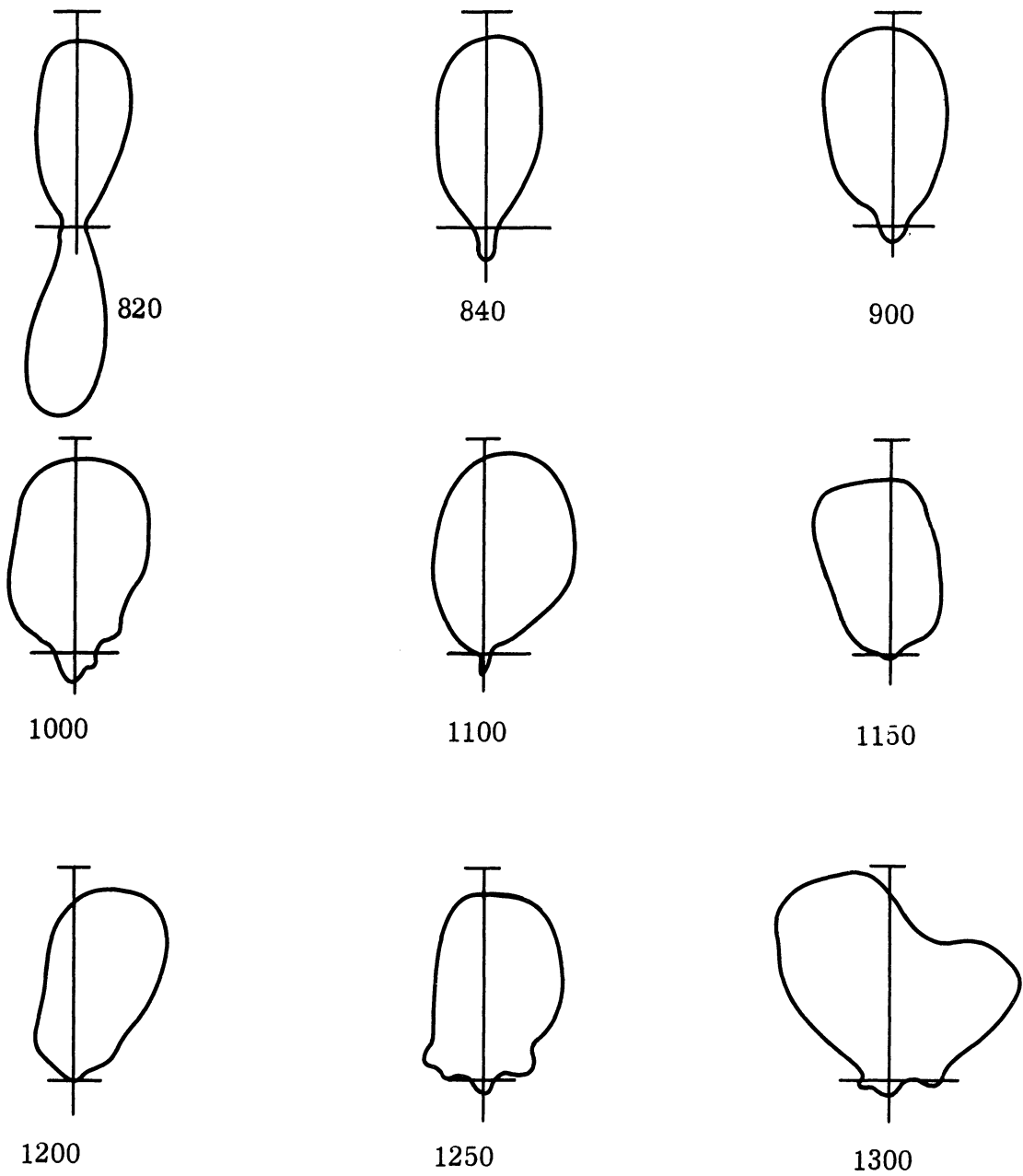


FIG. 2-4b: LINEAR POWER PATTERNS OF ANTENNA 238, AN INDUCTOR LOADED BIFILAR HELIX. ( $|E_{\theta}|^2$  Patterns in the  $\phi = 0$  Plane.)

THE UNIVERSITY OF MICHIGAN  
7848-7-Q

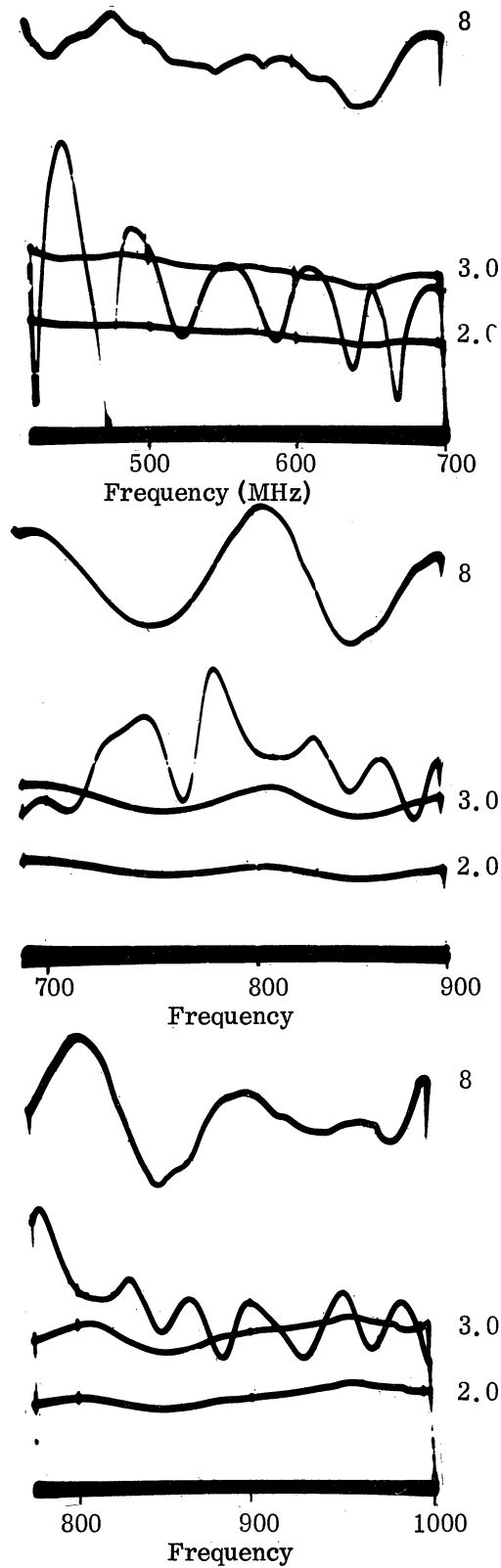


FIG. 2-5: VSWR OF ANTENNA 238, A BIFILAR HELIX WITH INDUCTANCE LOADING.

frequency range to find the characteristic impedance of the corresponding transmission line produced a characteristic impedance of 110 ohms. The input impedance of a helix antenna is usually in the range of 100 to 150 ohms. Thus, apparently using the input impedance of a helix antenna in the transmission line analogy correctly predicts the experimental results.

2) Even by itself, antenna 238 is a very interesting antenna. It covers almost the entire frequency range from 475 to 1250 MHz, except for a band of 80 MHz centered around 800 MHz.

3) Series inductance tends to reduce the size of a helix antenna but series capacitive loading will increase the size for a given frequency range of operation. (In the 840 to 1250 MHz range, the stubs were capacitive.)

4) However, the average impedance values measured tend not to support the transmission line analogy. The impedance was higher in the high band and lower in the low band, not the other way around as would be expected from the transmission line relation  $Z_0 = \sqrt{L/C}$ . (Note, that in the high band, the capacitance introduced would tend to reduce the inductance in the above formula.)

III

SLOT ARRAYS

Since the last Quarterly Report the effort on the fabrication of a ferrite loaded slot array has been completely reoriented. The work done under this task had previously been concentrated on using a waveguide section with slots cut in one of the broad faces. The material used had been type Q-3 solid ferrite. Unfortunately the electrical and magnetic characteristics of the ferrite were not satisfactory and not in accordance with the published data received by the manufacturer.

A new experimental arrangement has now been completed. This consists of three ferrite filled rectangular slots mounted in a metal ground plane. The ground plane is composed of copper screening 5' by 5' in overall size. In the center the metal screening has been replaced by a solid aluminum plate 27" by 20" in size. Three rectangular ferrite filled slots have been mounted on the center line parallel with the long direction of the rectangular plate. That is the H direction of the slots is parallel with the 27" direction of the aluminum plate. The slots are mounted 16 3/16" center-to-center. The central slot corresponds to the center of the ground plate. Each slot has dimensions 5" by 2" by 1 1/2" deep. The 5" dimension corresponds to the direction of the H field. The 2" direction corresponds to the direction of the E field in the aperture. Each slot is filled completely by solid type EAF-2 ferrite.

The array of slots just described has been made for operation about a central frequency of 350 MHz. The present status of the array utilizing physically small slot radiator elements is that it is now ready for preliminary experimental testing as an array.



IV

FERRITE ROD ANTENNAS

4.1 Theoretical Analysis

The field components of an isotropic infinite ferrite rod obtained by solving the homogeneous Helmholtz equation subject to the boundary conditions on the cylindrical surface of the rod for the  $HE_{11}$  mode are as follows where the time dependent factor  $e^{j\omega t}$  is understood. Field inside the rod ( $\rho < a$ ):

$$\begin{aligned}
 H_z &= A_i J_1(k_1 \rho) \cos \phi e^{-j\gamma z} \\
 H_\rho &= \left[ -A_i \frac{j\gamma}{k_1} J_1'(k_1 \rho) + B_i \frac{j\omega\epsilon_1}{k_1 \rho} J_1(k_1 \rho) \right] \cos \phi e^{-j\gamma z} \\
 H_\phi &= \left[ A_i \frac{j\gamma}{k_1 \rho} J_1(k_1 \rho) - B_i \frac{j\omega\epsilon_1}{k_1} J_1'(k_1 \rho) \right] \sin \phi e^{-j\gamma z} \\
 E_z &= B_i J_1(k_1 \rho) \sin \phi e^{-j\gamma z} \\
 E_\rho &= \left[ A_i \frac{j\omega\mu_1}{k_1 \rho} J_1(k_1 \rho) - B_i \frac{j\gamma}{k_1} J_1'(k_1 \rho) \right] \sin \phi e^{-j\gamma z} \\
 E_\phi &= \left[ A_i \frac{j\omega\mu_1}{k_1} J_1'(k_1 \rho) - B_i \frac{j\gamma}{k_1 \rho} J_1(k_1 \rho) \right] \cos \phi e^{-j\gamma z} \quad (4.1)
 \end{aligned}$$

Field surrounding the rod ( $\rho > a$ ):

$$H_z = A_o H_n^{(1)}(k_2 \rho) \cos \phi e^{-j\gamma z}$$

$$\begin{aligned}
 H_{\rho} &= \left[ -A_o \frac{j\gamma}{k_2} H_1^{(1)}(k_2\rho) + B_o \frac{j\omega\epsilon_o}{k_1\rho} H_1^{(1)}(k_2\rho) \right] \cos \phi e^{-j\gamma z} \\
 H_{\phi} &= \left[ A_o \frac{j\gamma}{k_2\rho} H_1^{(1)}(k_2\rho) - B_o \frac{j\omega\epsilon_o}{k_2} H_1^{(1)}(k_2\rho) \right] \sin \phi e^{-j\gamma z} \\
 E_z &= B_o H_1^{(1)}(k_2\rho) \sin \phi e^{-j\gamma z} \\
 E_{\rho} &= \left[ A_o \frac{j\omega\mu_o}{k_2\rho} H_1^{(1)}(k_2\rho) - B_o \frac{j\gamma}{k_2} H_1^{(1)}(k_2\rho) \right] \sin \phi e^{-j\gamma z} \\
 E_{\phi} &= \left[ A_o \frac{j\omega\mu_o}{k_2} H_1^{(1)}(k_2\rho) - B_o \frac{j\gamma}{k_2\rho} H_1^{(1)}(k_2\rho) \right] \cos \phi e^{-j\gamma z} \quad (4.2)
 \end{aligned}$$

where

$$\begin{cases}
 k_1^2 = \omega^2 \mu_1 \epsilon_1 - \gamma^2 & \text{inside the rod} \\
 k_2^2 = \omega^2 \mu_o \epsilon_o - \gamma^2 & \text{surrounding free space.}
 \end{cases} \quad (4.3)$$

Matching the tangential field components gives the proportion of field magnitudes inside and outside the rod as well as the magnitudes of the TM to TE waves

$$\frac{A_i}{A_o} = \frac{B_i}{B_o} = \frac{H_1^{(1)}(k_2 a)}{J_1(k_1 a)} \quad (4.4)$$

$$\frac{B_i}{A_i} = \frac{\frac{\gamma}{a} \left( \frac{1}{k_1^2} - \frac{1}{k_2^2} \right)}{\frac{\omega \epsilon_1}{k_1} \frac{J'_1(k_1 a)}{J_1(k_1 a)} - \frac{\omega \epsilon_0}{k_2} \frac{H'_1(1)(k_2 a)}{H_1(1)(k_2 a)}} = \frac{\frac{\omega \mu_1}{k_1} \frac{J'_1(k_1 a)}{J_1(k_1 a)} - \frac{\omega \mu_0}{k_2} \frac{H'_1(1)(k_2 a)}{H_1(1)(k_2 a)}}{\frac{\gamma}{a} \left( \frac{1}{k_1^2} - \frac{1}{k_2^2} \right)} \quad (4.5)$$

Equations (4.3) and (4.5) together give the characteristic equation:

$$\begin{aligned} & \left( \frac{\lambda_0}{2\pi a} \right)^2 \left[ \frac{(k_1 a)^2 - (k_2 a)^2 \mu_r \epsilon_r}{\mu_r \epsilon_r - 1} \right] \left[ \frac{1}{(k_1 a)^2} - \frac{1}{(k_2 a)^2} \right]^2 \\ & = \frac{\mu_r \epsilon_r}{(k_1 a)^2} \left[ \frac{J'_1(k_1 a)}{J_1(k_1 a)} \right]^2 + \frac{1}{(k_2 a)^2} \left[ \frac{H'_1(1)(k_2 a)}{H_1(1)(k_2 a)} \right]^2 \\ & - \left[ \frac{\mu_r + \epsilon_r}{(k_1 a)(k_2 a)} \right] \left[ \frac{J'_1(k_1 a) H'_1(1)(k_2 a)}{J_1(k_1 a) H_1(1)(k_2 a)} \right] \end{aligned} \quad (4.6)$$

where  $\lambda_0$  = wavelength in free space,  $\mu_1 = \mu_0 \mu_r$ ,  $\epsilon_1 = \epsilon_0 \epsilon_r$ . A graphical solution of Eq. (4.6) determine  $k_1$  and  $k_2$ , and together with Eq. (4.3) determines

the propagation constant  $\gamma$ . The phase velocity along the longitudinal axis is:

$$\frac{V_z}{c} = \left(\frac{2\pi}{\lambda_0}\right) \sqrt{\frac{\mu_r \epsilon_r - 1}{k_1^2 - k_2^2 \mu_r \epsilon_r}} \quad (4.7)$$

which corresponds to a slow wave for  $V_z < c$ .

The computed axial phase velocity for some selected ferrite materials with various diameters has been shown in the previous report, Lyon et al, 1967.

The electric and magnetic surface charge densities on the rod surface are:

$$\left\{ \begin{array}{l} \sigma_e = A_i J_1(k_1 a) \frac{1}{j\omega a} \left[ \frac{1}{k_2^2} - \frac{\mu_r \epsilon_r}{k_1^2} \right] \left[ \frac{k_1^2 - k_2^2}{\mu_r \epsilon_r - 1} - \left(\frac{2\pi}{\lambda_0}\right)^2 \right] \sin \phi e^{-j\gamma z} \\ \sigma_m = B_i J_1(k_1 a) \frac{1}{j\omega a} \left[ \frac{1}{k_1^2} - \frac{\mu_r \epsilon_r}{k_1^2} \right] \left[ \frac{k_1^2 - k_2^2}{\mu_r \epsilon_r - 1} - \left(\frac{2\pi}{\lambda_0}\right)^2 \right] \cos \phi e^{-j\gamma z} \end{array} \right. \quad (4.8)$$

$$\left\{ \begin{array}{l} \sigma_e = A_i J_1(k_1 a) \frac{1}{j\omega a} \left[ \frac{1}{k_2^2} - \frac{\mu_r \epsilon_r}{k_1^2} \right] \left[ \frac{k_1^2 - k_2^2}{\mu_r \epsilon_r - 1} - \left(\frac{2\pi}{\lambda_0}\right)^2 \right] \sin \phi e^{-j\gamma z} \\ \sigma_m = B_i J_1(k_1 a) \frac{1}{j\omega a} \left[ \frac{1}{k_1^2} - \frac{\mu_r \epsilon_r}{k_1^2} \right] \left[ \frac{k_1^2 - k_2^2}{\mu_r \epsilon_r - 1} - \left(\frac{2\pi}{\lambda_0}\right)^2 \right] \cos \phi e^{-j\gamma z} \end{array} \right. \quad (4.9)$$

These oscillating surface charges on the rod surface are equivalent to the volume electric polarization current and the magnetic polarization current in the rod due to the subatomic displacement of charge centers and charge of spin momenta. The magnitude ratio of  $\sigma_e$  to  $\sigma_m$  is the same as the ratio of TE to TM waves. In the limiting case with  $\mu_r = 1$ ,  $\epsilon_r = 1$  both electric and magnetic surface charges vanish.

The behavior of a finite ferrod antenna is more or less like a physically thick cylindrical antenna with the volume electric polarization current in ferrod equivalent to the conduction current in metal. A comparison of these two antenna types is given in the following table.

	Thick Metal Cylindrical Antenna	Ferrite Rod Antenna
1 Excitation	Voltage Source	Field Source
2 Material of Radiator	Metal Conductor	Ferrite Material
3 Source of Radiation	Surface Current	Polarization Volume Current
4 Dominant Wave Pattern	Standing Wave	Traveling Wave

At present there is still no exact solution for the field distribution at the junction of the waveguide to the rod and at the end of the rod. To simplify the problem it is assumed that  $HE_{\parallel}$  mode is traveling along the axis with an attenuation due to radiation and heat loss in the material. The reflection from the end is negligibly small.

Maxwell's equation in a homogeneous isotropic material media in the absence of conductance current can be written as:

$$\left\{ \begin{array}{l} \nabla \times \bar{E} = -\mu_0 \frac{\partial \bar{H}}{\partial t} - (\mu - \mu_0) \frac{\partial \bar{H}}{\partial t} \\ \nabla \times \bar{H} = \epsilon_0 \frac{\partial \bar{E}}{\partial t} + (\epsilon - \epsilon_0) \frac{\partial \bar{E}}{\partial t} \\ \nabla \cdot \bar{E} = \frac{\rho_e}{\epsilon} \\ \nabla \cdot \bar{H} = \frac{\rho_m}{\mu} \end{array} \right. \quad (4.10)$$

Let

$$\left\{ \begin{array}{l} \bar{J}_{eq} = (\epsilon - \epsilon_0) \frac{\partial \bar{E}}{\partial t} \\ \bar{M}_{eq} = (\mu - \mu_0) \frac{\partial \bar{H}}{\partial t} \end{array} \right. \quad (4.11)$$

The radiation field from the ferrod in unbounded free space arises from the magnetic and electric polarization currents in the rod or from the oscillating magnetic and electric surface charges on the rod. The field solution can be represented as the sum of a complementary and a particular solution. The particular solution due to the electric and magnetic polarization currents is

$$\begin{cases} \bar{\mathbf{E}} = -\nabla \times \bar{\mathbf{F}} - j\omega\mu_0 \bar{\mathbf{A}} + \frac{1}{j\omega\epsilon_0} \nabla(\nabla \cdot \bar{\mathbf{A}}) \\ \bar{\mathbf{H}} = \nabla \times \bar{\mathbf{A}} - j\omega\epsilon_0 \bar{\mathbf{F}} + \frac{1}{j\omega\mu_0} \nabla(\nabla \cdot \bar{\mathbf{F}}) \end{cases} \quad (4.12)$$

$$\begin{aligned} \bar{\mathbf{A}}(\mathbf{r}) &= \frac{1}{4\pi} \iiint \frac{\bar{\mathbf{J}}_{\text{eq}}(\mathbf{r}') e^{-jk|\mathbf{r}-\mathbf{r}'|}}{|\mathbf{r}-\mathbf{r}'|} d\mathbf{v}' \\ \bar{\mathbf{F}}(\mathbf{r}) &= \frac{1}{4\pi} \iiint \frac{\bar{\mathbf{M}}_{\text{eq}}(\mathbf{r}') e^{-jk|\mathbf{r}-\mathbf{r}'|}}{|\mathbf{r}-\mathbf{r}'|} d\mathbf{v}' \end{aligned} \quad (4.13)$$

If only the far field is considered for  $r \gg r'_{\text{max}}$ :

$$\begin{aligned} |\mathbf{r}-\mathbf{r}'| &= r - r' \cos \xi \\ r' \cos \xi &= \rho' \sin \theta \cos(\phi - \phi') + z' \cos \theta \end{aligned} \quad (4.14)$$

In the radiation zone, the components of the field are therefore given by:

$$\begin{cases} E_\theta = -j\omega\mu_0 A_\theta - jkF_\phi \\ E_\phi = -j\omega\mu_0 A_\phi + jkF_\theta \end{cases} \quad (4.15)$$

$$\frac{E_{\theta}}{H_{\phi}} = -\frac{E_{\phi}}{H_{\theta}} = \eta \quad . \quad (4.16)$$

The spherical components of any vector can be obtained from the rectangular components using the relationships:

$$\begin{cases} V_{\theta} = (V_x \cos \phi + V_y \sin \phi) \cos \theta - V_z \sin \theta \\ V_{\phi} = -V_x \sin \phi + V_y \cos \phi \end{cases} \quad . \quad (4.17)$$

The rectangular components of the electric field can be obtained by the transformation of coordinates and the relationships of the Bessel functions:

$$\begin{cases} E_x = E_{\rho} \cos \phi - E_{\phi} \sin \phi \\ E_y = E_{\rho} \sin \phi + E_{\phi} \cos \phi \end{cases} \quad (4.18)$$

$$\begin{cases} J_0(k_1 \rho) = \frac{J_1(k_1 \rho)}{k_1 \rho} + J_1'(k_1 \rho) \\ J_2(k_1 \rho) = \frac{J_1(k_1 \rho)}{k_1 \rho} - J_1'(k_1 \rho) \end{cases} \quad . \quad (4.19)$$

Thus the field components in rectangular coordinates are:

$$E_x = \frac{j [A_i \omega \mu_1 + B_i \gamma]}{2 k_1} J_2(k_1 \rho) \sin 2 \phi e^{-j \gamma z}$$

$$E_y = \left\{ \frac{j [A_i \omega \mu_1 - B_i \gamma]}{2 k_1} J_0(k_1 \rho) - \frac{j [A_i \omega \mu_1 + B_i \gamma]}{2 k_1} J_2(k_1 \rho) \cos 2 \phi \right\} e^{-j \gamma z}$$

$$\begin{aligned}
 H_x &= \left\{ \frac{-j \left[ A_i \gamma - B_i \omega \epsilon_1 \right]}{2k_1} J_0(k_1 \rho) + \frac{j \left[ A_i \gamma + B_i \omega \epsilon_1 \right]}{2k_1} J_2(k_1 \rho) \cos 2\phi \right\} e^{-j\gamma z} \\
 H_y &= \frac{j \left[ A_i \gamma + B_i \omega \epsilon_1 \right]}{2k_1} J_2(k_1 \rho) \sin 2\phi e^{-j\gamma z} \quad . \quad (4.20)
 \end{aligned}$$

Substitute Eq. (4.20) into Eqs. (4.11) and (4.13) and perform the integration by using Eq. (4.14) and Bessel-Fourier series

$$\begin{aligned}
 e^{jk\rho' \sin \theta \cos(\phi - \phi')} &= J_0(k\rho' \sin \theta) \\
 &+ \sum_{n=1}^{\infty} J_n(k\rho' \sin \theta) \cos n(\phi - \phi') \quad (4.21)
 \end{aligned}$$

and the Lommel integral formula

$$\begin{aligned}
 I_n &= \int_0^x x J_n(\alpha x) J_n(\beta x) dx = \frac{x}{\alpha^2 + \beta^2} \left[ J_n(\alpha x) \frac{\partial}{\partial x} J_n(\beta x) \right. \\
 &\quad \left. - J_n(\beta x) \frac{\partial}{\partial x} J_n(\alpha x) \right] \quad . \quad (4.22)
 \end{aligned}$$

Thus the vector potential components in rectangular coordinate are:

$$\begin{aligned}
 A_x &= \frac{j\omega(\epsilon_1 - \epsilon_0)}{8k_1} \left[ A_i \omega \mu_1 + B_i \gamma \right] I_2(k_1) \sin 2\phi f(r) f(\theta) \\
 A_y &= \frac{j\omega(\epsilon_1 - \epsilon_0)}{8k_1} \left\{ 2 \left[ A_i \omega \mu_1 - B_i \gamma \right] I_0(k_1) \right. \\
 &\quad \left. - \left[ A_i \omega \mu_1 + B_i \gamma \right] I_2(k_1) \cos 2\phi \right\} f(r) f(\theta)
 \end{aligned}$$



$$\begin{aligned}
 A_z &= \frac{\omega(\epsilon_1 - \epsilon_0)}{4} B_i I_1(k_1) \sin \phi f(r) f(\theta) \\
 F_x &= \frac{j\omega(\mu_1 - \mu_0)}{8k_1} \left\{ -2 \left[ A_i \gamma - B_i \omega \epsilon_1 \right] I_0(k_1) \right. \\
 &\quad \left. + \left[ A_i \gamma + B_i \omega \epsilon_1 \right] I_2(k_1) \cos 2\phi \right\} f(r) f(\theta) \\
 F_y &= \frac{j\omega(\mu_1 - \mu_0)}{8k_1} \left[ A_i \gamma + B_i \omega \epsilon_1 \right] I_2(k_1) \sin 2\phi f(r) f(\theta) \\
 F_z &= \frac{\omega(\mu_1 - \mu_0)}{4} A_i I_1(k_1) \cos \phi f(r) f(\theta) \tag{4.23}
 \end{aligned}$$

where

$$\begin{aligned}
 f(r) &= \frac{e^{-jkr}}{r} \\
 f(\theta) &= \frac{\left[ e^{j(k \cos \theta - \gamma)\ell} - 1 \right]}{k \cos \theta - \gamma}
 \end{aligned}$$

$$I_0(k_1) = \int_0^a \rho J_0(k_1 \rho) J_0(k \rho \sin \theta) d\rho$$

$$I_1(k_1) = \int_0^a \rho J_1(k_1 \rho) J_1(k \rho \sin \theta) d\rho$$

$$I_2(k_1) = \int_0^a \rho J_2(k_1 \rho) J_2(k \rho \sin \theta) d\rho .$$

Substituting Eq. (4.23) into Eq. (4.17) gives the spherical components of the vector potential A and F.

$$\begin{aligned}
 A_{\theta} &= \frac{j\omega(\epsilon_1 - \epsilon_0)}{8k_1} f(r)f(\theta) \sin \phi \left\{ 2 \left[ A_i \omega \mu_1 - B_i \gamma \right] I_0(k_1) \cos \theta \right. \\
 &\quad \left. + j 2k_1 B_i I_1(k_1) \sin \theta + \left[ A_i \omega \mu_1 + B_i \gamma \right] I_2(k_1) \cos \theta \right\} \\
 A_{\phi} &= \frac{j\omega(\epsilon_1 - \epsilon_0)}{8k_1} f(r)f(\theta) \cos \phi \left\{ 2 \left[ A_i \omega \mu_1 - B_i \gamma \right] I_0(k_1) \right. \\
 &\quad \left. - \left[ A_i \omega \mu_1 + B_i \gamma \right] I_2(k_1) \right\} \\
 F_{\theta} &= \frac{j\omega(\mu_1 - \mu_0)}{8k_1} f(r)f(\theta) \cos \phi \left\{ - 2 \left[ A_i \gamma - B_i \omega \epsilon_1 \right] I_0(k_1) \cos \theta \right. \\
 &\quad \left. + j 2k_1 A_i I_1(k_1) \sin \theta + \left[ A_i \gamma + B_i \omega \epsilon_1 \right] I_2(k_1) \cos \theta \right\} \\
 F_{\phi} &= \frac{j\omega(\mu_1 - \mu_0)}{8k_1} f(r)f(\theta) \sin \phi \left\{ 2 \left[ A_i \gamma - B_i \omega \epsilon_1 \right] I_0(k_1) \right. \\
 &\quad \left. + \left[ A_i \gamma + B_i \omega \epsilon_1 \right] I_2(k_1) \right\} . \tag{4.24}
 \end{aligned}$$

Thus the radiated field is obtained by substituting Eq. (4.24) in (4.15)

$$\begin{aligned}
 E_{\theta} &= f(r)f(\theta) \sin \phi \left\{ C_A \left[ 2(A_i \omega \mu_1 - B_i \gamma) I_0(k_1) \cos \theta \right. \right. \\
 &\quad \left. \left. + j 2k_1 B_i I_1(k_1) \sin \theta + (A_i \omega \mu_1 + B_i \gamma) I_2(k_1) \cos \theta \right] \right. \\
 &\quad \left. + C_F \left[ 2(A_i \gamma - B_i \omega \epsilon_1) I_0(k_1) + (A_i \gamma + B_i \omega \epsilon_1) I_2(k_1) \right] \right\} \tag{4.25}
 \end{aligned}$$

$$\begin{aligned}
 E_{\phi} = f(r)f(\theta) \cos \phi \left\{ C_A \left[ 2(A_i \omega \mu_1 - B_i \gamma) I_0(k_1) - (A_i \omega \mu_1 \right. \right. \\
 \left. \left. + B_i \gamma) I_2(k_1) \right] + C_F \left[ 2(A_i \gamma - B_i \omega \epsilon_1) I_0(k_1) \cos \theta \right. \right. \\
 \left. \left. - j 2 k_1 A_i I_1(k_1) \sin \theta - (A_i \gamma + B_i \omega \epsilon_1) I_2(k_1) \cos \theta \right] \right\} \quad (4.26)
 \end{aligned}$$

where

$$C_A = \frac{k^2 (\epsilon_r - 1)}{8 k_1} \quad C_F = \frac{\eta k^2 (\mu_r - 1)}{8 k_1} \quad \eta = \sqrt{\frac{\mu_0}{\epsilon_0}}$$

In case when  $\mu_1 = \mu_0$  then  $C_F = 0$  and the radiated field reduces to the pattern of a dielectric rod antenna. It is observed that the magnitude ( $B_i$ ) of the TM component of the hybrid mode should be as small as possible in order to lower sidelobe level and increase the directivity in the endfire direction.

#### 4.2 Experimentation

In the analysis of the ferrite rod wave guide it is seen that an increase in the permeability  $\mu$  or the permittivity  $\epsilon$  of the ferrite rod has the effect of increasing the propagation constant along the axis. This may be the cause of increasing the numbers of side lobes and its levels. In order to obtain end-fire narrow beam patterns it is preferable to have an axial propagation constant nearly equal to the free space propagation constant. Experimentally it appears that a cylindrical shell of ferrite will serve as well for a surface waveguide as the solid rod. As shown in Fig. 4-1 a cylindrical ferrite shell was used instead of a solid ferrite rod since there was insufficient ferrite material. EAF-2 ferrite powder with  $\mu_r = 2.2$ ,  $\epsilon_r = 3.8$  was inserted between two fiber glass tubes with a 6 inch and a 5 inch diameter respectively.

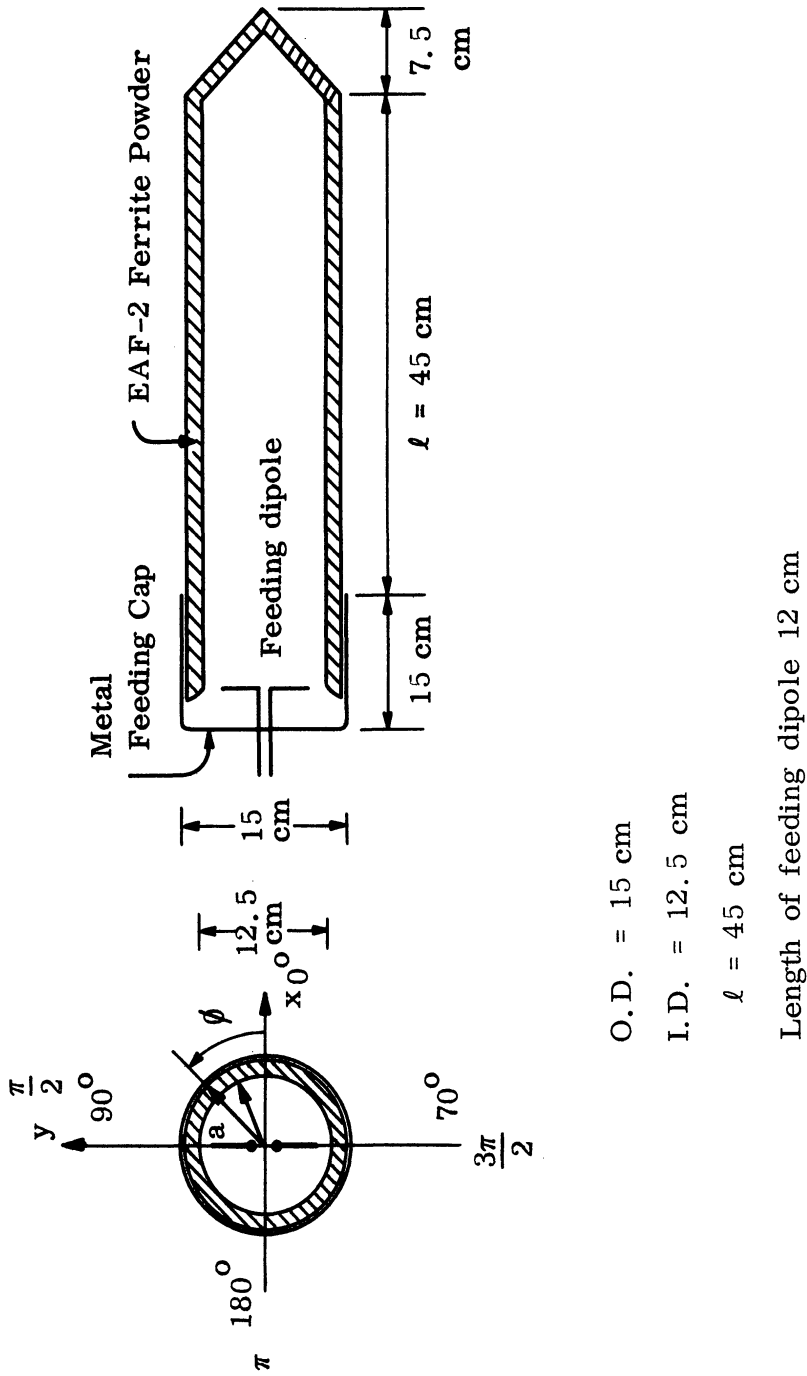


FIG. 4-1: GEOMETRY OF THE FERRITE TUBE ANTENNA.

One end of the tube was fitted tightly into a metal circular cylindrical cavity having 6 inches in depth. Excitation was by a symmetrical dipole inserted from the base of the cavity and mounted diametrically. In this way the ferrite radiator has a 1/2 inch shell layer, 6 inches of outer diameter, 18 inches of length and has a 45 degree conical shape with a tapered free end. The radiation patterns in the E-plane and in the H-plane are presented in Figs. 4-2 and 4-3 from 400 MHz to 1150 MHz. It should be pointed out that the  $TE_{11}$  mode cutoff frequency of the cylindrical guide without the loading of the ferrite tube is 1170 MHz. Below this cutoff frequency the radiated field is weak; it is difficult to detect it accurately at the far field zone. The patterns shown in the Figs. 4-2 and 4-3 show the effects of adding the ferrite tube. In the normal operation region above cutoff the directivity is more than 15 db above an isotropic source. The measured half power beamwidth and the side lobe level are plotted against frequency in Figs. 4-4 and 4-5. It is seen from the graph that the side lobes are more prominent in the H-plane than in the E-plane which is expected due to the asymmetric field distribution of the HE mode in the ferrite tube. Also it can be observed that the side lobe level is more than 4 db down from the main lobe.

The near field distribution along the outer surface of the ferrite tube has been measured by using a probe moving axially and along the circumference. Figures 4-6 and 4-7 show the  $E_{\rho}$  - distribution against the coordinate  $\phi$  taken at 2 inches from the feed end and 2 inches from the free end respectively. The  $E_{\rho}$  field is observed to be sinusoidal around the circumference and the sudden change of phase at  $\phi = \pi/2$  and  $\phi = 3\pi/2$  is to be expected. Figures 4-8 and 4-9 show the  $E_{\rho}$  - distribution along the tube axis at 600 MHz and 900 MHz. The observed pattern using a voltage probe appears to be standing

THE UNIVERSITY OF MICHIGAN

7848-7-Q

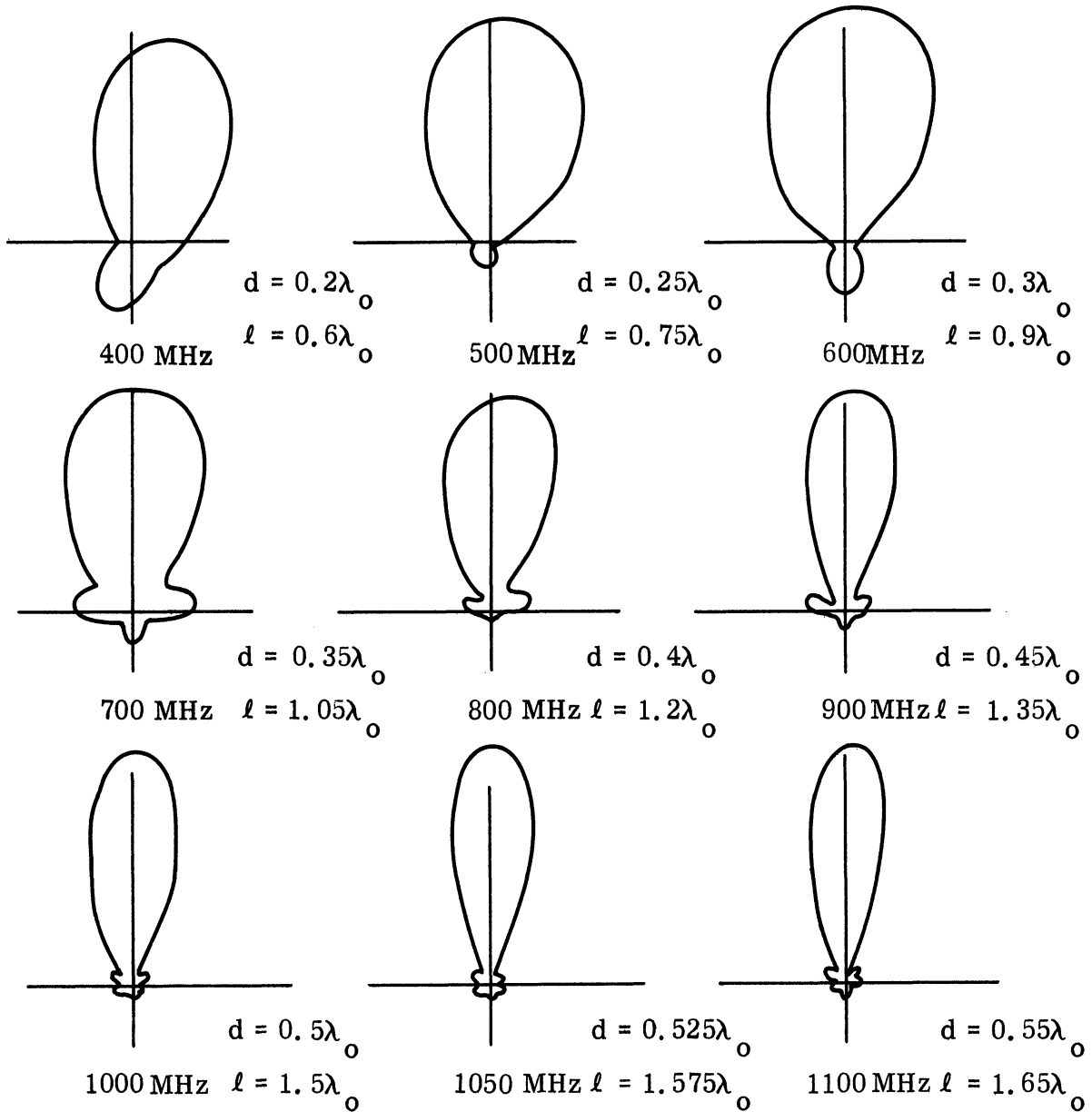


FIG. 4-2: LINEAR POWER PATTERNS OF THE FERRITE TUBE ANTENNA ( $|E_\theta|^2$  Patterns in the  $\phi = 0$  Plane).

THE UNIVERSITY OF MICHIGAN

7848-7-Q

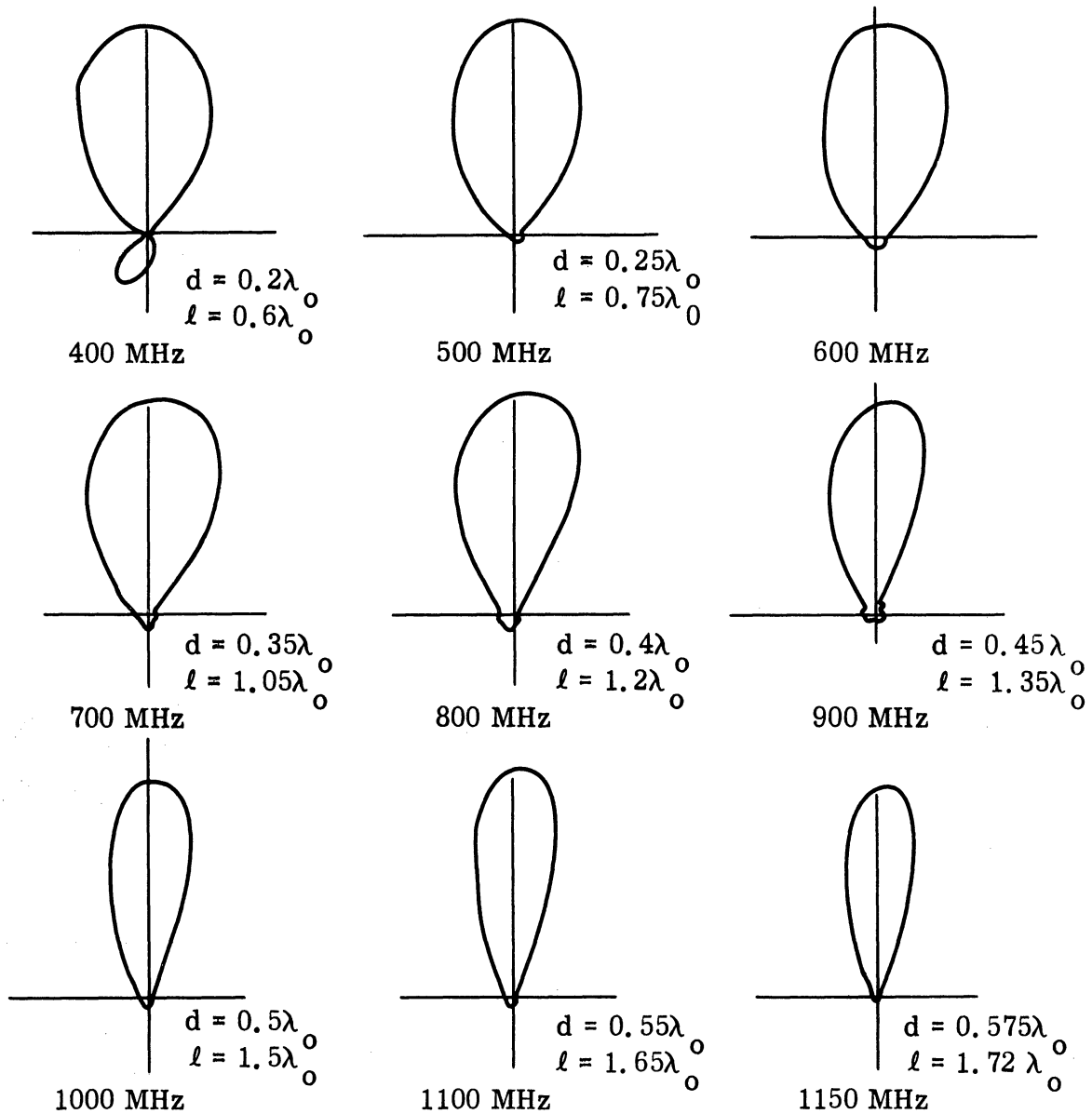


FIG. 4-3: LINEAR POWER PATTERNS OF THE FERRITE TUBE ANTENNA ( $|E_\theta|^2$  Patterns in the  $\phi = 90^\circ$  Plane).

THE UNIVERSITY OF MICHIGAN

7848-7-Q

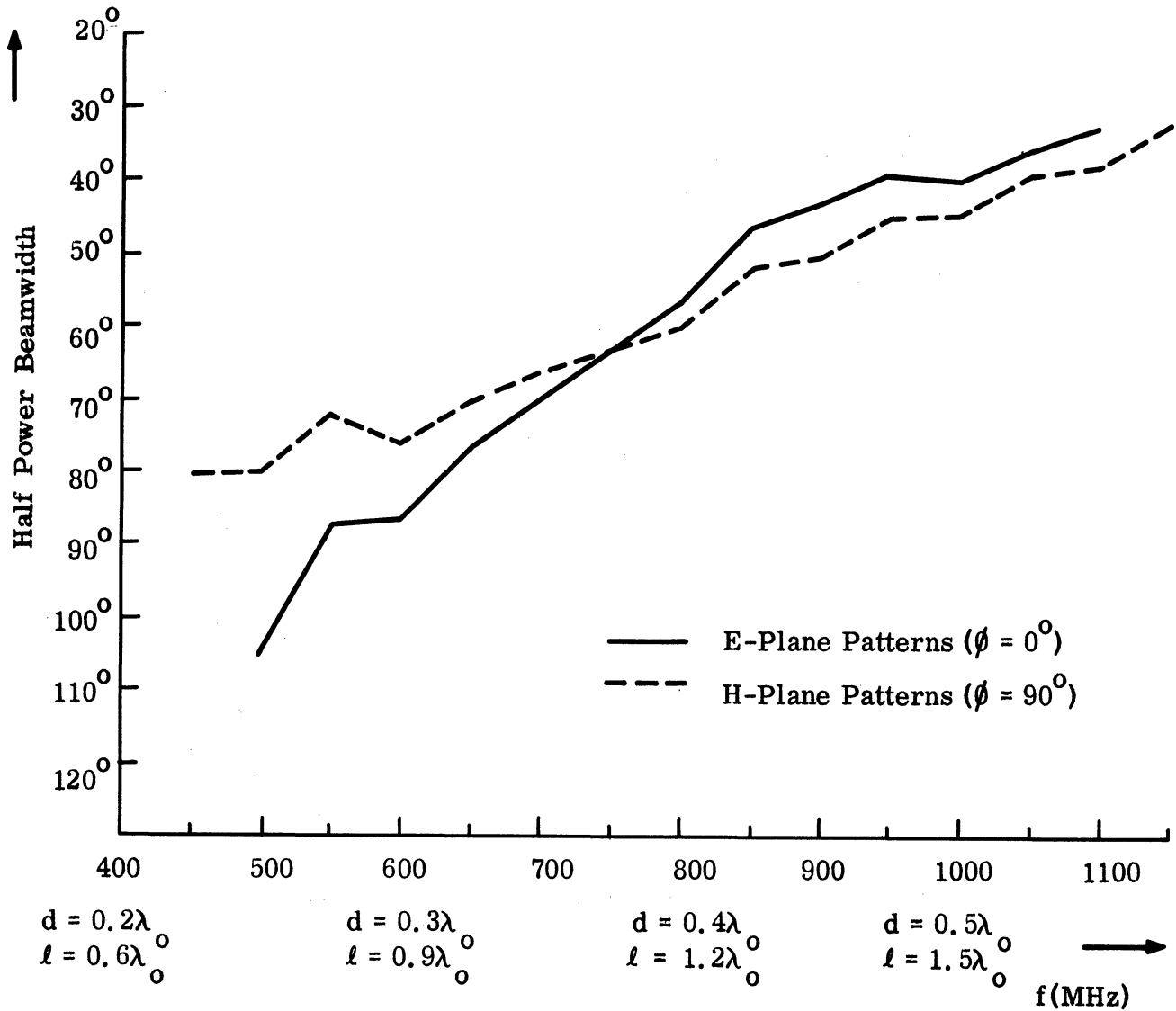


FIG. 4-4: HALF-POWER BEAMWIDTH AGAINST FREQUENCY OF THE FERRITE TUBE ANTENNA.



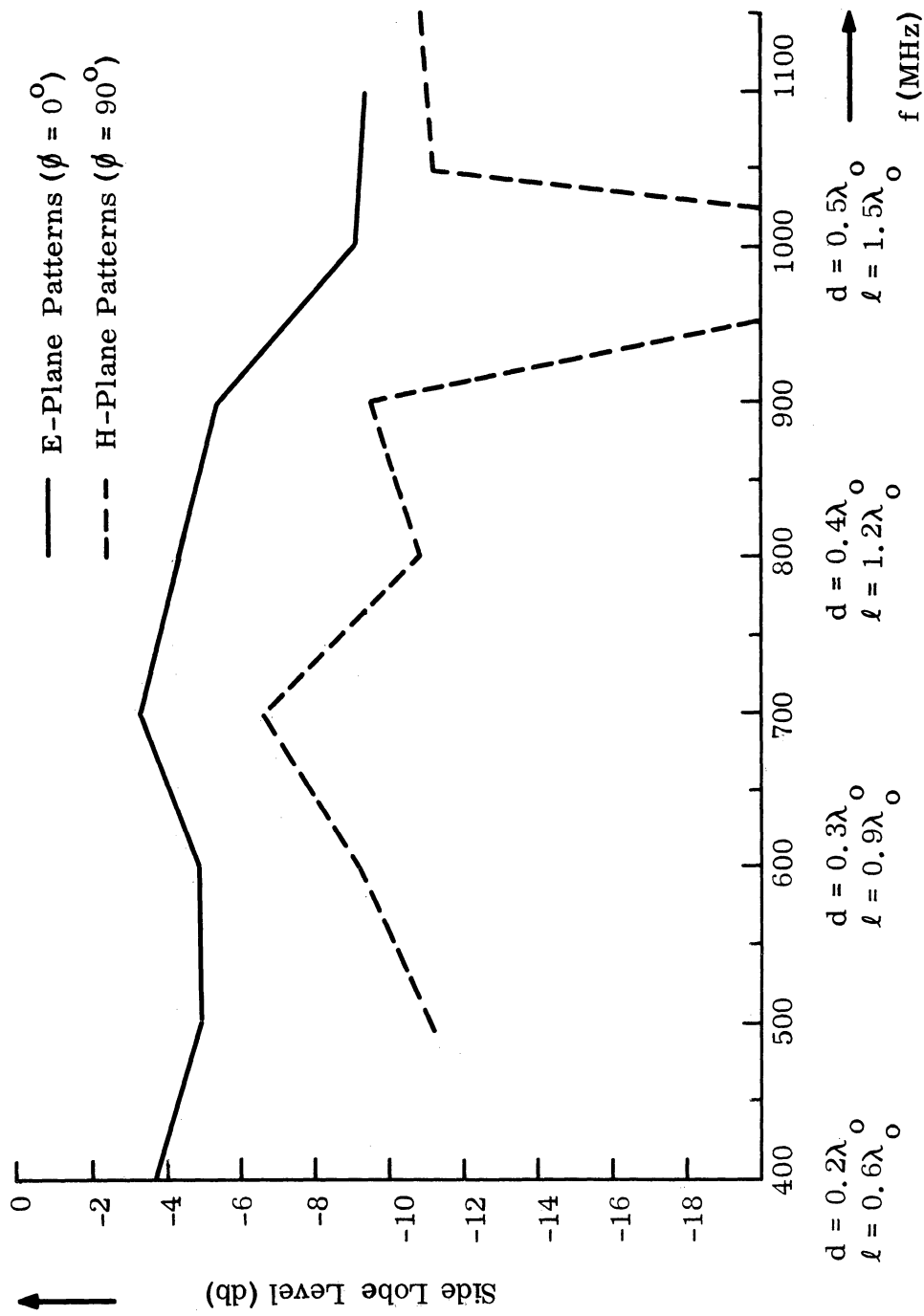


FIG. 4-5: SIDE-LOBE LEVEL AGAINST FREQUENCY OF THE FERRITE TUBE ANTENNA.

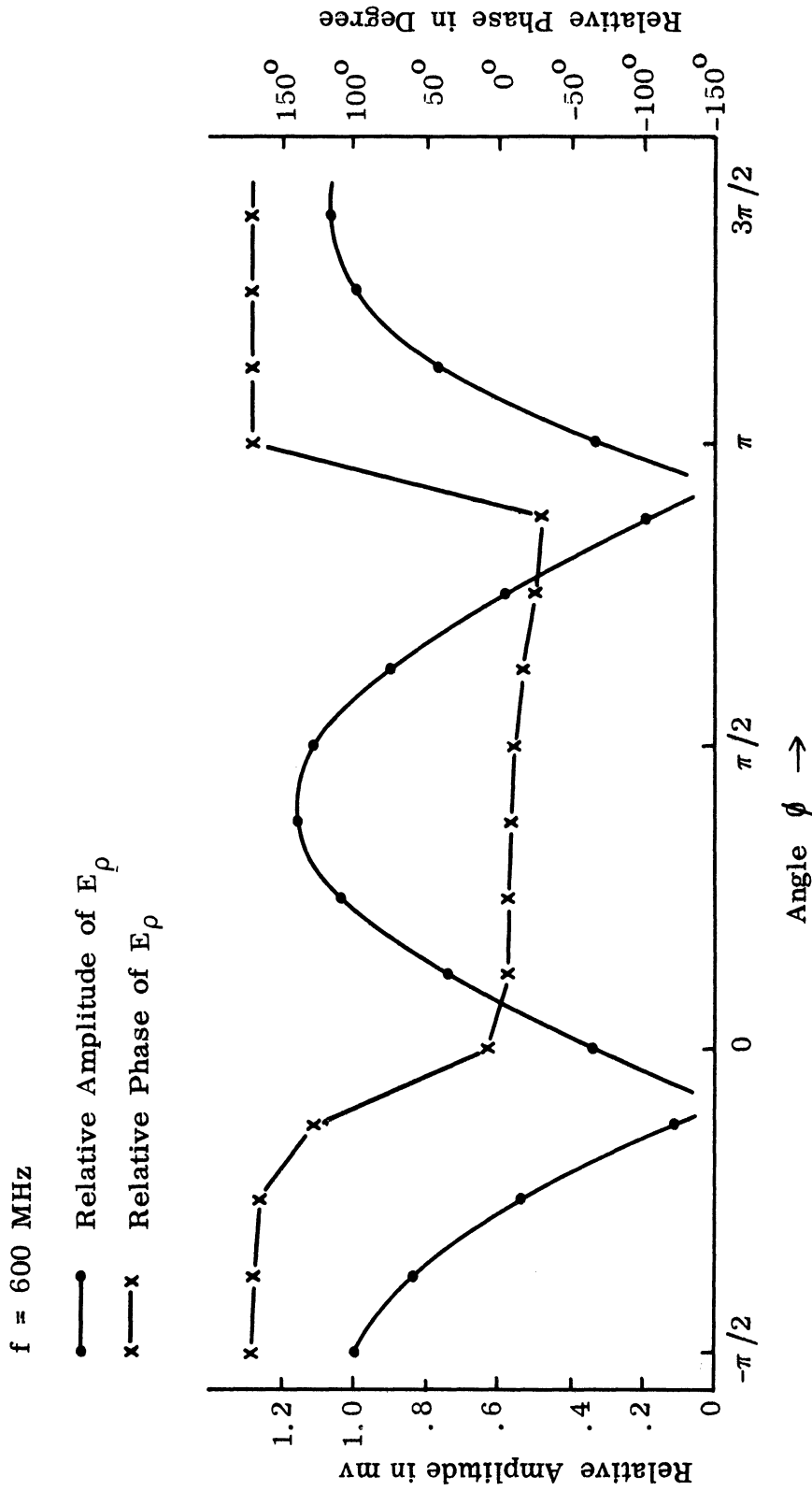


FIG. 4-6: NEAR FIELD MEASUREMENT, THE RELATIVE AMPLITUDE AND THE PHASE OF  $E_\rho$  AGAINST THE COORDINATE ANGLE  $\phi$ , TAKEN AT 5cm FROM THE FEED END OF THE FERRITE TUBE ANTENNA.

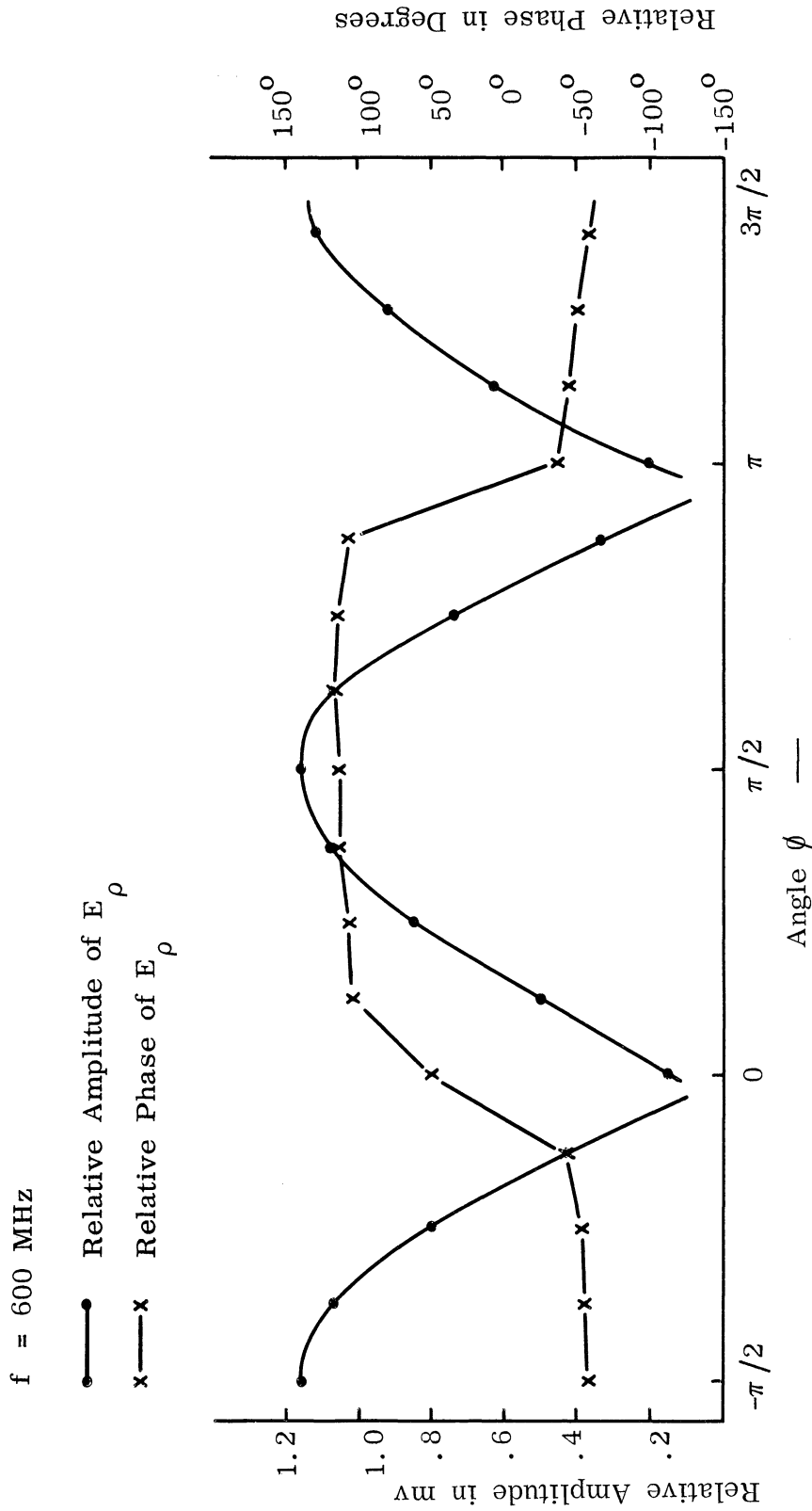


FIG. 4-7: NEAR FIELD MEASUREMENT, THE RELATIVE AMPLITUDE AND THE PHASE OF  $E_\rho$  AGAINST THE COORDINATE ANGLE  $\phi$ , TAKEN AT 5 cm THE FEED IN OF THE FERRITE TUBE ANTENNA.

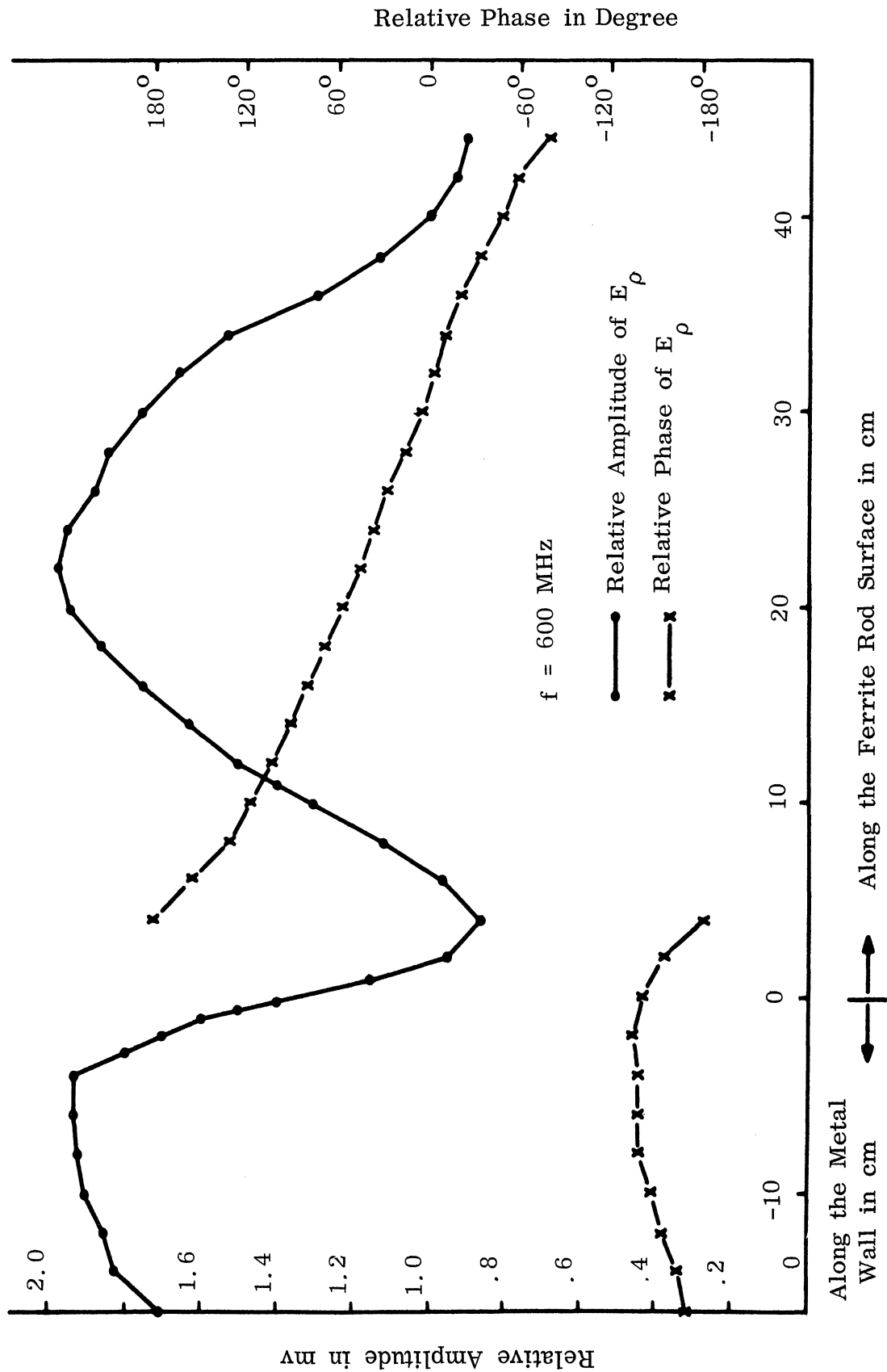


FIG. 4-8: NEAR FIELD MEASUREMENT, THE RELATIVE AMPLITUDE AND THE PHASE OF THE  $E_\rho$  AGAINST THE FERRITE TUBE AXIS AT 600 MHz IN  $\phi = \pi/2$  PLANE.

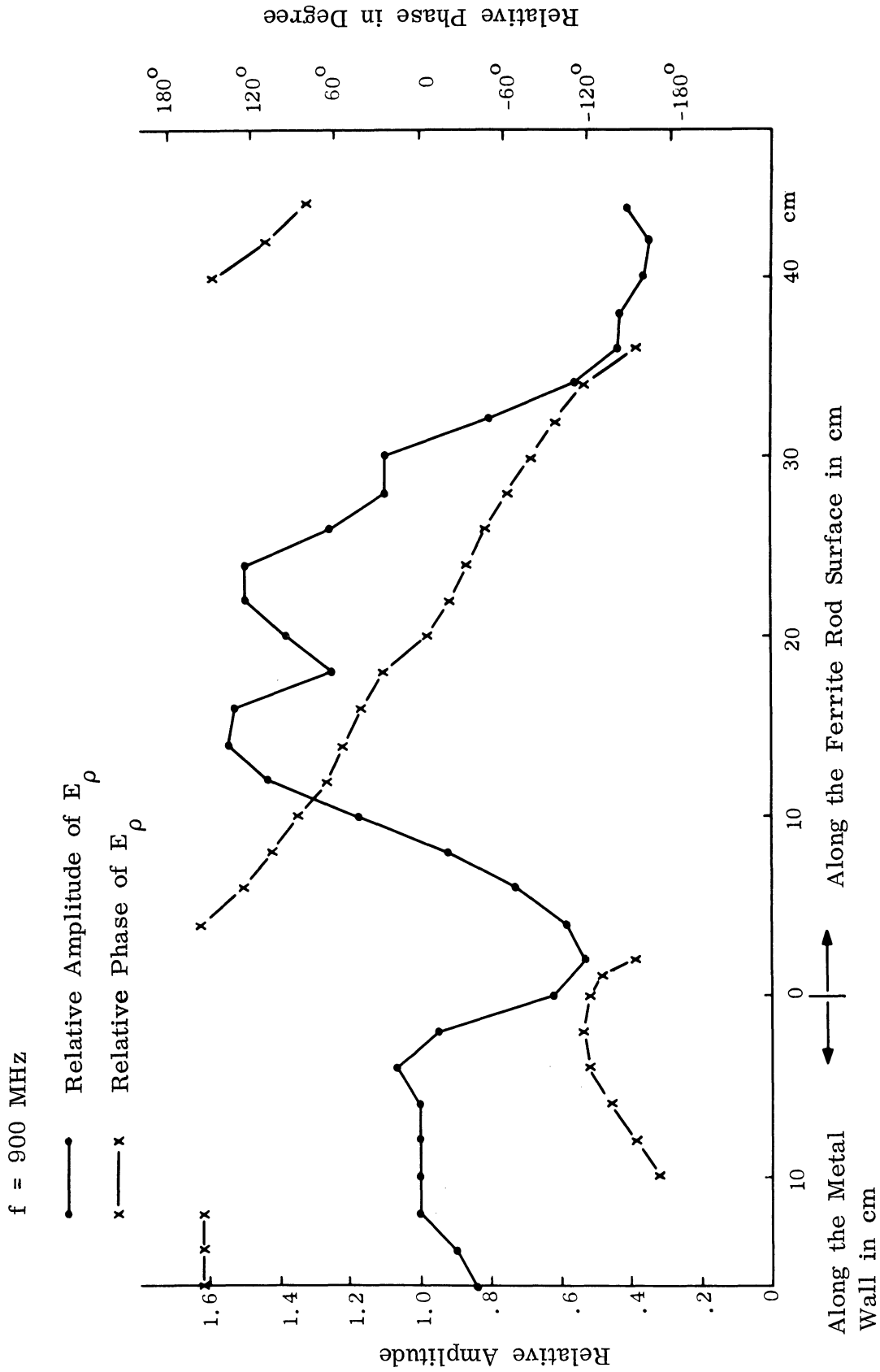


FIG. 4-9: NEAR FIELD MEASUREMENT, THE RELATIVE AMPLITUDE AND THE PHASE OF  $E_\rho$  AGAINST THE FERRITE TUBE AXIS AT 900 MHz IN  $\phi = \pi/2$  PLANE.

waves rather than traveling waves, probably because the conical cap free end and the short length ferrite tube form a resonance cavity. The continued investigation using experimental effort will be described in the next report. The exact mechanism governing the radiation properties of the tube antenna is not yet fully understood. It is hoped that the near field measurements will help to clarify the arguments among the existing theories. However, experimentally it has been found that the ferrite material used offered better guiding properties than the dielectric material.

## LOW FREQUENCY FERRITE ANTENNAS

The objective of this task is to investigate the design feasibility of new types of ferrite antennas that are usable at frequencies as low as 30 MHz. An effort has been made to identify realistic applications of ferrite loading to linear radiating elements. Accordingly, the investigation has focused upon applications which improve the performance of antennas that are relatively small. The range of sizes considered is  $0.1\lambda < 2h < 0.5\lambda$ , where  $\lambda$  = free space wavelength, and  $h$  = element half-length. The low end was chosen so as to avoid severe supergain limitations in element performance, while the high end was considered to be a practical size limit for a loaded 30 MHz element. Moreover, the detailed discussion is limited to center fed (or ground plane imaged) elements which support standing wave current distributions.

### 5.1 Tuning of Linear Elements Via Magnetic Biasing

Some inherent advantages of applying static biasing fields to material loaded multiple linear elements were discussed in Section 5.1 of the Sixth Quarterly Report, (Lyon et al, 1967). Section 5.2 of the same report described some magnetic biasing experiments which used small diameter material loaded helices as the linear slow wave structure. The interesting results of these experiments, combined with promising theoretical implications, has motivated a more thorough study of this particular slow wave structure. To this end, rather extensive design curves for small diameter core loaded helices have been prepared, and appear in Appendix A along with the details of the mathematical origin. An underlying assumption of isotropic core material is implied by the mathematics, so that strictly speaking the results are rigorous only for the unbiased structure. However, since saturation of the ferrite core

material represents a limit on the tuning range of magnetic biasing, the theory discussed in Section II was applied to obtain approximate results for this limit.

As an approximation, a helix filled with a ferrite material biased into saturation by a DC magnetic field can be assumed equivalent to one filled with only a dielectric material of the same dielectric constant as the ferrite. This approximation is deduced by noting that the magnetic properties of a ferrite biased into saturation do not effect the wave number of the wave equation for electromagnetic waves inside such a material. By assuming that there is no variation of the field in the  $\phi$  direction for the helix (which is not the case for anisotropic loading), the characteristic equation becomes identical to the isotropic loaded case with the relative permeability of the material identically unity. This approach yields a rough idea of the phase velocity reduction for a biased loading.

To establish the reduction in phase velocity, obtainable with ferrites that are available in our laboratory, the computer program described in Appendix A was used to obtain graphical solutions of the characteristic equation. Plots were made for the following core loadings: 1) Air, 2) EAF-2 ferrite powder, 3) Indiana General Q-3 ferrite at 100 MHz, 150 MHz, and 200 MHz, and 4) Eccorsorb CR at 300 MHz. Eccorsorb CR is an Emerson and Cuming Microwave absorber having fairly low electric and magnetic loss properties at the frequency of interest. In certain instances two plots were made for each loading so that the results could be read with greater resolution. The solution of the characteristic equation for an air core is given in Fig. A-1 for purposes of comparison with the loaded results. Figures A-2 through A-4 depict the approximate results when the indicated ferrite loadings are biased into saturation.



The results for a saturated core and an air core are seen to be nearly identical. Figures A-5a,b through A-9a,b depict rigorous results for the same ferrite loadings without magnetic bias. A substantial reduction in phase velocity is seen to occur for a given helix pitch angle. Intermediate values of bias field should produce phase velocity reductions between the no bias and saturation bias cases. For small helix pitch angles, the sheath helix is an excellent approximation to the physical problem, and close agreement between theoretical and experimental phase velocity reduction factors can be expected. At the larger helix pitch angles, the theoretical model would be more closely approximated by using multifilar windings connected in parallel at the feed. To date, good agreement between theoretical and experimental results has been obtained for the unbiased loadings. Since fields of sufficient intensity to saturate the ferrite have not yet been generated in the project laboratory, the accuracy of the graphs for the saturated core awaits experimental verification.

## 5.2 Computer Analysis of Multiple Linear Elements

A generalized analysis of two parallel linear elements was presented in Appendix A of the Fourth Quarterly Report, (Lyon et al, 1967). That analysis is the foundation from which ideas for several interesting design concepts are being exploited. Although the formulation was complete, rather limited numerical information was presented for the impedance associated with the symmetric excitation mode. This limitation was eliminated by the addendum which appeared in Appendix B of the Sixth Quarterly Report, (Lyon et al, 1967). This appendix developed the symmetric mode impedance of a small diameter helical slow wave structure. The formulas are also valid for describing the effects of material loading inside the helix, and are representative of the effects ob-

tainable from other slow wave structures. Due to the general utility of these results, they were put into a convenient graphical presentation to facilitate usage.

The addendum material in Appendix B of the Sixth Quarterly Report, along with the previously developed formulation in Appendix A of the Fourth Quarterly Report, has been incorporated into a general computer program. The computer program is useful as a diagnostic tool in designing meaningful experiments. In addition results from existing experiments can readily be compared to theory by inserting into the program the appropriate parameters of the experiment. At present the program calculates the input impedance  $Z_{in} = R + jX$  to a structure composed of two parallel linear slow wave structures with various lumped impedance terminations. The structure and associated nomenclature were specified in Appendix A of the Fourth Quarterly Report.

Computer results for the particular case corresponding to a folded dipole formed of two similar slow wave elements are presented in Figs. 4-1 through 4-6. The slow wave elements characterized were small diameter helices having symmetric and asymmetric mode phase velocity reduction factors of  $p_s$  and  $p_a$ , respectively, a length to thickness ratio of 55, and an asymmetric mode characteristic impedance of 250 ohms. As the figures clearly show, some interesting variations in impedance behavior result from different combinations of  $p_s$  and  $p_a$ . Figure 4-1 illustrates the input impedance for an ordinary open wire folded dipole since  $p_s = p_a = 1.0$ . Figure 4-3 illustrates an interesting negative reactance slope behavior near  $kh = \pi/2$  when  $p_s = 1.0$ ,  $p_a = 0.6$ . This structure may be realized by placing dielectric material between two linear conducting elements, thereby affecting only the asymmetric phase velocity reduction factor as is the case for TV "twin-lead" cable.

THE UNIVERSITY OF MICHIGAN

7848-7-Q

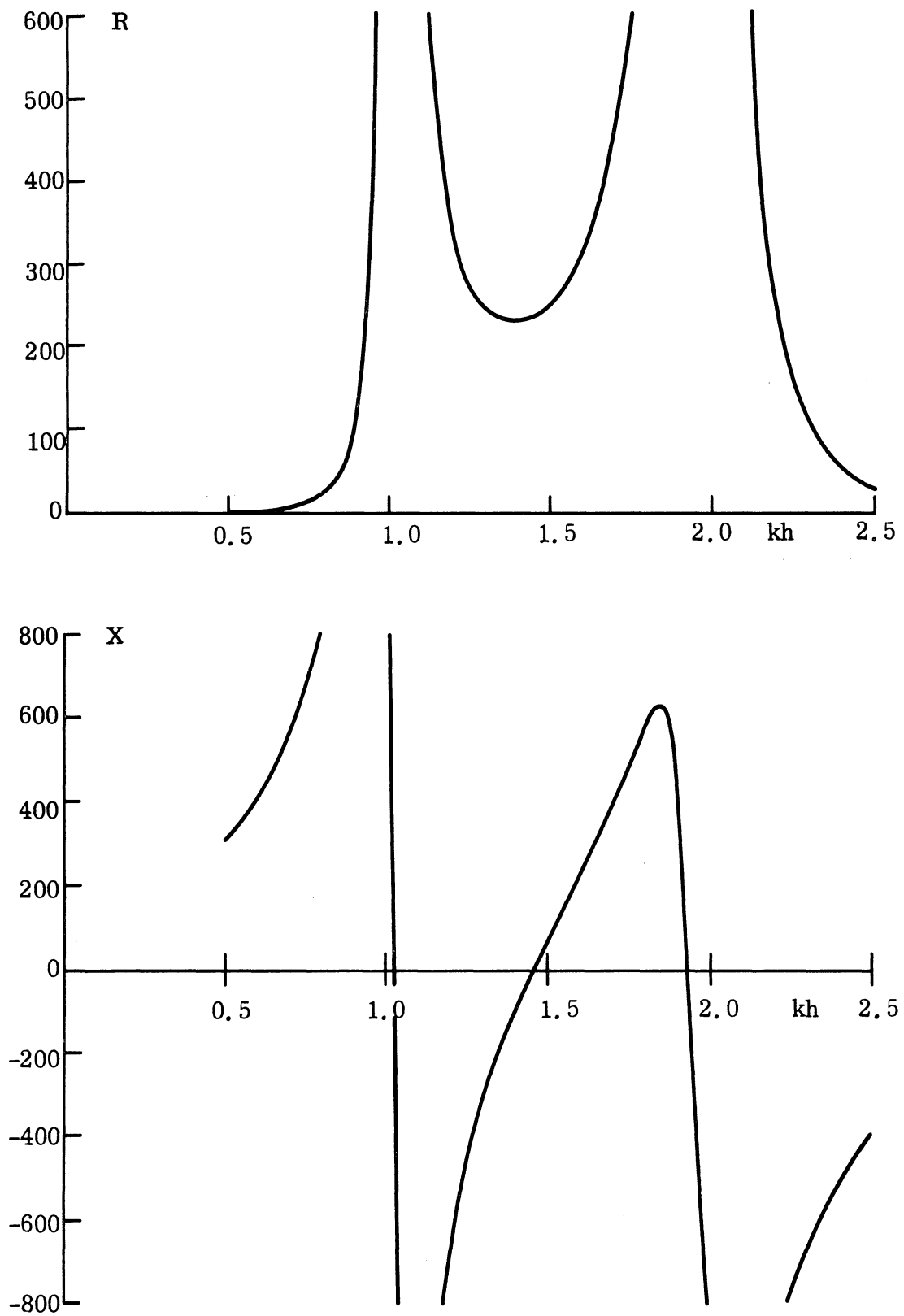


FIG. 5-1: INPUT RESISTANCE  $R$  AND REACTANCE  $X$  FOR FOLDED DIPOLE STRUCTURE WHERE  $p_s = 1.0$ ,  $p_a = 1.0$ .

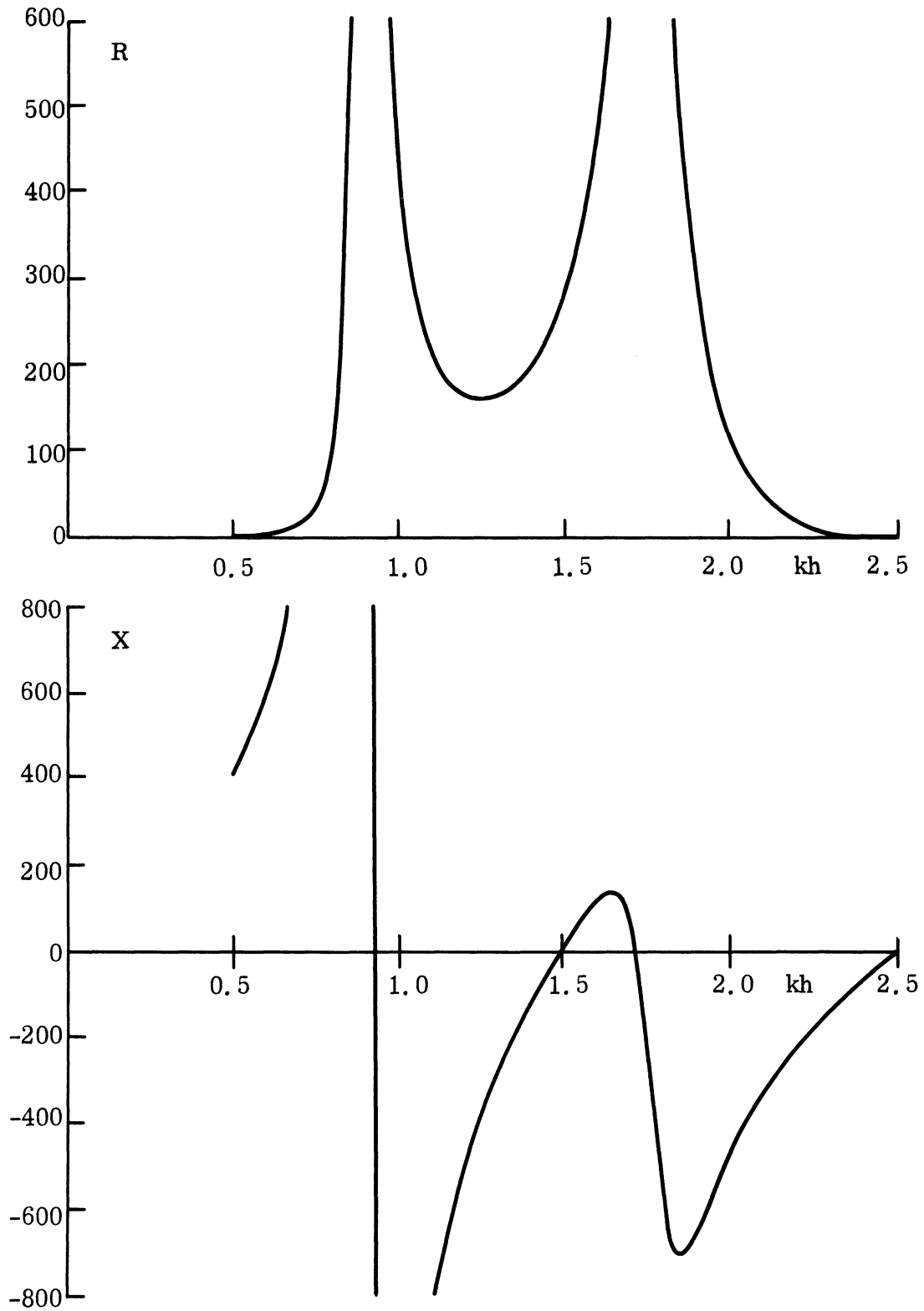


FIG. 5-2: INPUT RESISTANCE  $R$  AND REACTANCE  $X$  FOR FOLDED DIPOLE STRUCTURE WHERE  $p_s = 1.0$ ,  $p_a = 0.8$ .

THE UNIVERSITY OF MICHIGAN

7848-7-Q

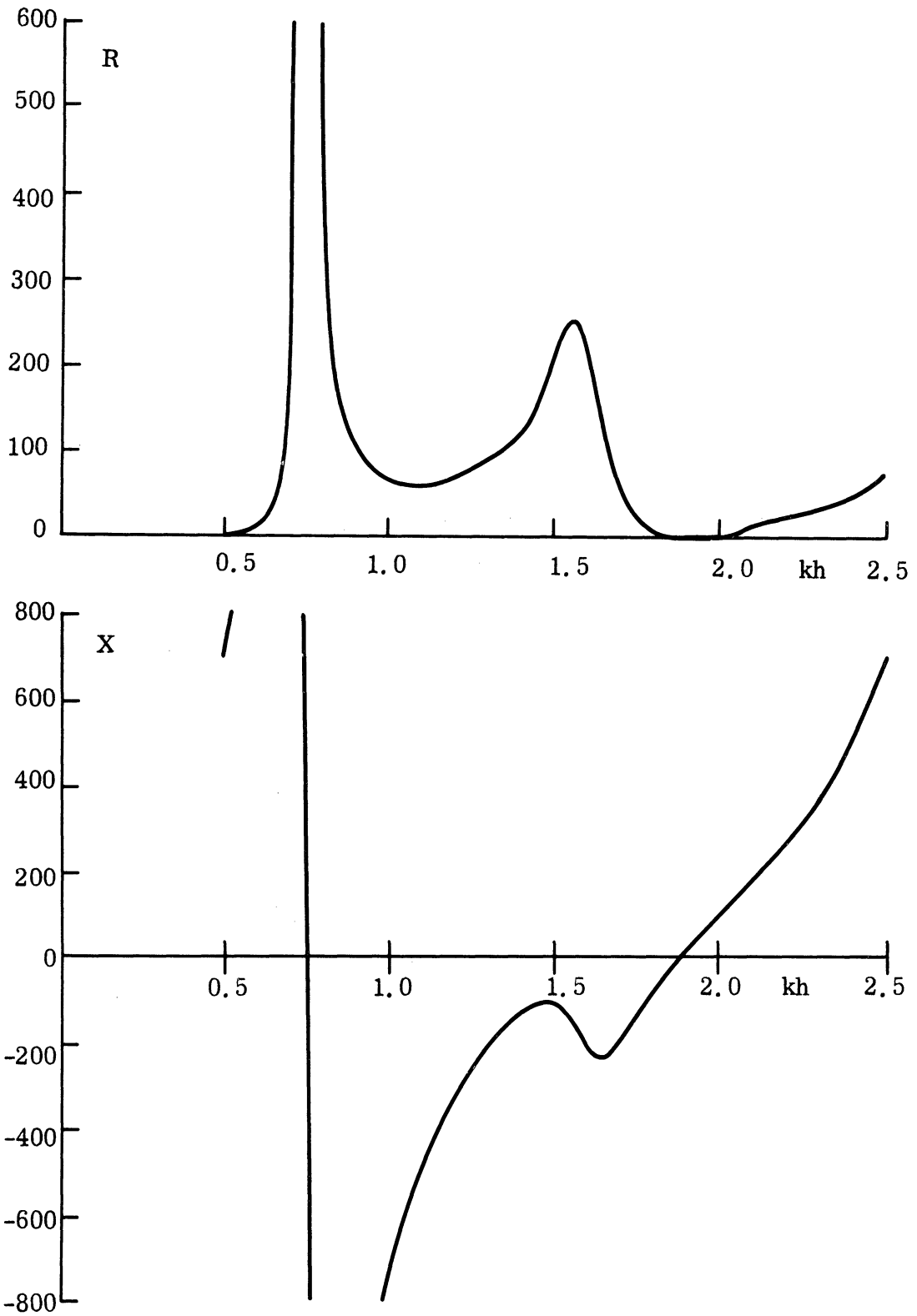


FIG. 5-3: INPUT RESISTANCE  $R$  AND REACTANCE  $X$  FOR FOLDED DIPOLE STRUCTURE WHERE  $p_s = 1.0$ ,  $p_a = 0.6$ .

THE UNIVERSITY OF MICHIGAN

7848-7-Q

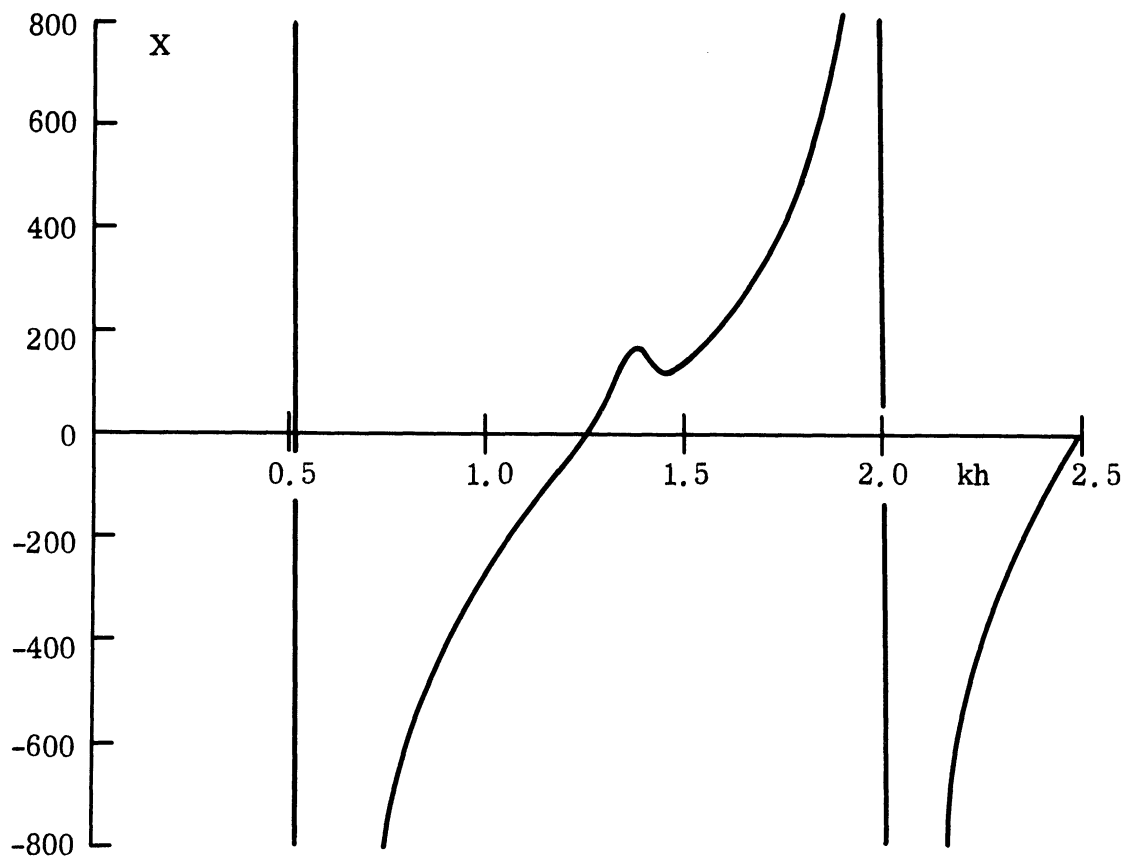
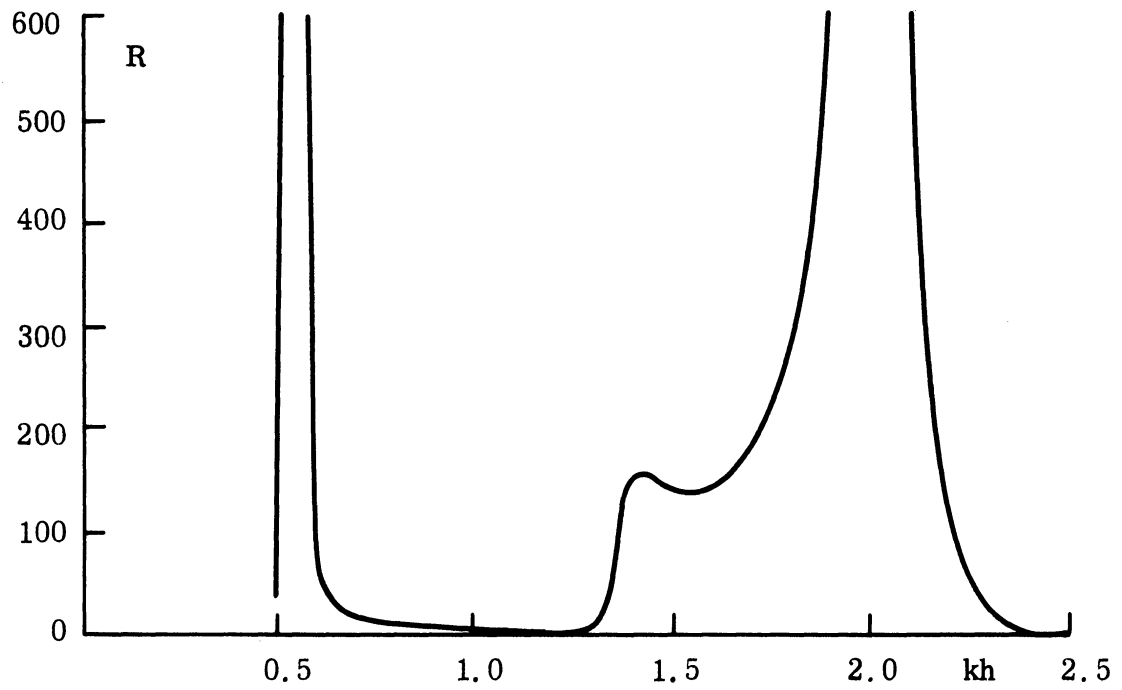


FIG. 5-4: INPUT RESISTANCE  $R$  AND REACTANCE  $X$  FOR FOLDED DIPOLE STRUCTURE WHERE  $p_s = 1.0$ ,  $p_a = 0.4$ .

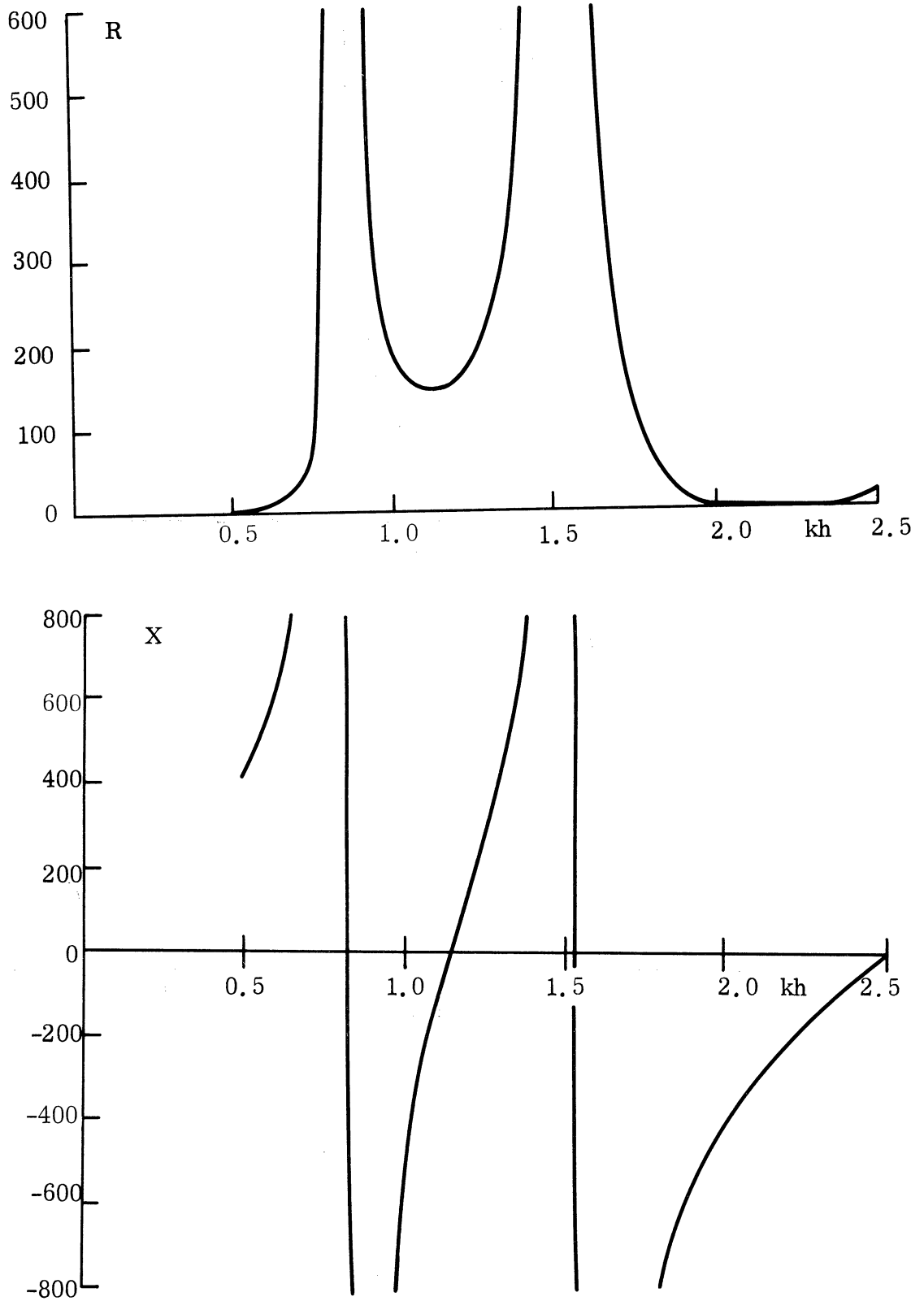


FIG. 5-5: INPUT RESISTANCE R AND REACTANCE X FOR FOLDED DIPOLE STRUCTURE WHERE  $p_s = 0.8$ ,  $p_a = 0.8$ .

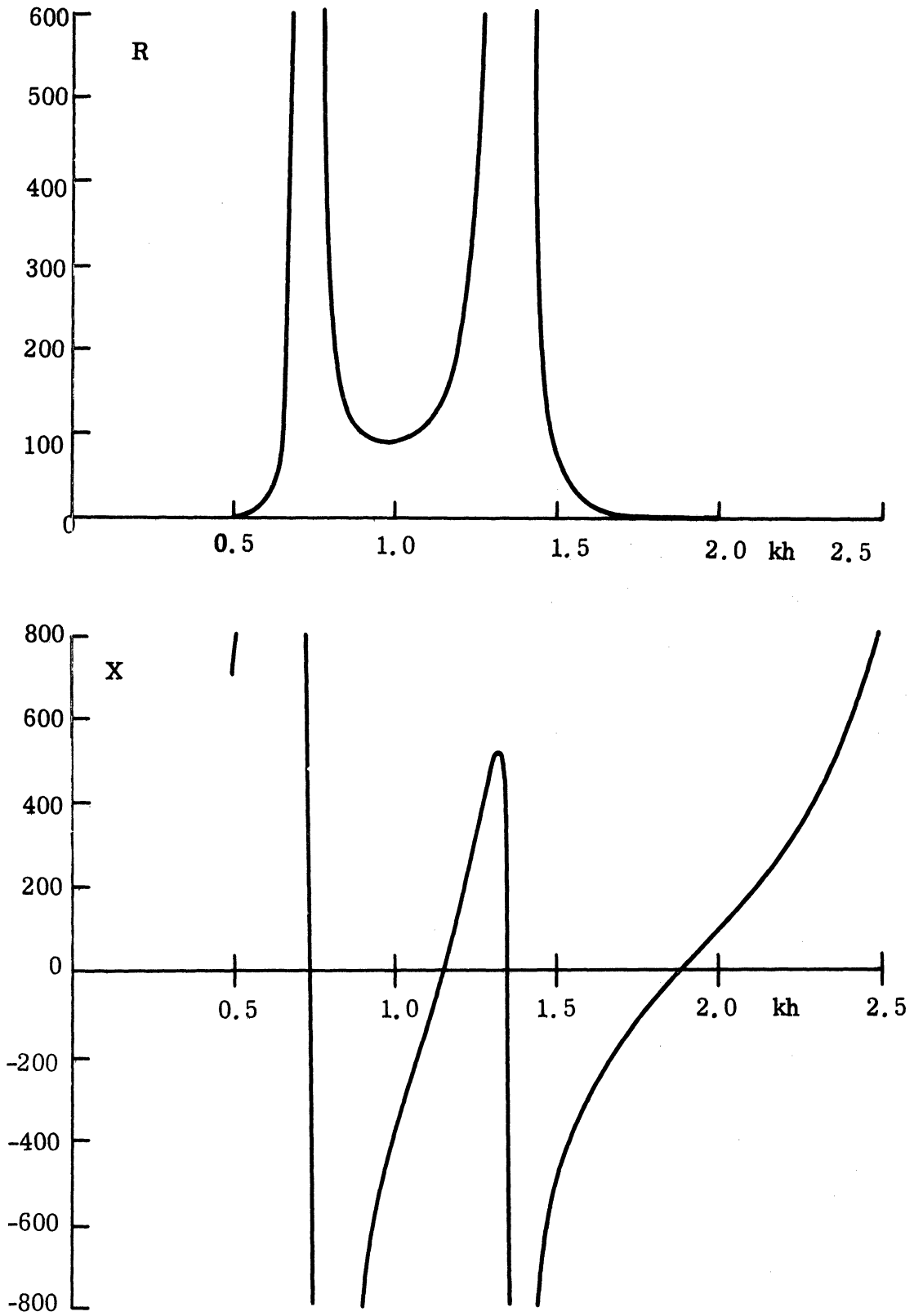


FIG. 5-6: INPUT RESISTANCE R AND REACTANCE X FOR FOLDED DIPOLE STRUCTURE WHERE  $p_s = 0.8$ ,  $p_a = 0.6$ .



VI

CONCLUSIONS

Both analysis and experiments have verified that a log conical spiral antenna can be reduced substantially in size. The present methods available, which have been investigated experimentally, are such as to assure the success of designing a log conical spiral antenna operable in the range from 200 to 600 MHz with a reduction in size. Although it is not anticipated that anisotropic loading will be utilized in the final design of this antenna, this type of loading does appear to be worthy of future study.

It has been decided to utilize a slot array of only three ferrite filled rectangular slots for establishing the feasibility and usefulness of the suggested concept. If there appear to be substantial advantages in this small array, including a reduction in near field effects due to small size of elements, then it is expected that justification can be extended to larger arrays.

It can be definitely concluded that the utilization of ferrite loading material for end fire rod antennas produces satisfactory results if the ferrite loading material is used in the form of a cylindrical shell. The experimental results confirm that such ferrite tube antennas have superior performance to ferrite rod antennas.

The study of ferrite loaded antennas down to 30 MHz has given considerable emphasis to the tuning of such antennas utilizing magnetic bias. For reasonably small size antennas in this frequency region, the radiating elements must certainly be of the highly tuned type. Therefore, in order to achieve reasonable coverage in frequency, it appears necessary to use either multiple tuning or continuously variable tuning, such as represented by magnetic bias.

VII

FUTURE EFFORT

In the next few weeks, a decision must be made as to which manner of loading is most appropriate for size reduction of the log conical spiral antenna. Quite aside from the physical outline size, it is important to maintain a reasonable weight for the final design. A choice must be made among the various alternative methods of loading which have been studied so far.

It is expected that the analytical work on ferrite tube radiators will be completed during the next report period. A careful study of the correctness of the analytical work will be made through a comparison of radiation patterns obtained both analytically and experimentally. In the future, all of the effort on this task will be on the ferrite tube rod radiator, which has a hollow air-space in the center of the core.

In the next few weeks, the array of three ferrite loaded rectangular slots will be thoroughly tested experimentally to obtain its actual radiation pattern. These tests will be performed on the roof-top antenna range. It is expected that pattern measurements will be made in a fairly narrow range of frequencies centered about 300 MHz. Supplementing these pattern measurements, there will be work done on the driving point impedance of each of the three slots. Effort will then be made to take this information and extend it to the prediction of driving point impedances of slots arranged in a still larger square array.

A careful comparison between experimental and theoretical results for elements useful down to 30 MHz will be completed. This should establish the accuracy of the mathematical techniques developed, and add support to the useful applications indicated by the study.

APPENDIX A

DESIGN CURVES FOR SMALL DIAMETER LOADED HELICES

In designing a small diameter helix to function as a linear slow wave structure, it is essential to know the dependence of the phase velocity reduction factor ( $\lambda_g/\lambda$ ) upon the helix pitch angle ( $\psi$ ). This information may be obtained from the solution to the characteristic equation for a sheath model of a helical transmission line. The characteristic equation for an arbitrary isotropic material loading in the helix core was derived by Li (1958) in his doctoral thesis. For a small diameter helix, the characteristic equation is

$$2 (ka)^2 \left\{ \ln \left( \frac{2}{ka} \right) - \gamma \right\} \left[ \frac{2 + \mu_r (ka)^2 \left\{ \ln(2/ka) - \gamma \right\}}{2 + \epsilon_r (ka)^2 \left\{ \ln(2/ka) - \gamma \right\}} \right] = \mu_r (\beta_0 a)^2 \cot^2 \psi$$

where  $k^2 = \beta^2 - \beta_0^2$ ,  $\beta$  is the wave number in the longitudinal direction,  $\beta_0$  is the free space wave number, "a" is the radius of the helix,  $\psi$  is the pitch angle of the sheath winding, and  $\gamma$  is Eulers constant (0.5772157). (Note: Li's notation is used only throughout this appendix. The notation appearing on subsequent figures is consistent with both this appendix and the remainder of the report.)

A computer program was written for the IBM 7090 computer at the University of Michigan Computing Center in Fortran II that would solve the characteristic equation and plot the required pitch angle ( $\psi$ ) vs  $\beta_0 a$  for a family of specified phase velocity reduction factors. With the slight modifications that are indicated by comment cards, the main program may be used on any computer system compatible with Fortran II. The subroutine that does

the plotting, however, calls on many local subroutines to use the IBM 763/789 plotter and is not compatible with other systems. Nevertheless, both the main program and the subroutine are included in the event that they may be useful to others wishing to solve the characteristic equation for other ferrites.

Solutions to the characteristic equation for a number of different core loadings are graphed in Figs. A-1 through A-9. The loadings are characterized by the relative permittivity ( $\epsilon_r$ ) and permeability ( $\mu_r$ ) of the core material. The materials which the  $\epsilon_r$  and  $\mu_r$  represent are stated in parentheses. While various engineering implications relating to the core material are discussed in Section 4.1, a few mathematical observations will be stated here. Li pointed out that little phase velocity reduction beyond that of an air core ( $\epsilon_r = \mu_r = 1$ ) is obtained with just dielectric loading of small diameter helices. This is illustrated in Figs. A-1 through A-4, where the relatively minor effect of increasing just  $\epsilon_r$  is seen to be more prominent for larger values of  $2\pi a/\lambda$  and smaller values of  $\lambda_g/\lambda$ . On the other hand, the utilization of ferrite loading to increase  $\mu_r$  results in a substantial phase velocity reduction for a specified helix pitch angle. The effect is illustrated in Figs. A-5a,b through A-9a,b, where two scales have been used to facilitate accuracy.

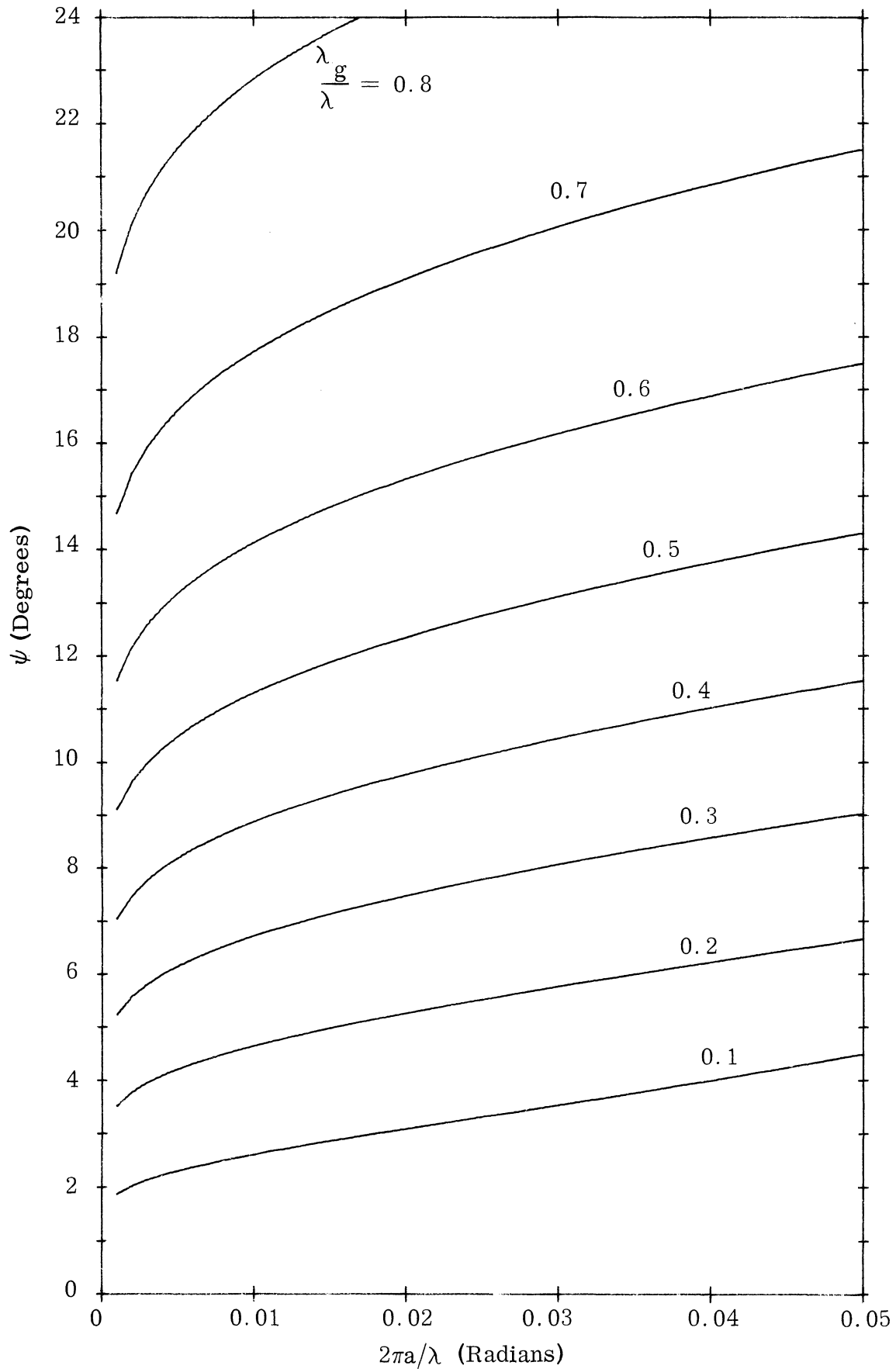


FIG. A-1: SOLUTION OF THE CHARACTERISTIC EQUATION FOR HELIX HAVING CORE PARAMETERS  $\epsilon_r = 1.00$ ,  $\mu_r = 1.00$ ; (Air).

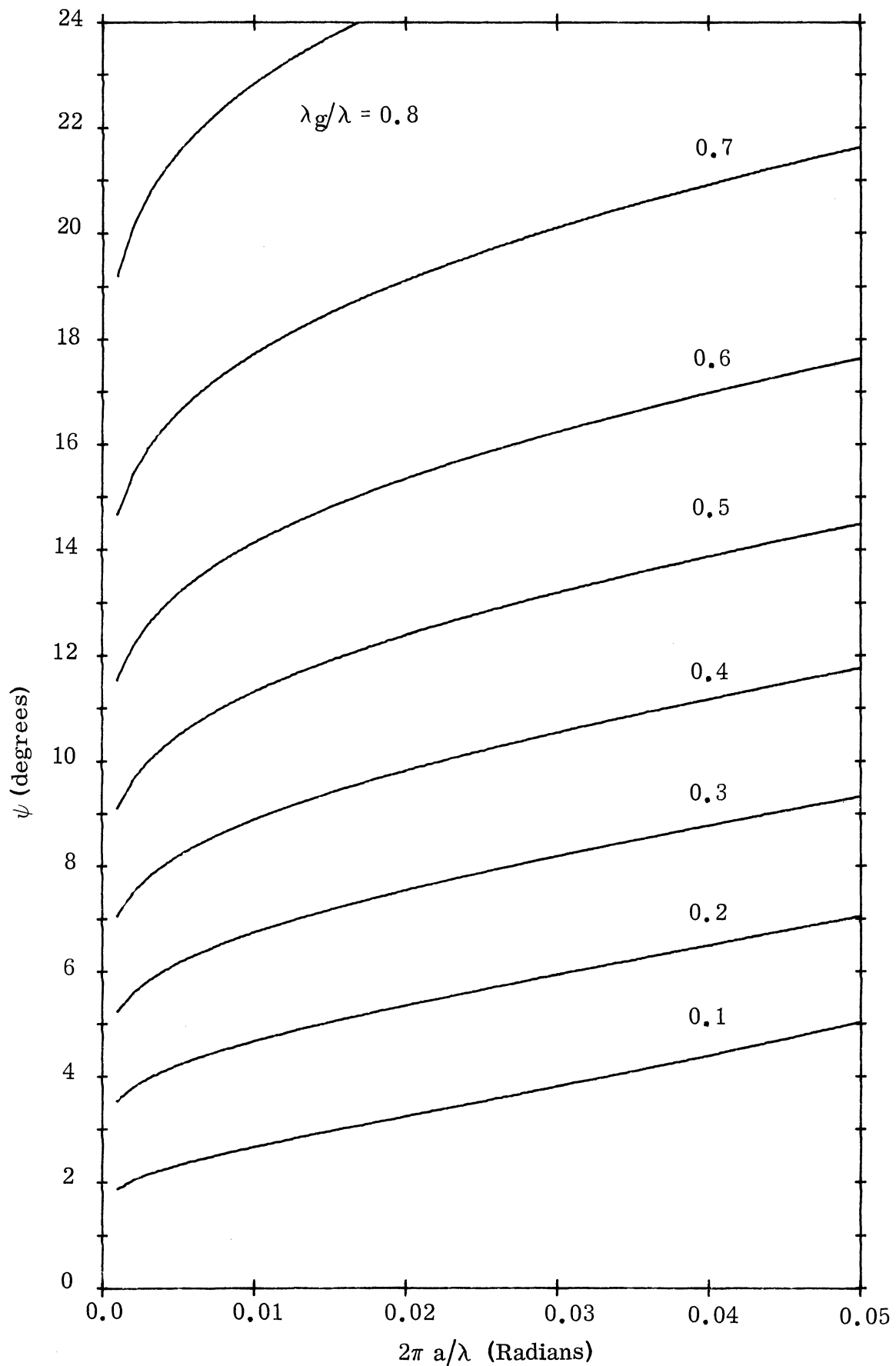


FIG. A-2: SOLUTION OF THE CHARACTERISTIC EQUATION FOR HELIX HAVING CORE PARAMETERS  $\epsilon_r = 3.77$ ,  $\mu_r = 1.00$ ; (EAF-2 Powder Ferrite Biased into Saturation).

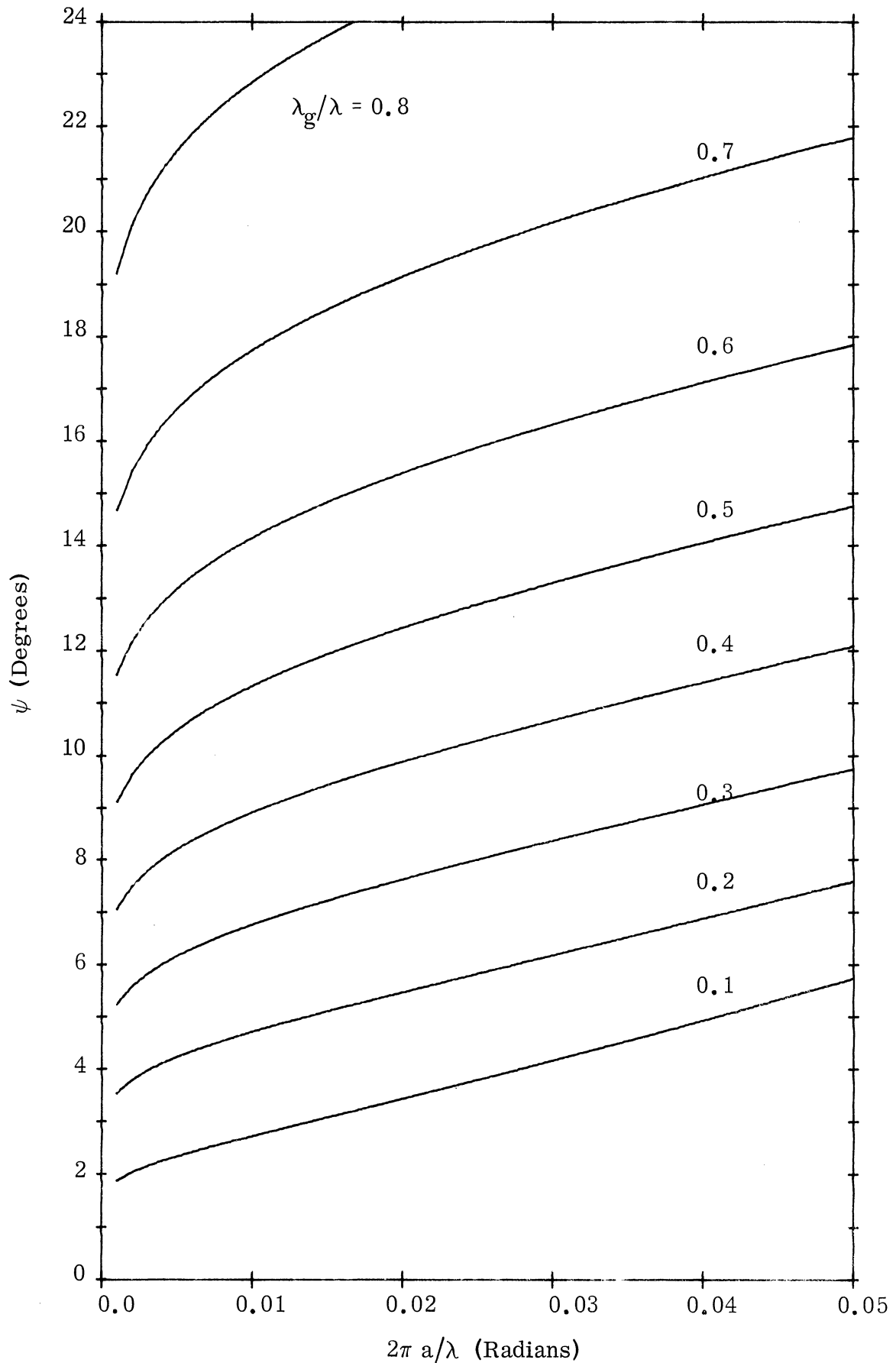


FIG. A-3: SOLUTION OF THE CHARACTERISTIC EQUATION FOR HELIX HAVING CORE PARAMETERS  $\epsilon_r = 7.88$ ,  $\mu_r = 1.00$ ; (Q-3 Ferrite at 150 MHz Biased into Saturation).

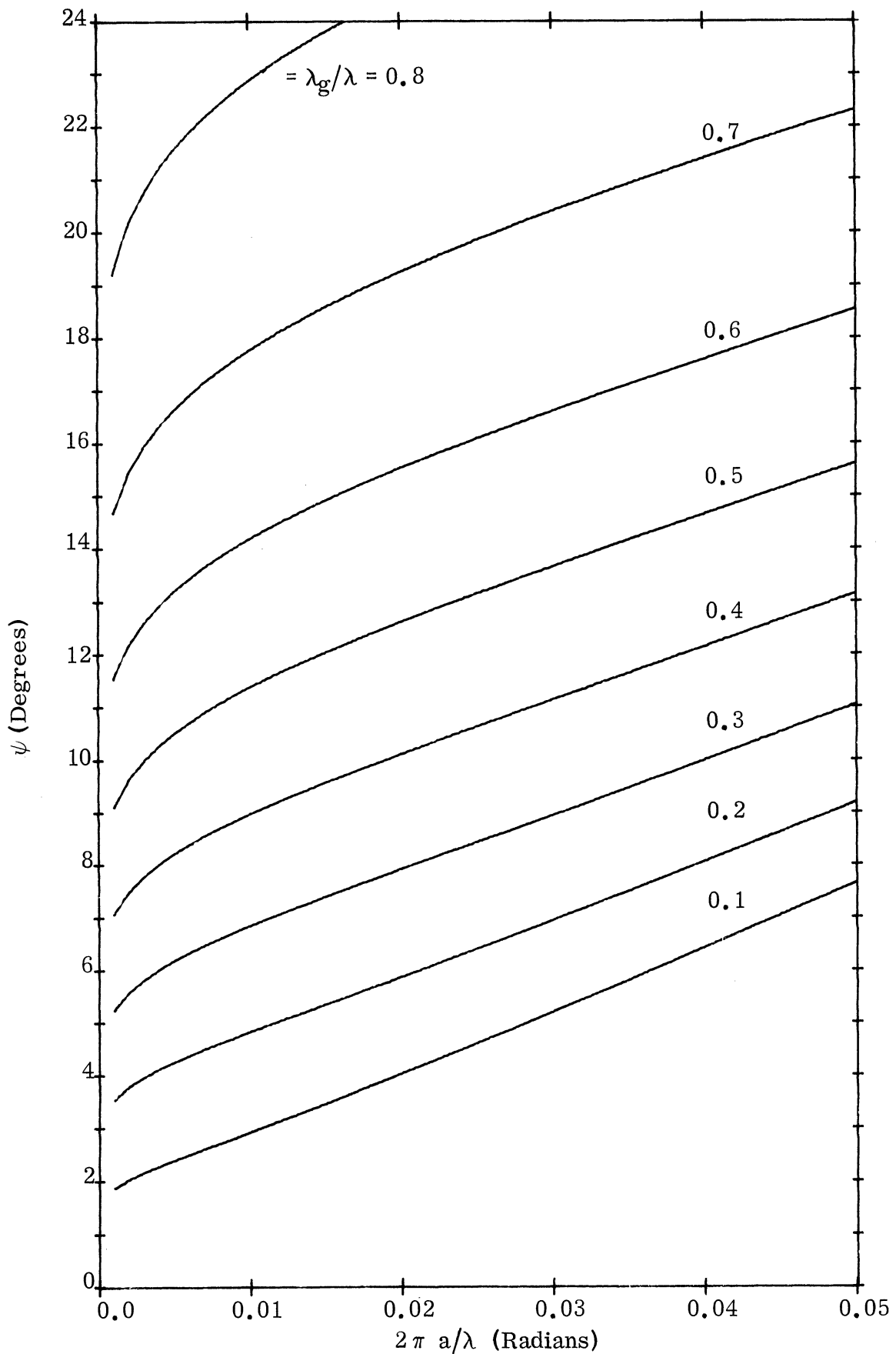


FIG. A-4: SOLUTION OF THE CHARACTERISTIC EQUATION FOR HELIX HAVING CORE PARAMETERS  $\epsilon_r = 22.0$ ,  $\mu_r = 1.00$ ; (Eccosorb CR at 300 MHz Biased into Saturation).



7848-7-Q

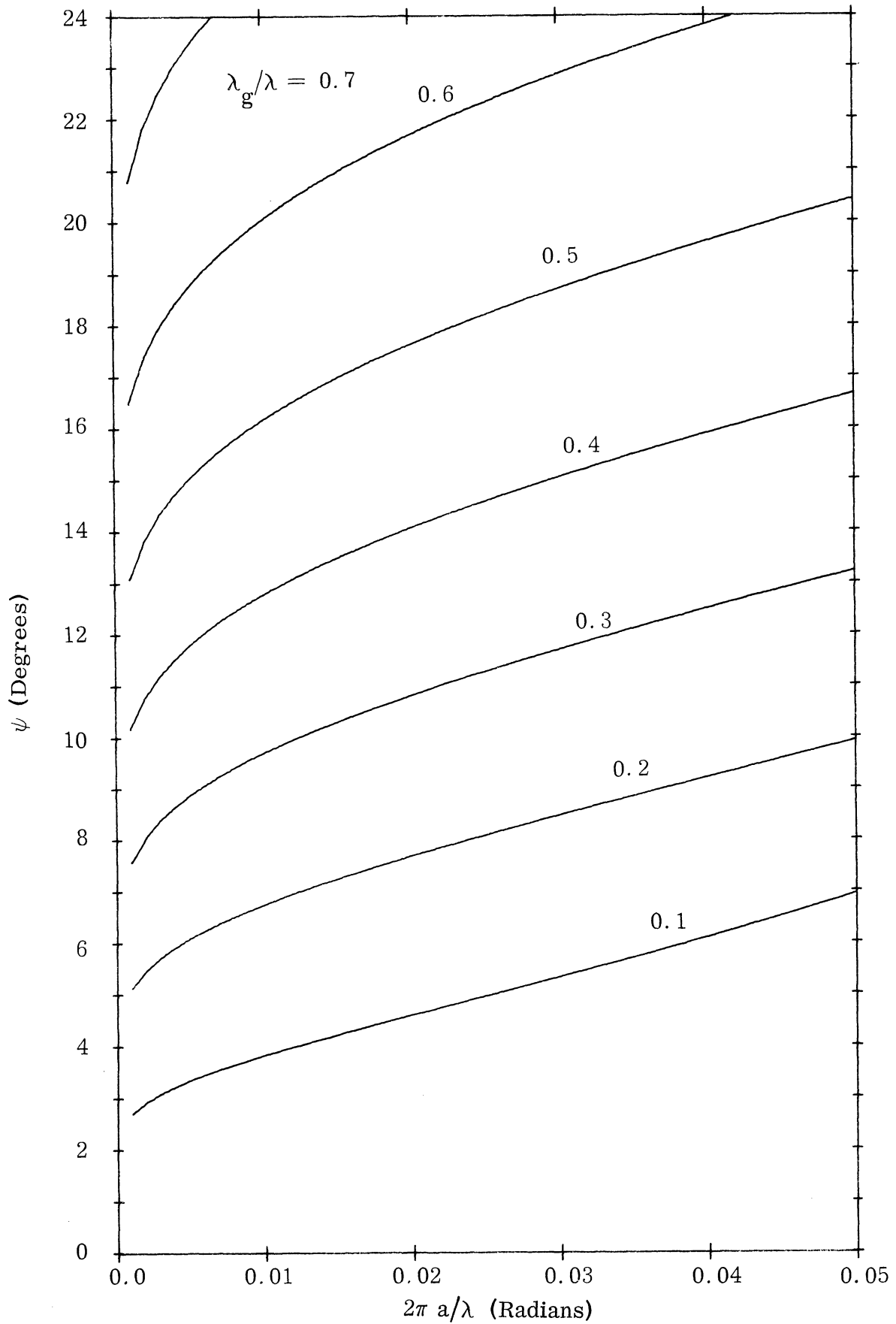


FIG. A-5a: SOLUTION OF THE CHARACTERISTIC EQUATION FOR HELIX HAVING CORE PARAMETERS  $\epsilon_r = 3.77$ ,  $\mu_r = 2.10$ ; (EAF-2 Powder Ferrite).

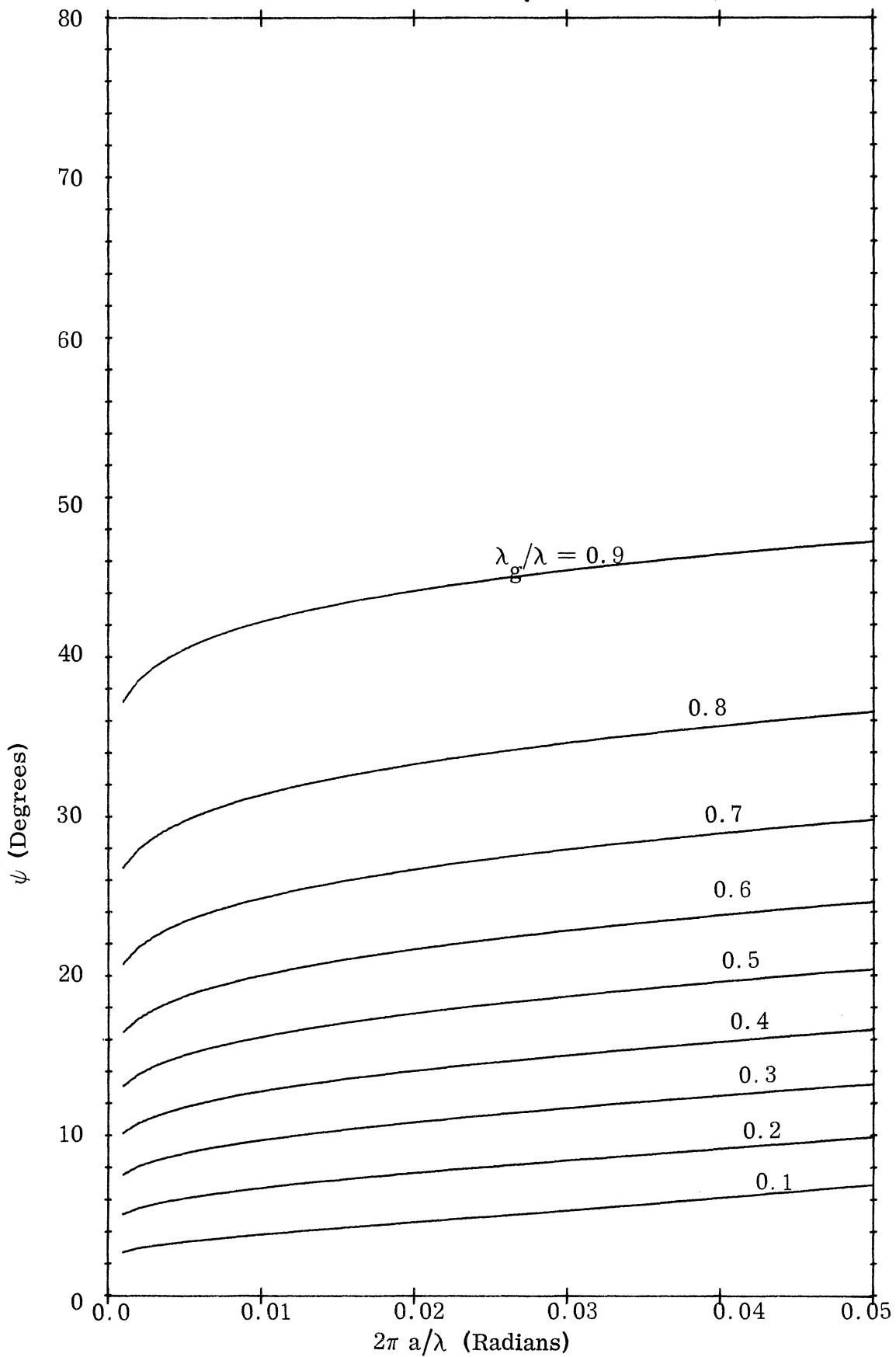


FIG. A-5b: SOLUTION OF THE CHARACTERISTIC EQUATION FOR HELIX HAVING CORE PARAMETERS  $\epsilon_r = 3.77$ ,  $\mu_r = 2.10$ ; (EAF-2 Powder Ferrite).

THE UNIVERSITY OF MICHIGAN

7848-7-Q

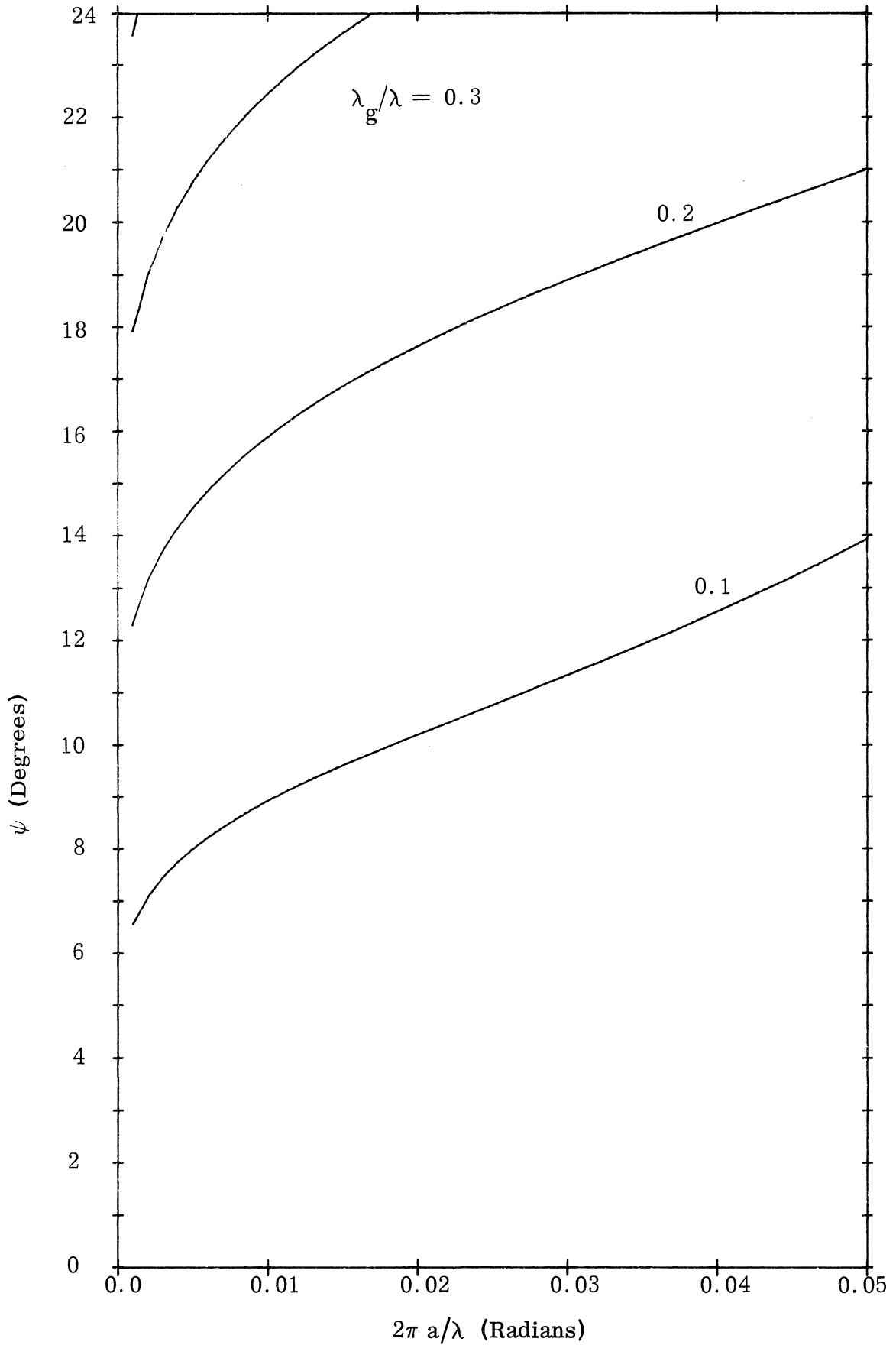


FIG. A-6a: SOLUTION OF THE CHARACTERISTIC EQUATION FOR HELIX HAVING CORE PARAMETERS  $\epsilon_r = 7.96$ ,  $\mu_r = 12.4$ ; (Q-3 Ferrite at 100 MHz).

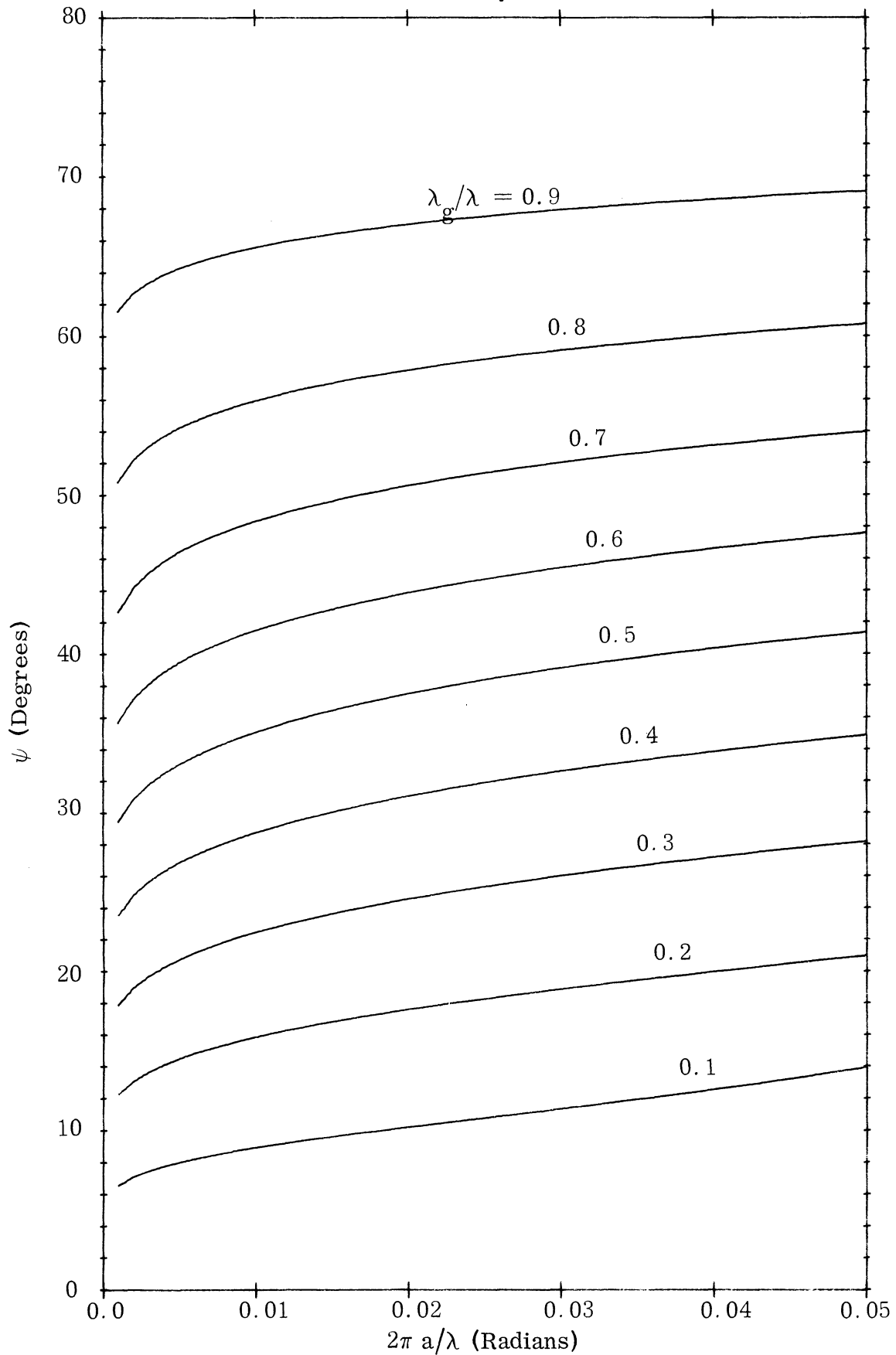


FIG. A-6b: SOLUTION OF THE CHARACTERISTIC EQUATION FOR HELIX HAVING CORE PARAMETERS  $\epsilon_r = 7.96$ ,  $\mu_r = 12.4$ ; (Q-3 Ferrite at 100 MHz).

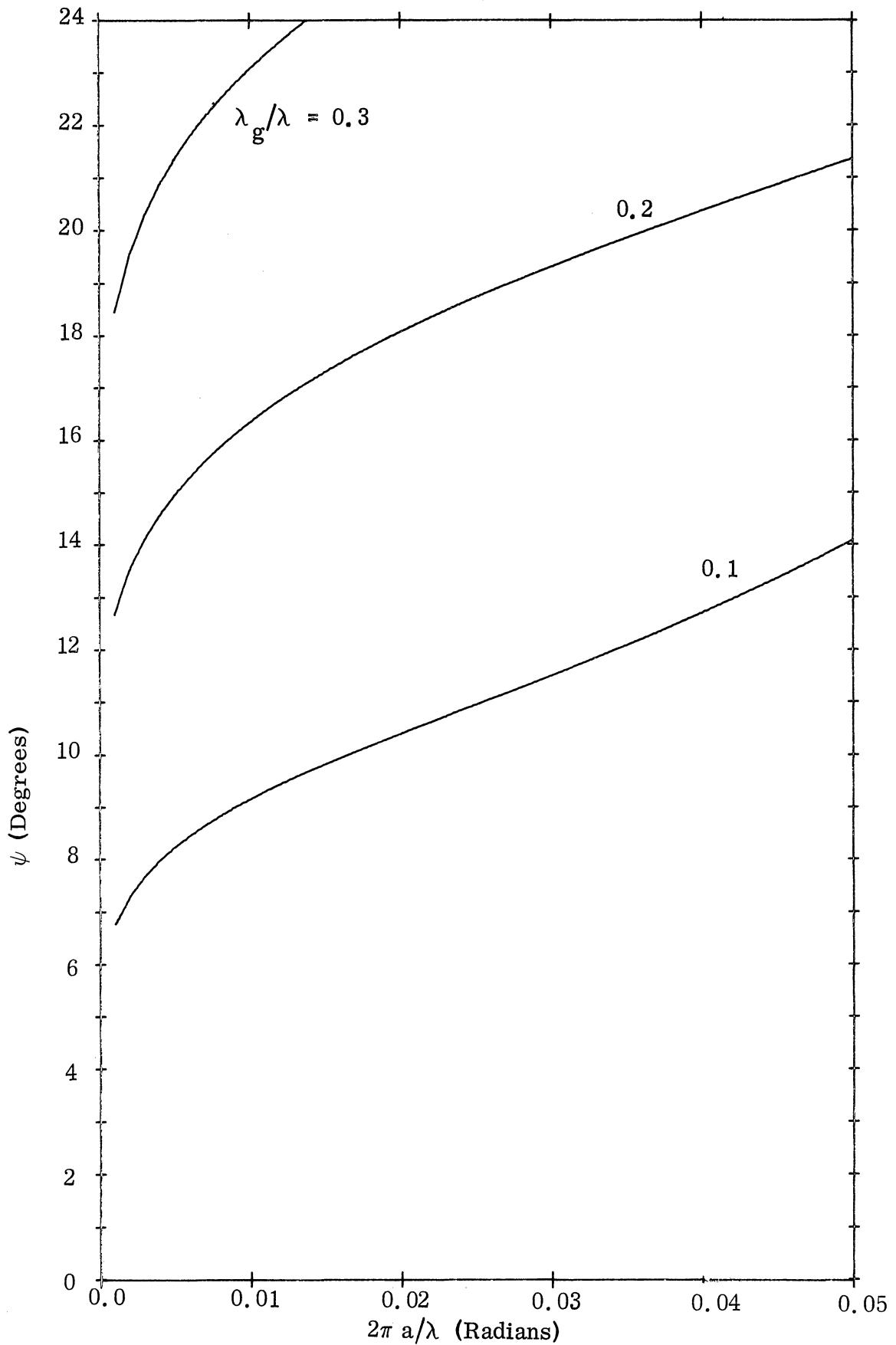


FIG. A-7a: SOLUTION OF THE CHARACTERISTIC EQUATION FOR HELIX HAVING CORE PARAMETERS  $\epsilon_r = 7.88$ ,  $\mu_r = 13.2$ ; (Q-3 Ferrite at 150 MHz).

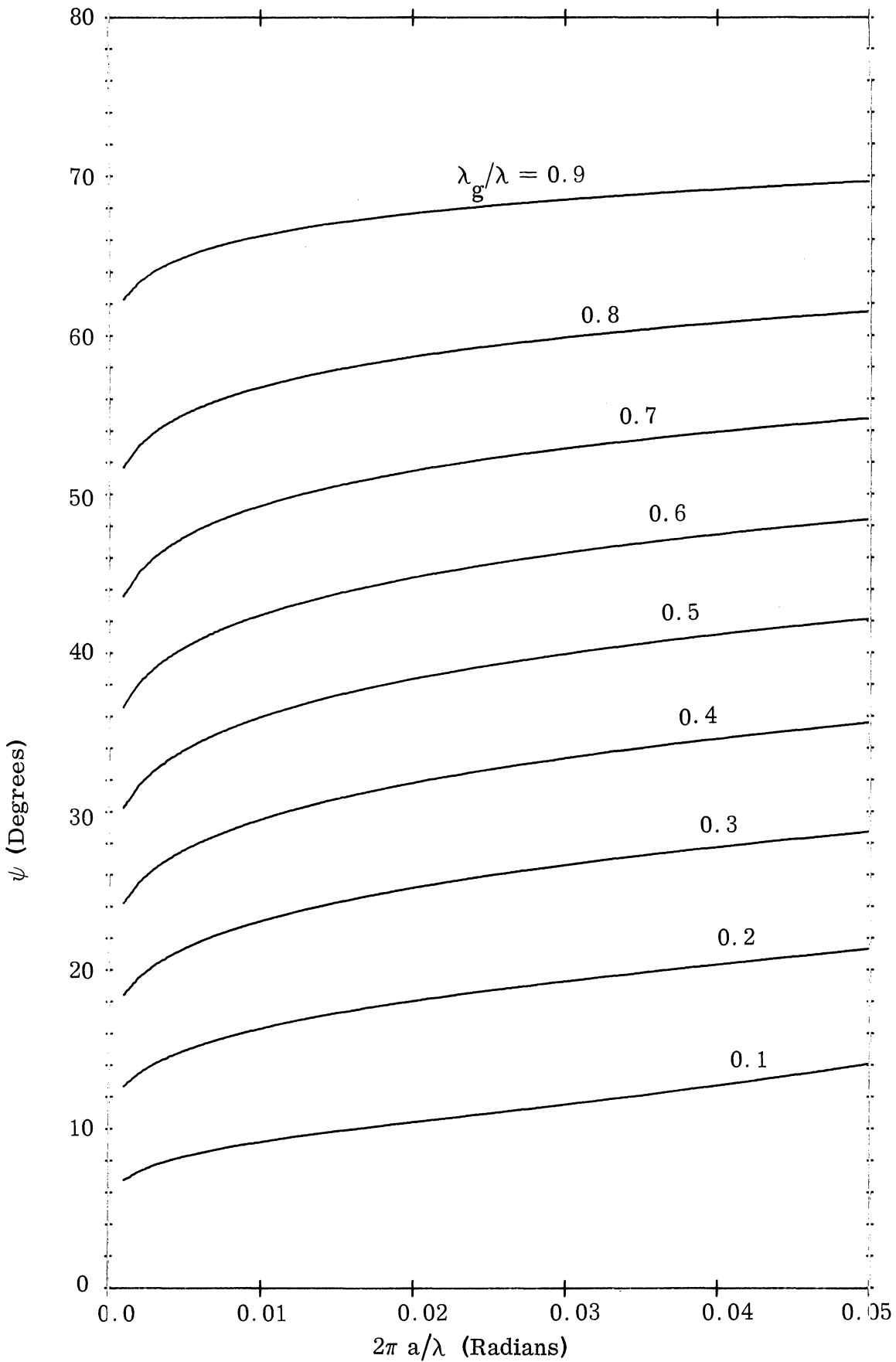


FIG. A-7b: SOLUTION OF THE CHARACTERISTIC EQUATION FOR HELIX HAVING CORE PARAMETERS  $\epsilon_r = 7.88$ ,  $\mu_r = 13.2$ ; (Q-3 Ferrite at 150 MHz).

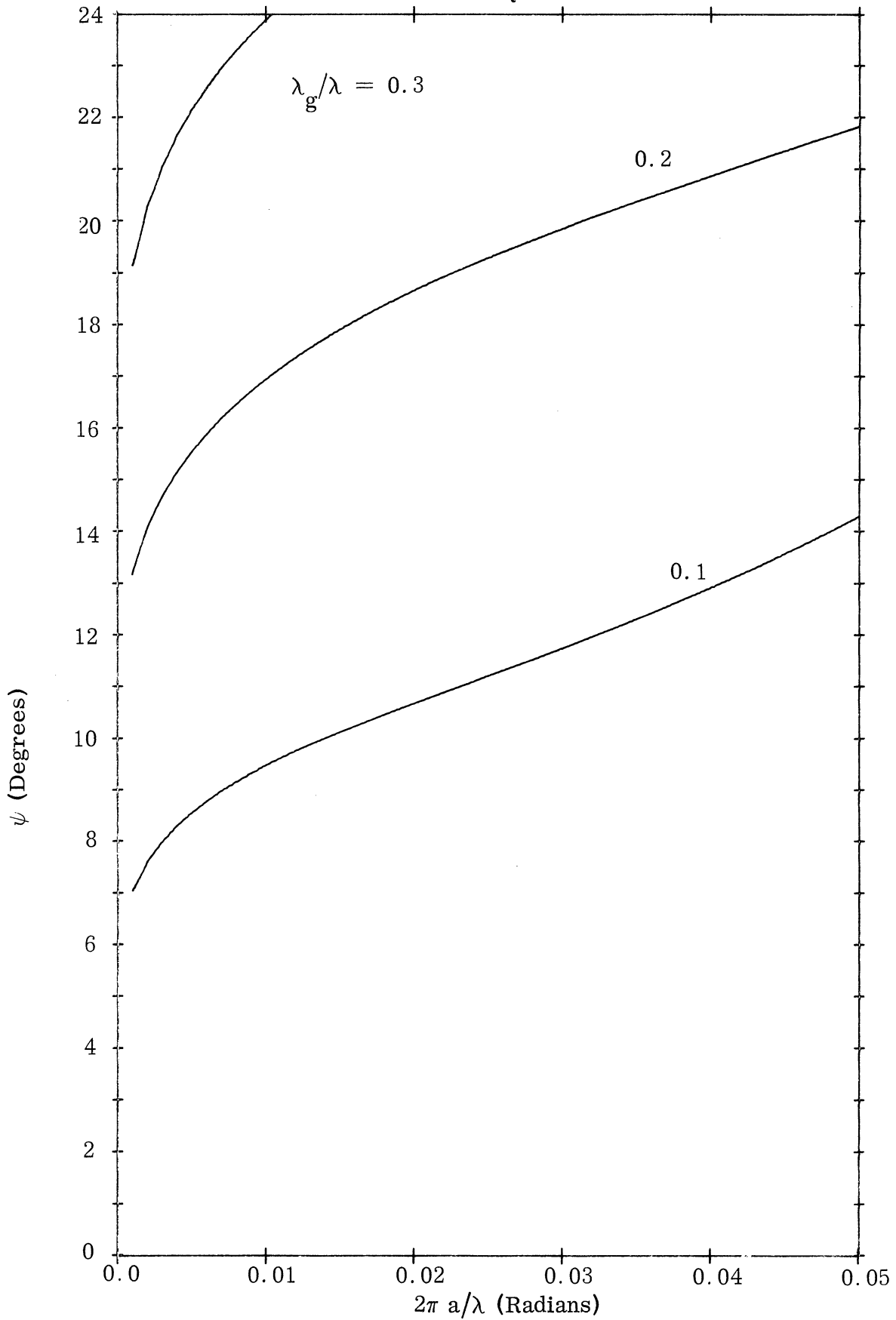


FIG. A-8a: SOLUTION OF THE CHARACTERISTIC EQUATION FOR HELIX HAVING CORE PARAMETERS  $\epsilon_r = 7.81$ ,  $\mu_r = 14.3$ ; (Q-3 Ferrite at 200 MHz).

THE UNIVERSITY OF MICHIGAN

7848-7-Q

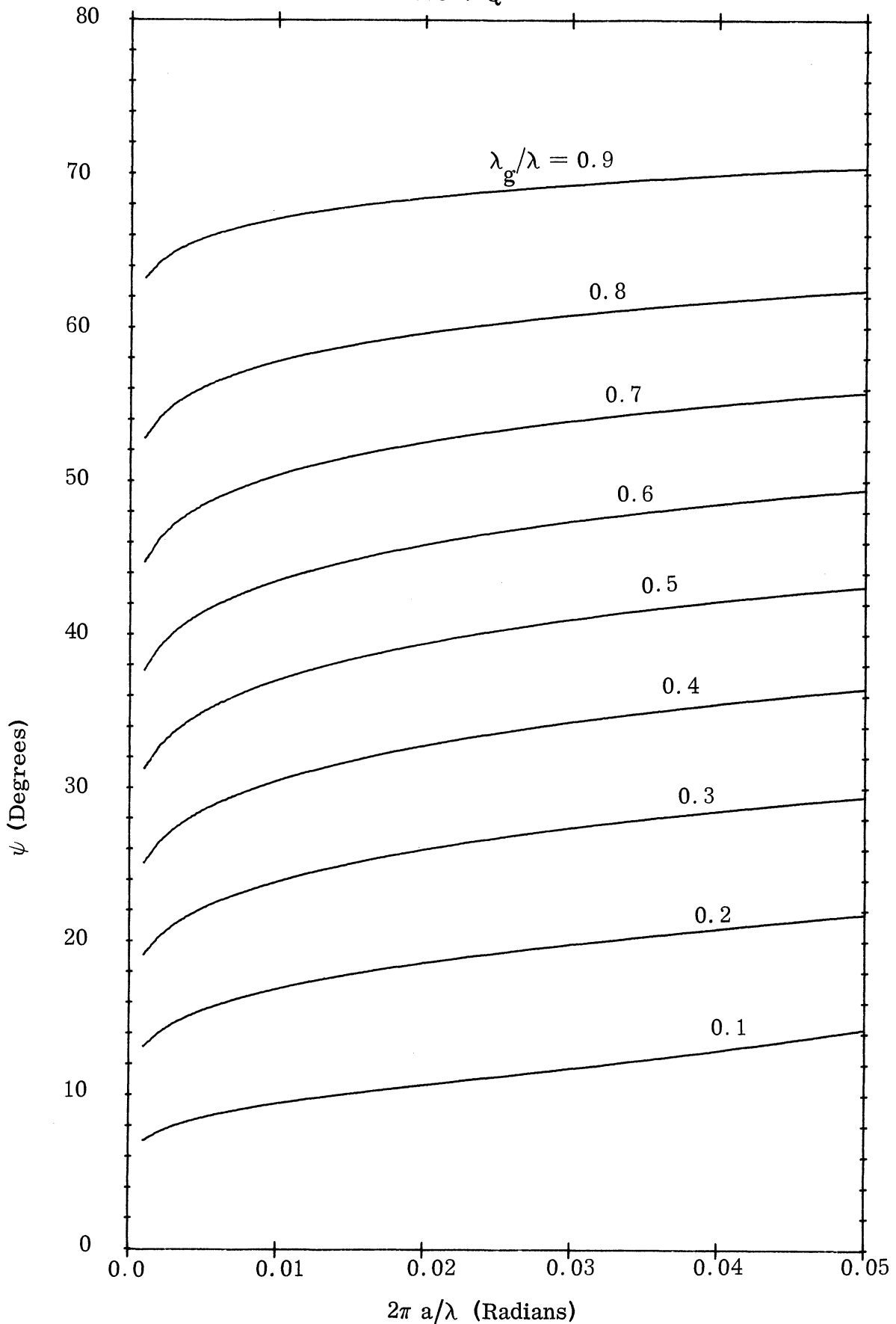


FIG. A-8b: SOLUTION OF THE CHARACTERISTIC EQUATION FOR HELIX HAVING CORE PARAMETERS  $\epsilon_r = 7.81$ ,  $\mu_r = 14.3$ ; (Q-3 Ferrite at 200 MHz).



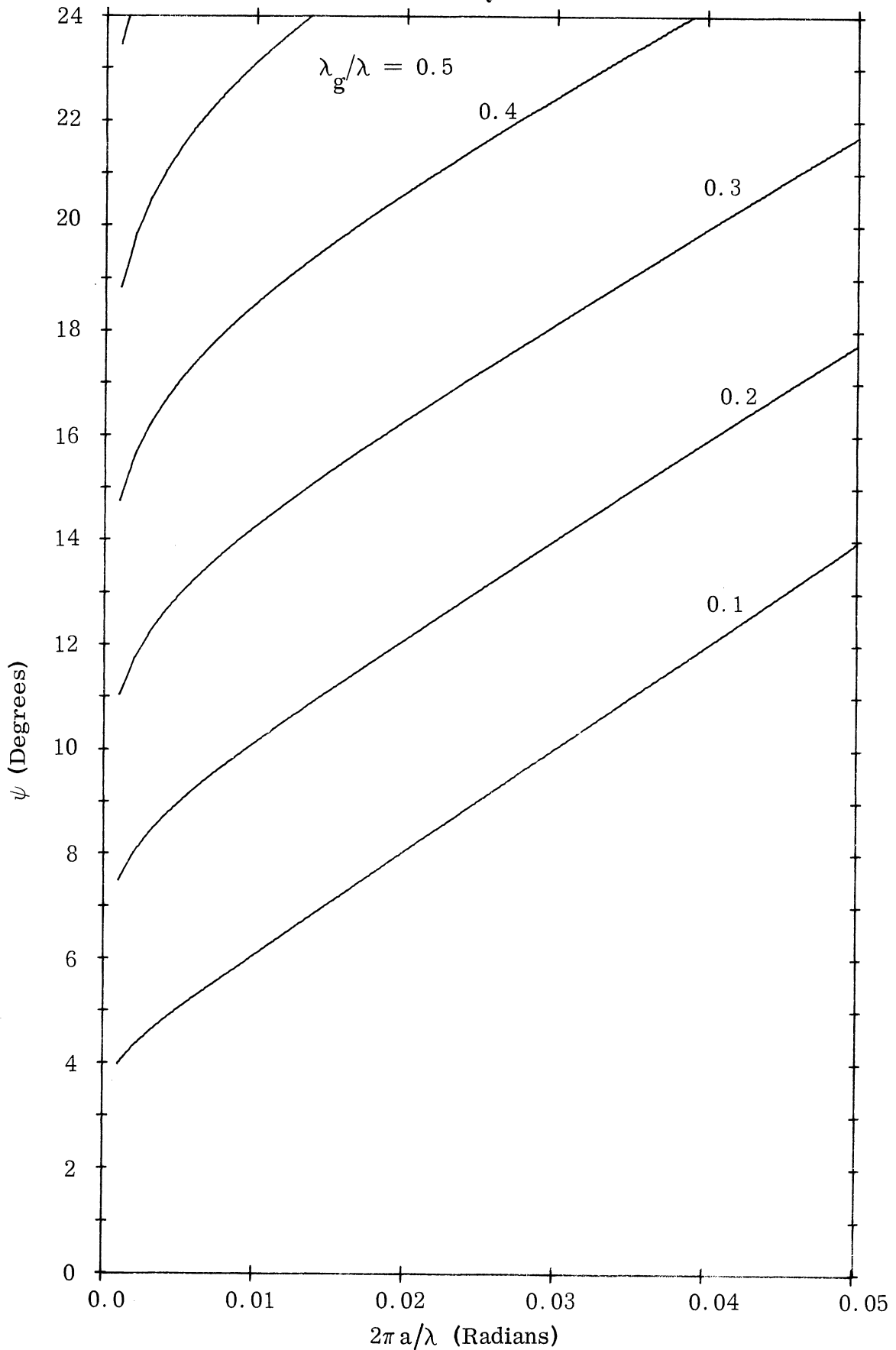


FIG. A-9a: SOLUTION OF THE CHARACTERISTIC EQUATION FOR HELIX HAVING CORE PARAMETERS  $\epsilon_r = 22.0$ ,  $\mu_r = 4.51$ ; (Eccosorb CR at 300 MHz).

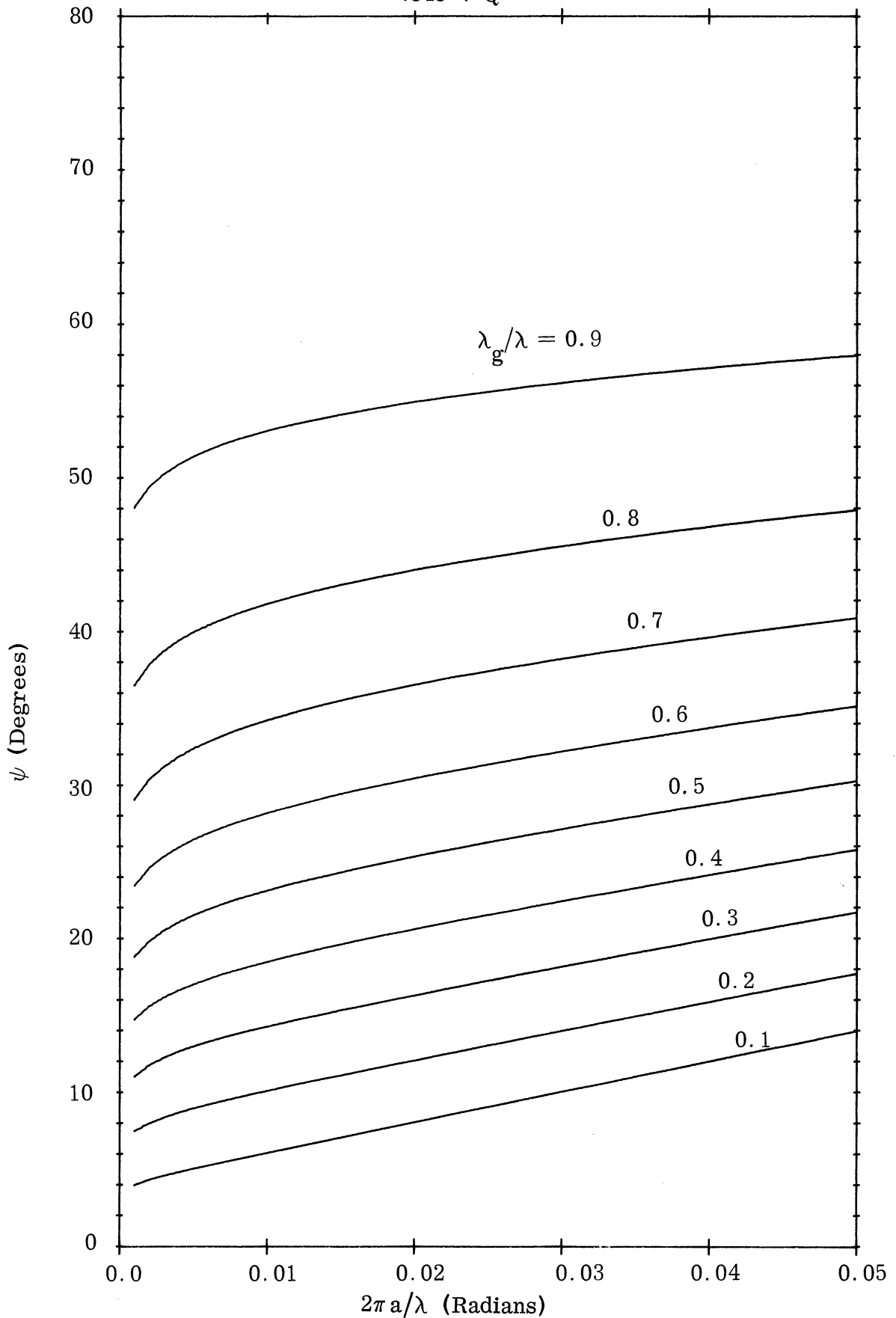


FIG. A-9b: SOLUTION OF THE CHARACTERISTIC EQUATION FOR HELIX HAVING CORE PARAMETERS  $\epsilon_r = 22.0$ ,  $\mu_r = 4.51$ ; (Eccosorb CR at 300 MHz).

```

DIMENSION PSI(450), X(450)
C TAPE 7 IS THE INPUT TAPE, AND TAPE 6 THE OUTPUT TAPE OF THE UNIVERSITY OF
C MICHIGAN SYSTEM
C
10 READ INPUT TAPE 7,20, RELMU, RELEPS
20 FORMAT (2E10.0)
21 WRITE OUTPUT TAPE 6,22,RELMU,RELEPS
22 FORMAT(32H1THE RELATIVE MU AND EPSILON ARE 1P2E20.8,
1 // 52H R, BETA(0)*A AND PSI ARE PRINTED OUT IN THAT ORDER.)
25 I=1
26 J=1
30 R=0.1
40 BOA=0.001
45 WRITE OUTPUT TAPE 6,46
46 FORMAT(/)
50 BA=BOA/R
60 XKAE2= (BA**2)-(BOA**2)
C
C SORT IS A LOCAL FUNCTION FOR CALCULATING THE SQUARE ROOT.
C
70 XKA=SQRT(XKAE2)
C
C ELOG IS A LOCAL FUNCTION FOR CALCULATING THE NATURAL LOGRITHM.
C
25 LINES PRINTED
    
```

```

80 BRACK=ELOG(2.0/XKA)
90 BRACK=BRACK-0.5772157
100 CT2PSI=(2.0*XKAE2*BRACK*(2.0+(RELMU*XKAE2*BRACK)))/(RELMU*(BOA**2)
      1*(2.0+(RELEPS*XKAE2*BRACK)))
110 COTPSI=SQRT(CT2PSI)
C
C ATAN IS A LOCAL FUNCTION FOR CALCULATING THE ARCTANGENT.
C THE RETURN OF ATAN IS IN RADIANS , STATEMENT 130 CONVERTS THIS TO DEGREES.
C
120 PSI(I)=ATAN(1.0/COTPSI)
130 PSI(I)=PSI(I)/(1.745329E-2)
135 X(I)=BOA
136 IF (J-5) 153,140,140
140 WRITE OUTPUT TAPE 6, 150,R,BOA, PSI(I)
150 FORMAT (1P3E20.8)
152 J=0
153 J=J+1
155 I=I+1
160 BOA=BOA+0.001
170 IF (BOA-0.05) 50,50,180
180 R=R+0.1
190 IF (R-0.99)40,195,195
195 CALL GRAPH (X,PSI)
200 GO TO 10
      END

```

25 LINES PRINTED

THE UNIVERSITY OF MICHIGAN  
7848-7-Q

```

C THIS SUBROUTINE DOES THE GRAPH USING THE CALPLOT SUBROUTINES.
C
C PLTXMX IS NOT CALLED FOR SINCE 8.5 INCHES OF GRAPH PAPER IS SUFFICIENT.
C PSCALE IS NOT CALLED FOR SINCE THE SCALE FACTORS ARE KNOWN APRIORI.
C THESE APRIORI VALUES ARE FED INTO PLTOFS.
C
C SUBROUTINE GRAPH (BOA,PSI)
  DIMENSION PSI(450), BOA(450)
C
C STATEMENT 10 SPECIFIES THE RELATIVE ORIGIN.
C
10 CALL PLTOFS(0.0,0.01,0.0,10.0,1.0,1.0)
C
C STATEMENT 30 DRAWS AND LABELS THE X AXIS. 35 DOES THE UPPER X AXIS.
C 40 DRAWS AND LABELS THE Y AXIS. 45 DOES THE RIGHT Y AXIS.
C
30 CALL PAXIS(1.0,1.0,1H,-1,-5.0,0.0,0.0,0.01,1.0)
35 CALL PAXIS(1.0,9.0,1H,-1,-5.0,0.0,0.0,0.01,1.0)
40 CALL PAXIS(1.0,1.0,1H,1,-8.0,90.0,0.0,10.0,0.2)
45 CALL PAXIS(6.0,1.0,1H,1,-8.0,90.0,0.0,10.0,0.2)
C
C SINCE THE NORMAL MODE OF PLOTTING IS LINEAR-RECTANGULAR, THE MODE NEED NOT BE
  C DEFINED.
C 50 PLOTS PSI VS. BETA(0)*A USING A SOLID LINE.
C PRSTER, PONRST, AND POFRST ARE CALLED TO PREVENT PLOTTING OUTSIDE
  C THE DESIRED PLOTTING REIGON.
C
47 SWT=PRSTER(1.0,1.0,5.0,8.0)
48 SWT=PONRST(0)
50 DO 60 I=1,9
55 K=1+(I-1)*50
60 CALL PLINE(BOA(K),PSI(K),50,1,0,0,1)
65 SWT=POFRST(0)
C
C 70 INDICATES THE PLOTTING IS ALL FINISHED.
C
70 CALL PLTEND
80 RETURN
  END

```

## REFERENCES

- Collin, Robert C. (1960) Field Theory of Guided Waves, McGraw-Hill Book Company Inc., New York.
- Fradin, A. Z. (1961), Microwave Antennas, Pergamon Press, London.
- Hach, R. C. (1966), Conductron Corporation, Private Communication with one of the Authors.
- James, J. R. (1967), "Theoretical Investigation of Cylindrical Dielectric Rod Antennas," Proc. IEEE, 114, pp. 309-319.
- Kiely, D. G. (1953), "Dielectric Aerials," Methuen Monograph.
- Li, T. (1958), "The Small-Diameter Helical Antenna and its Input-Impedance Characteristics," Doctoral Thesis, Northwestern University.
- Lyon, J. A. M., N. G. Alexopoulos, G. G. Rassweiler, D. L. Smith, J. C. Parker, W. W. Parker and P. R. Wu (1966), "Study and Investigation of a UHF-VHF Antenna," The University of Michigan Radiation Laboratory Report No. 7848-2-Q. UNCLASSIFIED.
- Lyon, J. A. M., G. G. Rassweiler, N. G. Alexopoulos, J. C. Parker, D. L. Smith and P. R. Wu (1967), "Study and Investigation of a UHF-VHF Antenna," The University of Michigan Radiation Laboratory Report No. 7848-4-Q. UNCLASSIFIED.
- Lyon, J. A. M., C. C. Chen, E. S. Greene, J. C. Parker, and D. L. Smith (1967), "Study and Investigation of a UHF-VHF Antenna," The University of Michigan Radiation Laboratory Report No. 7848-6-Q. UNCLASSIFIED.
- Rassweiler, G. G. (1967), "Helical and Log-Conical Helical Antennas Loaded with an Isotropic Material," Doctoral Thesis, also The University of Michigan Radiation Laboratory Report No. 7848-3-Q. (November, 1966) UNCLASSIFIED.
- Walter, C. H. (1965), Traveling Wave Antennas, McGraw-Hill Book Co., New York.
- Wolff, E. A. (1966) Antenna Analysis, John Wiley and Sons, Inc., New York.

Destination	Number of Copies
Adams-Russell Company Library - Antenna Section 280 Bear Hill Road Waltham, Mass. 02154	1
Aero Geo Astro Security Officer Edsall and Lincolnia Blvd. Alexandria, Va.	1
Aerospace Corporation Robert C. Hansen 2400 E. El Segundo Blvd. Los Angeles, Calif. 90045	1
Cutler-Hammer Division, Airborn Instruments Labs. Librarian - Antenna Section Walt Whitman Road Melville, L.I., New York 11729	1
All Products Company Mr. James Buzbee Mineral Wells, Texas	1
Americal Electronic Laboratories, Inc. Antenna Section Box 552 Lansdale, Pa.	1
Andrew Alfred Consulting Engineers Librarian - Antenna Section 299 Atlantic Ave. Boston, Mass. 02110	1
AVCO Res. and Adv. Development Division Research Library 201 Lowell Wilmington, Mass. 01887	1
AVCO Electronic and Ordnance Division Technical Library 2630 Glendale-Milford Road Cincinnati, Ohio 45241	1
Bell Aircraft Corporation Technical Library - Antennas Buffalo, New York 14205	1
Bell Telephone Laboratories Inc. Technical Reports Library - Room 2A165 Whippany, New Jersey 07961	1

AF 33(615)-3609

Proj. 07848

Bendix Radio Division Technical Library - Dept. 462-4 East Joppa Road Baltimore, Md. 21204	1
Bendix Research Laboratories Technical Library 20800 10 1/2 Mile Road Southfield, Michigan 48076	1
Boeing/Wichita - Antenna Systems Staff Unit Technical Library 3801 South Oliver Wichita, Kansas 67201	1
Boeing Aerospace Division Technical Library - Antenna and Radomes Box 3707 Seattle, Washington 98124	1
Bunker-Ramo Corporation, Defense Systems Div. 8433 Fall Brook Avenue Canoga Park, California 91304	1
Canoga Electronics - Advanced Programs Dept Box 2086 Canoga Park, California 91306	1
Chance-Vought Aircraft, Inc. BuAer Representative Technical Library - Antenna Section Box 1500 Arlington, Texas 75222	1
Collins Radio Research Division Technical Library 5200 C NE Cedar Rapids, Iowa 52406	1
Collins Radio Corporation Dr. Robert L. Carrel - Antenna Section Dallas, Texas 75207	1
Dalmo Victor Company Technical Library - Antennas 1515 Industrial Way Belmont, California	1



AF 33(615)-3609

Proj. 07848

Dorne and Margolin, Inc. Technical Library - Antenna Section 29 New York Avenue Westbury, L.I., N.Y. 11591	1
Douglas Aircraft MSSD Technical Library Antenna Section 3000 Ocean Park Blvd. Santa Monica, Calif. 90406	1
Dynatronics, Inc. Technical Library - Antennas Hwy 17 and 92 N. Castlebury Orlando, Florida	1
Electronic Communications Research Division Technical Library 1830 York Road Timonium, Md.	1
Emerson and Cuming, Inc. E. J. Luoma 869 Washington St. Canton, Mass. 02021	1
Fairchild Aircraft and Missiles Division Technical Library - Antennas Hagerstown, Maryland	1
Fairchild Hiller Corporation Technical Library 1455 Research Blvd. Rockville, Md. 20850	1
General Dynamics/Convair Technical Library - Antennas Grants Lane P.O. Box 748 Fort Worth, Texas 76101	1
General Electric Electronics Laboratory Technical Library Electronics Park Syracuse, New York 13201	1
General Electric Light Military Electronics Dept. 901 Broad Street Utica, New York 13503	1

General Electric General Engineering Laboratory Building 371, Room 478 Schenectady, New York 12305	1
General Electronics Laboratories, Inc. Technical Library - Antennas 18 Ames Street Cambridge, Mass	1
General Precision Laboratory Technical Library - Antennas 63 Bedford Road Pleasantville, N. Y.	1
Goodyear Aircraft Arizona Division Antenna Department Box. 85 Litchfield Park, Arizona 85340	1
Grumman Aircraft Engineering Corporation Technical Library - Avionics Engineering South Oyster Bay Road Bethpage, N. Y.	1
Hallcrafters Company Technical Library - Antennas 4401 West Fifth Avenue Chicago, Illinois 60624	1
Hoffman Laboratories, Inc. 4501 North Arden Drive El Monte, California 91734	1
Hughes Aircraft Corporation Technical Library - Antennas Centinela and Teale Streets Culver City, California 90232	1
Hughes Aircraft Communications and Videasonics Div. Antenna Section 1901 West Malvern Avenue Fullerton, California	1
ITT Federal Laboratories Technical Library - Antennas 500 Washington Ave. Nutley, N. J. 07110	1

AF 33(615)-3609

Proj. 07848

Laboratory for Electronics, Inc. Antenna Department 1079 Commonwealth Avenue Boston, Mass. 02115	1
Ling-Temco-Vought Military Electronics Div. Librarian - Antennas 1200 Jupiter St. Garland, Texas	1
Litton Systems, Amecom Division Technical Library - Antennas 1140 E. W. Highway Silver Spring, Md. 20910	1
Lockheed Marietta Division South Cobb Drive Marietta, Georgia 30061	1
Lockheed Electronic and Armaments System Office P. O. Box 551 Burbank, California 91503	1
The Martin/Denver Division Headquarters Antenna Laboratory Mail Nr. T-0453 P. O. Box 179 Denver, Colorado 80201	1
The Martin/Orlando Company Technical Library - Microwaves Box 5837 Orlando, Florida	1
The Martin/Baltimore Company Technical Library - Antennas Baltimore, Md. 21203	1
Maxon Electronics Corporation Sunrise Highway Great River, L. I., New York 11739	1
McDonnell Aircraft Corporation Technical Library - Antennas Box 516 St. Louis, Missouri 63166	1
Melpar, Inc. Technical Library - Antennas 3000 Arlington Blvd. Falls Church, Va. 22047	1

MITRE Corporation  
Technical Library  
Electronic Warfare Department D-21  
Middlesex Turnpike  
Bedford, Mass. 01730 1

Motorola Western Military Electronics Division  
8201 E. McDowell  
Scottsdale, Arizona 85252 1

North American Aviation, Inc.  
Technical Library - Dept. 56  
International Airport  
Los Angeles, California 90009 1

North American Aviation, Autonetics Division  
System Technology Department  
3370 Miraloma Avenue  
Anaheim, California 92803 1

North American Aviation/Columbus Division  
Technical Library - Engineering Dept.  
4300 E. Fifth Avenue  
Columbus, Ohio 43216 1

Northrop/Norair Division  
3901 West Broadway  
Technical Information (3924-3)  
Hawthorne, California 90250 1

Northrop/Ventura  
Technical Information Center  
1515 Rancho Conejo Blvd.  
Newbury Park, California 91320 1

Philco Communications and Electronics  
Government and Industrial Division  
Technical Library - Antennas  
4700 Wissachickon Ave.  
Philadelphia, Pa. 19144 1

Radiation Systems, Inc.  
Engineering Department  
440 Swann Avenue  
Alexandria, Va. 1

Radiation Products Division  
Technical Library  
Box 37  
Melbourne, Fla. 31511 1

RCA Missile and Service Radar Division  
Manager, Antenna Engineering Skill Center  
Marne Highway  
Moorestown, New Jersey 08057 1

Rantec Corporation  
Librarian - Antenna Laboratory  
24003 Ventura Blvd.  
Calabasas, California 91302 1

Raytheon Equipment Division  
Library - Mr. J. Portsch  
P. O. Box 520  
Waltham, Mass. 02154 1

Raytheon Missile Systems Division  
Research Library  
Hartwell Street  
Bedford, Mass. 1

Raytheon Space and Information Systems Div.  
528 Boston Post Road  
Sudbury, Mass. 1

Sanders Associates  
Librarian - Antennas  
95 Canal Street  
Nashua, New Hampshire 1

Sichak Associates.  
Mr. W. Sichak  
518 Franklin Ave.  
Nutley, New Jersey 1

HRB Singer Corporation  
Attn: Library - Antennas  
Box 60, Science Park  
State College, Pa. 16801 1

Southwest Research Institute  
Librarian - Antenna Laboratory  
8500 Culebra Road  
San Antonio, Texas 78206 1

Space Technology Laboratory  
Research Library  
One Space Park  
Redondo Beach, California 90278 1

Sperry Gyroscope Division Librarian - Antenna Laboratory Great Neck, L. I., New York 11020	1
Sperry Microwave Electronics Division Librarian - Antenna Laboratory Box 1828 Clearwater, Florida	1
Stanford Research Institute Librarian - Antennas 333 Ravenswood Street Menlo Park, California 94025	1
Sylvania Electronic Products Librarian - Antennas Box 188 Mountain View, California	1
Sylvania Electronic Systems Division Librarian - Antennas and Microwaves 40 Sylvan Waltham, Mass 02154	1
Teledyne Communications System Division 12964 Panama Street Los Angeles 66, California	1
Texas Instruments, Inc. Librarian - Antennas 13500 N. Central Expressway Dallas, Texas 75209	1
A. S. Thomas, Inc. Librarian - Antennas 355 Providence Highway Westwood, Mass. 02081	1
Westinghouse Aerospace Division P. O. Box 746 Baltimore, Md. 21203	1
Wheeler Laboratories Librarian - Antennas Box 561 Smithtown, New York 11787	1

AFCRL C. J. Sletten CRD L G Hanscom Field Bedford, Mass. 01731	2
AFETRL - Technical Library Patrick AFB, Fla. 32925	1
AFMDC - Technical Library Holloman AFB, New Mexico 88330	1
APGC, Hq. 3208 Test Group Eglin AFB, Fla. 32542	1
ASD - ASEP B. Brooks Wright-Patterson AFB, Ohio 45433	1
RADC - EMATA, Griffiss AFB, New York 13442	1
RADC EMLT-1 Griffiss AFB, New York 13442	1
RADC EMIAD - R F Davis Griffiss AFB, New York 13442	1
SEG - SEAEM Mr. Mulligan Wright-Patterson AFB, Ohio 45433	1
SEG - SEACC Y. E. Stahler Wright-Patterson AFB, Ohio 45433	1
SEG - SEPIE Wright-Patterson AFB, Ohio 45433	1
AFSC - SCSE Andrews AFB, Wash. D. C. 20331	1
RTD - RTGS Bolling AFB, Washington, D. C. 20332	1
Hq, USAF, AFRDR, Lt. Col. B. Lieber Washington, D. C. 20330	1
Hq, USAF AFXSAI, Air Battle Analysis Center Dep. Dir. Plans for War Plans Washington, D. C. 20330	1
RTD RTHR Bolling AFB, Washington, D. C. 20332	1
FTD TD-EE Wright-Patterson AFB, Ohio 45433	1

U. S. Army Electronics Command SIGRA/NAI Ft. Monmouth, N J	1
U. S. Army White Sands Missile Range Technical Library ORDBS-OM RR-312 White Sands, New Mexico 88002	1
Ballistic Research Laboratory Technical Library - Antennas Aberdeen Proving Ground, Md. 21005	1
Harry Diamond Laboratories Connecticut Ave. , and Vann Ness Street, NW Attn: 240 Washington, D. C. 20438	1
U S Army Electronics R and D Activity SELWS-ED White Sands Missile Range, N. Mexico 88002	1
USAFSS ESD/ESG Mr. A. Martinez San Antonio, Texas 78241	1
Director, Surveillance Dept. Evans Area Technical Document Center Belmar, New Jersey	1
ONR Branch Office Box 39 FPO, New York 09510	1
Chief, Bureau of Ships Code 312 Main Navy Building Washington, D. C. 20360	1
Naval Research Laboratory Code 5200 Washington, D. C. 20390	1
U S Naval Air Test Center WSST-54, Antenna Section Patuxent River, Md. 20910	1
Materials Laboratory New York Naval Shipyard Code 932 Brooklyn, N. Y. 11201	1



U. S. Navy Electronics Laboratory Code 3220 - Library San Diego, California 92152	1
U. S. Naval Ordnance Test Station Mr. J. A. Mosko - Code 4021 China Lake, California 93557	1
U. S. Naval Ordnance Laboratory Technical Library Corona, California 91720	1
Office, Assist. Sec'y Def. R and D Technical Library 3E1065, Pentagon Washington, D. C. 20330	1
Air University Library 3T-AUL-59-30 Maxwell AFB, Alabama 36112	1
NASA Goddard Space Flight Center Antenna Branch Greenbelt, Md. 20771	1
V. DeSanti, Exchange Section DCD Scientific/Technical Information Facility P O Box 5700 Bethesda, Md.	1
GIT Engineering Experiment Station Technical Library - Electronics Division Atlanta, Ga. 30313	1
JHU Applied Physics Laboratory 8621 Georgia Avenue Silver Springs, Md. 20910	1
JHU Carlyle Barton Laboratory Charles and 34th Streets Baltimore, Md. 22218	1
MIT-Lincoln Laboratory Document Room Box 73 Lexington, Mass. 02173	1
New Mexico State University Antenna Department Physical Science Dept. University Park, New Mexico	1

Northeastern University Dodge Library Boston, Mass. 02115	1
Ohio University Technical Library - EE Dept. Athens, Ohio	1
Ohio State University Research Foundation Technical Library - Antenna Laboratory 2024 Neil Ave. Columbus, Ohio 43210	1
Ohio State University Antenna Laboratory Technical Library 1320 Kinnear Road Columbus Ohio 43212	1
PIB Microwave Research Institute Professor A. A. Oliner 55 Johnson St. Brooklyn, N. Y. 11201	1
Stanford Electronics Laboratory Librarian - Antennas Stanford, California 94025	1
Syracuse University Dr. Jose Perih - Electrical Engineering Dept. Syracuse, N. Y. 13210	1
University of Dayton Research Institute Professor Douglas Hanneman 300 College Park Dayton, Ohio 45409	1
University of Southern California W. V. Trusch - EE Dept. University Park Los Angeles, California 90007	1
University of Texas - EE Res. Lab. Route 4 Box 189 Austin, Texas	1

AF 33(615)-3609

Proj. 07848

Cornell Aeronautical Laboratory  
Research Library  
Buffalo, New York 14221

1

University of Illinois EE Res. Laboratory  
Engineering Experiment Station  
Urbana, Illinois

1

Air Force Avionics Laboratory  
AVWE-3  
Wright-Patterson AFB, Ohio 45433

5 +reproducible

Defense Documentation Center  
Alexandria Virginia 22314

20 + card

---

163 + reproducible



DOCUMENT CONTROL DATA - R & D

(Security classification of title, body of abstract and indexing annotation must be entered when the overall report is classified)

1. ORIGINATING ACTIVITY (Corporate author)  
The University of Michigan Radiation Laboratory, Dept. of  
Electrical Engineering, 201 Catherine Street,  
Ann Arbor, Michigan 48108

2a. REPORT SECURITY CLASSIFICATION

Unclassified

2b. GROUP

3. REPORT TITLE

Study and Investigation of a UHF-VHF Antenna

4. DESCRIPTIVE NOTES (Type of report and inclusive dates)

Seventh Quarterly Report 1 July 1967 through 30 September 1967

5. AUTHOR(S) (First name, middle initial, last name)

Lyon, John A.M., Chen, C-C, Parker, J.C. and Smith, D.L.

6. REPORT DATE

October 1967

7a. TOTAL NO. OF PAGES

70

7b. NO. OF REFS

12

8a. CONTRACT OR GRANT NO.

AF 33 (615)-3609

b. PROJECT NO.

6278

c.

Task 627801

d.

9a. ORIGINATOR'S REPORT NUMBER(S)

7848-7-Q

9b. OTHER REPORT NO(S) (Any other numbers that may be assigned  
this report)

10. DISTRIBUTION STATEMENT

Qualified requestors may obtain copies of this report from DDC. This document is subject to special export controls and transmittal to foreign governments or foreign nationals may be made only with prior approval of AFAL(AVPT), Wright-Patterson AFB, Ohio

11. SUPPLEMENTARY NOTES

12. SPONSORING MILITARY ACTIVITY

Air Force Avionics Laboratory AVWE  
Research and Technology Division, AFSC  
Wright-Patterson AFB, Ohio 45433

13. ABSTRACT

This report covers the work effort in the various tasks of the project for a three-month period. The report goes into considerable detail since it includes substantial analysis, computer results, and experimental data. In all of the tasks, substantial progress has been made. However, in one task, a complete reorientation of the work program has been made. Under Task II, on slot arrays, it has been found necessary to simplify the work and also to avoid difficulties with materials. This should allow development of new array utilizing ferrite filled rectangular slots developed in the prior contract work of this group.

14. KEY WORDS	LINK A		LINK B		LINK C	
	ROLE	WT	ROLE	WT	ROLE	WT
ANTENNAS FERRITE LOADING TECHNIQUES PHYSICALLY SMALL ANTENNAS						



UNIVERSITY OF MICHIGAN



3 9015 03465 8636